SKB

TECHNICAL REPORT 91-63

An electrochemistry-based model for the dissolution of UO_2

D W Shoesmith, S Sunder

AECL Research, Whiteshell Laboratories, Pinawa, Manitoba, Canada

December 1991

SVENSK KÄRNBRÄNSLEHANTERING AB
SWEDISH NUCLEAR FUEL AND WASTE MANAGEMENT CO

BOX 5864 S-102 48 STOCKHOLM

TEL 08-665 28 00 TELEX 13108 SKB S
TELEFAX 08-661 57 19

AN ELECTROCHEMISTRY-BASED MODEL FOR THE DISSOLUTION OF UO_2

D W Shoesmith, S Sunder

AECL Research, Whiteshell Laboratories, Pinawa, Manitoba, Canada

December 1991

AECL RESEARCH

AN ELECTROCHEMISTRY-BASED MODEL FOR THE DISSOLUTION OF UO_2

by

D.W. Shoesmith and S. Sunder

Whiteshell Laboratories
Pinawa, Manitoba ROE 1LO
1991

AECL-10488

AN ELECTROCHEMISTRY-BASED MODEL FOR THE DISSOLUTION OF UO_2

by

D.W. Shoesmith and S. Sunder

ABSTRACT

A model to predict the dissolution of UO_2 fuel under both oxidizing and non-oxidizing conditions is presented and compared with other available models for fuel dissolution. Dissolution rates under oxidizing conditions are predicted by extrapolating steady-state electrochemical currents for the anodic dissolution of UO_2 to the corrosion potentials measured in solutions containing various oxidants, including dissolved oxygen, hydrogen peroxide, and the products of the gamma or alpha radiolysis of water. Where possible, these predictions are compared with dissolution rates measured chemically and available in the literature. With a few exceptions, the agreement between our predictions and published rates is good.

For non-oxidizing conditions, the dissolution rate of UO_2 is not well known. Attempts to measure this rate are fraught with difficulties, and the published values are difficult to rationalize within the framework of our model. Consequently, we briefly reviewed the literature on the dissolution of similar p-type semiconducting oxides and chose to estimate the chemical dissolution rate of UO_2 by analogy to the well-studied oxide NiO. In this manner we have managed to establish a threshold rate below which the rate of oxidative dissolution becomes negligible in comparison with the rate of chemical dissolution. This threshold agrees quite well with that established electrochemically.

Using these extrapolated rates we predict that the rate for oxidative dissolution of CANDU (CANada Deuterium Uranium) fuel due to gamma radiolysis will fall below this threshold after ~200 a, a time period that is short in comparison with the anticipated lifetimes of titanium waste containers, which are expected to last for a period greater than ~1200 a. For dissolution due to alpha radiolysis, oxidative rates are uncertain, but could be above this threshold for a period of 500 to 10 000 a for CANDU fuel, and 500 to 30 000 a for pressurized water reactor (PWR) fuel. The uncertainty in these ranges reflects the poor quality and limited number of corrosion potential measurements in the presence of alpha radiolysis. Experiments are in progress to obtain additional data to ascertain the impact of alpha radiolysis.

AECL Research
Whiteshell Laboratories
Pinawa, Manitoba R0E 1L0
1991

AECL-10488

CONTENTS

		Page
1.	INTRODUCTION	1
2.	CHEMISTRY OF UO_2 DISSOLUTION	3
3.	MODELLING UO_2 DISSOLUTION	5
	3.1 SOLUBILITY-BASED DISSOLUTION MODEL	5
	3.2 KINETIC MODELS	7
	3.3 ELECTROCHEMISTRY-BASED DISSOLUTION MODEL	8
4.	UO_2 DISSOLUTION IN OXYGENATED SOLUTIONS	11
5.	UO_2 DISSOLUTION IN HYDROGEN PEROXIDE SOLUTIONS	14
6.	IMPACT OF GAMMA RADIOLYSIS ON UO_2 DISSOLUTION	15
7.	IMPACT OF ALPHA RADIOLYSIS ON UO_2 DISSOLUTION	17
8.	SUMMARY	21
	ACKNOWLEDGEMENTS	24
	REFERENCES	24
	FIGURES	29
APPENDIX A	EVIDENCE FOR A THRESHOLD FOR OXIDATIVE DISSOLUTION	51
APPENDIX B	UO_2 OXIDATION AND DISSOLUTION DURING GAMMA RADIOLYSIS	55
APPENDIX C	REDOX CONDITIONS FOR WHICH THE SOLUBILITY-BASED MODEL FOR FUEL DISSOLUTION IS APPROPRIATE	61

continued...

CONTENTS (concluded)

		Page
APPENDIX D	BASIS FOR AN ELECTROCHEMISTRY-BASED DISSOLUTION MODEL	67
APPENDIX E	CHEMICAL DISSOLUTION OF METAL OXIDES	79
APPENDIX F	PEROXIDE-DECOMPOSITION AND OXIDATIVE DISSOLUTION IN H_2O_2-CONTAINING SOLUTIONS	85
APPENDIX G	RELATIONSHIP BETWEEN ALPHA-SOURCE STRENGTH USED IN EXPERIMENTS AND THE ALPHA PLUS BETA ACTIVITY-TIME PROFILE FOR IRRADIATED CANDU FUEL	95

1. INTRODUCTION

Any environmental assessment of used-fuel disposal requires a prediction of the release rates of radionuclides from the fuel once contact with groundwater is established. Experimental studies on the leaching and dissolution of used fuel have shown that the rate of release of radionuclides depends largely on their location within the fuel element. The radionuclide release model used in the safety assessment of the Canadian Nuclear Fuel Waste Management Program (NFWMP) acknowledges three main release mechanisms (Johnson and Shoesmith 1988):

(1) the rapid release of volatile fission products (e.g., Cs and I) from the fuel/cladding gap;

(2) the leaching of fission products (e.g., Cs, I, Tc) from the fuel grain boundaries; and

(3) the slow release of radionuclides from the fuel matrix as a result of dissolution of the fuel grains.

A review of the source terms developed to describe such releases has been published (Garisto and Garisto 1990).

Understanding the factors controlling these releases has proved difficult, and extremely conservative approaches have been adopted. Thus, the present analysis disregards the difference in kinetics for release from the fuel/cladding gap and from grain boundaries: we assume radionuclides at both sites are instantly released on contact with groundwater. The great majority of radionuclides are contained within the grains of the fuel pellets and will be released at a rate governed by the dissolution rate of the uranium oxide matrix.

The problem of measuring and predicting UO_2 dissolution rates is complicated by the sensitivity of uranium solubility to redox conditions (Lemire and Tremaine 1980, Paquette and Lemire 1981, Garisto and Garisto 1985, Lemire and Garisto 1989). Although UO_2 is highly insoluble, the solubility of uranium increases by many orders of magnitude under oxidizing conditions. This makes the release rates of the large majority of radionuclides potentially very dependent on vault redox conditions.

Even though non-oxidizing conditions are expected to prevail in a dosposal vault in granitic rock by the time waste containers fail, the possibility

that water radiolysis, due to ionizing radiation within the fuel, will maintain oxidizing conditions close to the fuel surface needs to be examined. The gamma-radiation field at the surface of the fuel will decay to insignificant levels after ~500 a, and should be of little consequence unless containers fail at times shorter than this. By contrast, alpha, and to some extent beta, radiation fields will remain significant for more than 10^5 a, and could maintain surface oxidizing conditions well beyond the expected lifetime of most containers. Such localized oxidizing conditions could be particularly important in internal cracks in the fuel, since cracks are invariably present in irradiated nuclear fuels.

In this report we will attempt to assess the impact of potential oxidants on the dissolution of UO_2. We will review briefly the impact of redox conditions on the mechanism of oxidation and dissolution of UO_2, and discuss the modelling approaches currently used to assess fuel behaviour. However, our primary aim is to present the framework of a model capable of predicting the dissolution rate of fuel as vault redox conditions change from initially oxidizing to eventually non-oxidizing. This model is based on the extrapolation of electrochemical data to natural corrosion conditions and has been outlined previously (Johnson et al. 1988).

Our experimental approach and the results obtained are discussed in detail. Where possible, these results are compared with those reported by other researchers. On the basis of such comparisons we hope to enhance the credibility of our approach. Unfortunately, in some cases, particularly for results obtained in the presence of alpha radiolysis, comparison is impossible because no similar measurements have been attempted elsewhere. Since our experimental program is incomplete, this model must be considered preliminary, and predictions are likely to change as further advances in understanding are achieved and a more accurate and complete database is accumulated. A significant deficiency in the model is the lack of any assessment of the impact of parameters likely to influence the reactivity of UO_2. Such changes in reactivity may exert a significant influence on the dissolution rate, and are the key to applying the results of this model to the prediction of used fuel, as opposed to unirradiated UO_2, behaviour. Despite these reservations, a comparison of rates obtained by extrapolation of electrochemical data with rates obtained chemically with used fuel (Shoesmith et al. 1989) are encouraging.

2. CHEMISTRY OF UO_2 DISSOLUTION

The dissolution of UO_2 has been studied under both oxidizing (Johnson and Shoesmith 1988, Sunder and Shoesmith 1991) and non-oxidizing (Bruno et al. 1988, 1991) conditions. In the presence of radiolytically decomposed water, the possible reactions that could occur on the surface of fuel are numerous, as illustrated in Figure 1, and include, besides oxidative dissolution, radical recombination, hydrogen peroxide decomposition, the reduction of oxidized surface layers, and radical recombination catalyzed by redox-active species in the surrounding environment (e.g., Fe^{II}/Fe^{III}). Although many of these processes have been experimentally observed at one time or another, a detailed mechanistic understanding has not yet been achieved. Our present mechanistic understanding has been reviewed elsewhere (Johnson and Shoesmith 1988, Sunder and Shoesmith 1991). Here we discuss only those aspects of the oxidative dissolution process essential to an understanding of the model to be presented.

The chemistry of UO_2 dissolution as a function of electrochemical potential is summarized in Figure 2. The potential scale in this figure represents the redox condition established at the UO_{2+x} surface ($0 < x \leq 1$), not the redox potential in the surrounding solution or environment. As such, it is a measure of the kinetic balance between the anodic (oxidation) and cathodic (reduction) reactions possible on the surface. It is appropriate to think in terms of coupled electrochemical reactions, since Nicol and Needes have demonstrated the electrochemical nature of the oxidative dissolution of UO_2 in the presence of a variety of oxidizing agents (Nicol et al. 1975, Needes et al. 1975).

The degree of oxidation of the surface ($UO_{2+x} \longrightarrow UO_{2.67}$) has been established both as a function of applied electrochemical potential and under natural corrosion conditions using X-ray photoelectron spectroscopy (XPS). Electrochemical experiments have also shown that significant oxidative dissolution does not occur until a surface composition close to $UO_{2.33}$ is achieved. This composition is taken as a threshold composition beyond which oxidative dissolution becomes significant. This threshold is indicated by the second horizontal shaded area in Figure 2, and some of our experimental evidence supporting the choice of -100 mV (vs. SCE, standard calomel electrode) as the threshold potential is presented in Appendix A.

A composition of $UO_{2.33}$ represents the end of the fluorite structure range for UO_{2+x}. More extensive oxidation leads to major structural modifications of the surface (to $UO_{2.67}$), accelerating dissolution (as UO_2^{2+}), and

to the formation of secondary precipitates ($UO_3 \cdot xH_2O$). The composition of these secondary precipitates will depend on the nature and composition of the surrounding environment (Johnson and Shoesmith 1988, Sunder and Shoesmith 1991). Dissolution, illustrated schematically in Figure 3(a), can be represented by the following reactions:

$$UO_2 + 0.33H_2O \longrightarrow UO_{2.33} + 0.66H^+ + 0.66e \quad (1)$$

$$UO_{2.33} + 0.66H^+ \longrightarrow UO_2^{2+} + 0.33H_2O + 1.34e \quad (2)$$

Both of these reactions are oxidations and must be accompanied by the reduction of available oxidants.

When surface oxidation is confined to the region below $UO_{2.33}$ (U_3O_7), the fluorite structure is maintained and oxidation occurs by the uptake of oxygen as O^{2-} at interstitial sites within UO_{2+x}. Under such redox conditions we anticipate that oxidative dissolution rates will be extremely low, and it may be more appropriate to think of dissolution as chemical and not involving electrochemical rate parameters. In reality, the process is still oxidative in nature, since dissolution would involve the ion transfer across the oxide-solution interface of uranium species in at least two oxidation states, U^{4+} and U^{6+}, and under steady-state conditions further oxidation must occur to maintain the surface composition. For this situation to apply, surface oxidation would have to be rapid, and dissolution controlled by the slower ion transfer of U^{4+} and U^{6+} species:

$$UO_2 + xH_2O \longrightarrow UO_{2+x} + 2xH^+ + 2xe \quad (3)$$

$$UO_{2+x} + n(1 - x)OH^- + (x - 2)H_2O \longrightarrow (1 - x)U(OH)_n^{(4-n)+} + xUO_2^{2+} + (2x - 4)H^+ \quad (4)$$

This situation is illustrated schematically in Figure 3(b) and is equivalent to an overall oxidative dissolution process controlled by the rate of chemical ion transfer, Reaction (4). Experimental evidence for rapid surface oxidation in the potential region from -400 to -100 mV is discussed briefly in Appendix B.

Under non-oxidizing conditions, any oxidized layer on the surface will dissolve, and, in the absence of oxidant to maintain the surface composition, dissolution would eventually become fully chemical in nature, involving only the ion transfer of U^{4+} species (Figure 3(c)). Attempts to

measure the dissolution rate of UO_2 under reducing conditions have been made, and in the range $7 \leq pH \leq 11$, Bruno et al. (1988,1989) have obtained a dissolution rate independent of pH (~4 x 10^{-3} $\mu g \cdot cm^{-2} \cdot d^{-1}$) for the overall reaction,

$$UO_2 + (n - 2)H_2O \longrightarrow U(OH)_n^{(4-n)+} + (n - 4)H^+ \qquad (5)$$

The two double-hatched horizontal zones in Figure 2 represent the corrosion potential ranges observed for UO_2 electrodes exposed to aerated solutions and argon-purged solutions. The width of these zones is a measure of the reproducibility of the corrosion-potential measurements. The separation between the two zones reflects the range of potentials measured between definitely oxidizing conditions and those that are as non-oxidizing as experimentally achievable in argon-purged solutions in an anaerobic chamber.

3. MODELLING UO_2 DISSOLUTION

3.1 SOLUBILITY-BASED DISSOLUTION MODEL

In the Canadian NFWMP a solubility-based dissolution model has been developed to determine the rate of used-fuel dissolution. Such a model is considered appropriate since redox conditions within a waste vault are not expected to be oxidizing for any significant length of time. Oxygen initially present within the vault will be consumed either by reaction with reducing agents, such as S^{2-}, Mn^{2+} and Fe^{2+} present in minerals, or by corrosion of the metal container.

The form of this model is illustrated schematically in Figure 4, and the assumptions implicit in its use are discussed in Appendix C. The transport of dissolved uranium and released radionuclides is represented by a one-dimensional diffusion-convection equation modified to include radioactive decay. Details of the mass transport modelling and the justification for the use of a one-dimensional model have been given elsewhere (Garisto and Garisto 1988, Garisto and LeNeveu 1989). This diffusion-convection equation is solved with a steady-state concentration boundary condition at the fuel/buffer interface (J_1 at $x = 0$ in Figure 4), which specifies that

$$\text{Dissolution Rate} = J_1 A = k_{UO_2} A(c_{SOL} - c(0,t)) \qquad (6)$$

where k_{UO_2} is the dissolution rate constant of the fuel, A is the surface

area of the fuel (taken as equal to the surface area of the container in this one-dimensional model), c_{SOL} is the solubility of the used-fuel matrix, and c(0,t) is the concentration of dissolved uranium at the fuel surface (x = 0) at time t. The source term for a specific radionuclide is then obtained by multiplying this rate by the fractional inventory of that radionuclide in the used-fuel matrix. The development of the source terms for individual radionuclides has been discussed (Lemire and Garisto 1989, Garisto and Leneveu 1989), and the development of the solubility term, c_{SOL}, for uranium and other actinides has been described in detail elsewhere (Lemire and Garisto 1989, Garisto and Garisto 1985).

Under transport-controlled conditions, when the dissolution (interfacial ion transfer) reaction is near equilibrium (i.e., $c(0,t) \sim c_{SOL}$), the relationship given in Equation (6) is a reasonable approximation (Segall et al. 1988). However, the use of this equation requires that a value be specified for the kinetic constant, k_{UO_2}. At present, a value for this constant is deduced from fuel-leaching experiments. The major advantage of using Equation (6) is that it allows dissolution to be modelled in the absence of any mechanistic understanding of the interfacial processes involved. When used in this manner, k_{UO_2} is an empirical rate constant.

Other problems arise with an approach of this nature. To calculate solubilities, a detailed knowledge of chemical conditions within the vault is required. Such a calculation requires large amounts of thermodynamic data, much of which is poorly known and difficult to obtain. Also, the model is limited to the redox potential range from UO_2 to $UO_{2.25}$ (Appendices A to C). When solubilities are computed for oxidation potentials at which $UO_{2.25}$ undergoes oxidative dissolution to U^{VI} species, dissolved uranium concentrations exceed 10^{-4} mol·kg^{-1} (Figure C-2, Appendix C). Such high local concentrations will inevitably lead to precipitation. In this case, as stated by Garisto and Garisto (1990), the solid transformation rate, rather than the transport of dissolved uranium away from the fuel/buffer interface, would control the release of radionuclides. Under such conditions, the approximation embodied in Equation (6) is unlikely to be justified.

The implications of coupling precipitation processes with a mass transport model for dissolution involving a reversible interfacial step have been documented (Garisto and Garisto 1988, Garisto 1986). The situation is illustrated schematically in Figure 5. In essence, the formation of secondary phases on the dissolving surface cannot proceed with $c(0,t) \sim c_{SOL}$, as required in the application of the boundary condition specified in Equation (1). Under such conditions, dissolution will be proceeding far

from equilibrium and will be controlled by the kinetic parameters of the interfacial reaction.

3.2 KINETIC MODELS

It is impossible to circumvent the difficulties described above within the framework of a solubility-based model. It is also difficult to assess the impact of radiolysis processes, which are intrinsically non-thermodynamic and kinetically oxidizing in character. For an assessment of radiolysis effects to be meaningful, it is necessary to attempt the development of a kinetic model for oxidative dissolution processes.

To avoid the difficulties inherent in an experimental approach, attempts have been made to develop models that assess the effect of alpha radiolysis on fuel dissolution rates. Alpha radiolysis is considered the only significant source of radiolytic oxidants, since gamma-radiation fields will have decayed to negligible levels by the time the container fails and fuel comes in contact with groundwater.

It is assumed that all the alpha energy, calculated from the energy spectrum of alpha particles emitted from used fuel, is deposited in a thin layer of water (30 to 50 μm thick) on the surface of the fuel. Using this model, Garisto and Garisto (1990) estimated that the fractional fuel dissolution rate is about 2×10^{-7} d^{-1}. Several other assumptions are also used in this calculation: (i) the effective surface area of a fuel pellet (including cracks) is five times the geometric surface area; (ii) the surface-to-volume ratio is independent of time; and (iii) each mole of H_2O_2 can dissolve one mole of UO_2. This rate is considered an upper bound for the impact of radiolysis and is six to seven orders of magnitude larger than the rate calculated using the solubility-based model with a UO_2 solubility of 10^{-10} $mol \cdot kg^{-1}$ (Garisto and LeNeveu 1989).

A similar approach to modelling the impact of alpha radiolysis on fuel dissolution has been adopted by Werme et al. (1990). They assumed that UO_2 will oxidize in radiolytically decomposed water at a rate identical to that observed for the oxidation of Fe^{2+} in solution. On the basis of calculations by Christensen and Bjergbakke (1987a), showing that the rate of oxidation of Fe^{2+} to Fe^{3+} is directly proportional to alpha dose rate, Werme et al. (1990) calculated the extent of fuel oxidation assuming the dissolution rate was equal to the oxidation rate of UO_2. Provided the container survives for 1000 a, this rate is $\sim 2.5 \times 10^{-7}$ d^{-1}. This value is comparable to that observed in used-fuel corrosion tests with 15-a-old fuel, if the rate of strontium release is accepted as a monitor of the rate of matrix dissolution/alteration (Werme et al. 1990).

3.3 ELECTROCHEMISTRY-BASED DISSOLUTION MODEL

Given the uncertainties in the approaches to modelling, and the wide divergence in the predicted behaviour of fuel by the models described above (i.e., a difference of six to seven orders of magnitude in predicted dissolution rates), we have adopted a wide-ranging experimental program to determine the mechanism and kinetics of fuel dissolution over a wide range of redox conditions. Our aim is to develop a kinetic statement for the dissolution of UO_2 that is applicable over the full range of redox conditions expected under waste vault conditions. This statement would replace the semi-empirical Equation (1) as the flux boundary condition at the fuel/buffer interface in the transport-based model outlined schematically in Figure 4.

We have been attempting to measure dissolution rates using a combination of electrochemical and natural corrosion experiments. Electrochemical techniques are ideal for this purpose, since they enable us to control the potential at the surface of UO_2. Using such techniques, we can separate a corrosion reaction into its component half reactions, and study the dependence of rate on applied potential for each half reaction. Our experimental approach is outlined in Figure 6.

At positive applied potentials we have measured the steady-state current resulting from the anodic dissolution of UO_2 according to the half reaction

$$UO_2 \longrightarrow UO_2^{2+} + 2e \qquad (7)$$

as a function of applied potential. Similar measurements have been made on selected cathodic half reactions:

$$O_2 + 2H_2O + 4e \longrightarrow 4OH^- \qquad (8)$$

$$H_2O_2 + 2e \longrightarrow 2OH^- \qquad (9)$$

As expected for a steady-state electrochemical reaction uncomplicated by transport processes, the current is logarithmically dependent on potential, provided the applied potential is sufficiently positive or negative (Shoesmith et al. 1989, Hocking et al. 1991).

Under natural corrosion conditions, Reaction (7) will couple with either, or both, Reactions (8) and (9) if the oxidative dissolution of UO_2 is being driven by O_2 and/or H_2O_2. This coupling of half reactions can only occur

at a single value of corrosion potential, E_{CORR}, at which the current resulting from anodic dissolution (I_A) must equal that arising from oxidant reduction ($-I_C$). The corrosion potential can be measured easily in solutions of known oxidant concentration, and the arrow in Figure 6 shows the range of corrosion potentials measured in solutions containing O_2, H_2O_2 or the products of water radiolysis. By extrapolating the electrochemical data measured at positive and negative potentials to the corrosion potential under a given chemical/radiochemical condition, we can obtain a measure of the corrosion current (equal to the dissolution rate) under that condition.

For this extrapolation to be valid, two conditions must be met:

(1) the two half reactions must be genuinely coupled; i.e., the extrapolations from both positive and negative potentials must yield the same value of corrosion current, I_{CORR}; and

(2) the mechanism of the electrode process must not change over the range of the extrapolations.

Changes in composition of the UO_2 electrode surface with potential make these extrapolations uncertain. However, on the basis of a clear and detailed understanding of the mechanisms involved, we can justify this approach. A justification is presented in Appendix D.

If we can determine the dependence of these log I-E relationships on the range of parameters likely to control the dissolution, then mathematical expressions can be developed for both half reactions. The anodic current (≡ dissolution rate) will be expressed by equations of the type

$$I_A = k_{UO_2} N[X]^m[Y]^p \exp(bE) \qquad (10)$$

where k_{UO_2} is the heterogeneous rate constant for oxidative dissolution and the rate is dependent on the concentration of species X and Y (probably HCO_3^- and H^+), with reaction orders m and p respectively. The term exp(bE) expresses the dependence of dissolution rate on applied potential, E, and b is the slope of the log I-E plot. The term N would take into account variations in reactivity of the UO_2 and is a difficult parameter to quantify. The question of reactivity has been discussed elsewhere (Johnson and Shoesmith 1988), and we have recently summarized our approach to studying reactivity effects in UO_2 oxidation and dissolution (Hocking et al., in preparation).

At negative potentials, similar relationships can be developed for the oxidant reduction reaction; i.e.,

$$I_c = k_{ox}N'[Ox]^q \exp(-b'E) \quad (11)$$

where the parameters have the same significance as in Equation (10) and Ox is the oxidant. Since we have shown that the kinetics of oxygen reduction are affected by species, such as carbonate, that compete with oxygen molecules for active sites on the UO_2 surface (Hocking et al. 1991), the addition of extra concentration terms to Equation (11) may be required. If more than one oxidant is involved, then the total cathodic current will be the sum of the individual components,

$$(I_c)_{Total} = (I_c)_{O_2} + (I_c)_{H_2O_2} + (I_c)_{OH} \cdots \quad (12)$$

These equations can be combined for $E = E_{CORR}$ to yield an expression for the corrosion current (dissolution rate) in terms of the parameters that control dissolution. This expression would then provide the desired replacement for the semi-empirical Equation (6) as the flux boundary condition at the fuel/buffer interface in the transport-based model outlined in Figure 4. Two published examples serve to illustrate the usefulness of this approach. Nicol and Needes developed a relationship to describe UO_2 dissolution under ore-leaching conditions (Nicol et al. 1975, Needes et al. 1975), and Marsh and Taylor (1988) used an approach similar to that described here to develop a model for the corrosion of iron and carbon steel waste containers under nuclear waste vault conditions.

At present, this model is incompletely developed (Appendix D), and the dissolution rates presented here are based on an extrapolation using only the log I-E relationship for the anodic dissolution reaction, Equation (7). Hence, our rates are semi-empirical but based on a good understanding of the dissolution kinetics. The procedure to obtain these rates is outlined schematically in Figure 7.

A number of points are worth emphasizing before we present our results.

(1) All results were obtained on electrodes of the same type of UO_2 (i.e., from the same batch of sintered fuel pellets); consequently, they do not reflect the impact of variations in reactivity.

(2) Our data were all recorded in 0.1 $mol \cdot L^{-1}$ $NaClO_4$, a generally non-complexing solution, at pH = 9.5, a value relevant to groundwater buffered with small amounts of HCO_3^-/CO_3^{2-}.

(3) All measurements are for room temperature.

(4) Our electrochemical results for the anodic dissolution of UO_2 were recorded under conditions where the accumulation of solid corrosion products on the electrode surface was unlikely. As such they represent the maximum dissolution rates, unattenuated by the presence of surface films. The implications of surface-film formation are discussed in Appendix D.

(5) The development of a mathematical expression (log I-E) for the electrochemical reduction of radiolytically produced radical oxidants is beyond the scope of our experimental method. At achievable dose rates with either gamma or alpha sources, the radiolysis product concentrations are too low to generate a steady-state reduction current. Consequently, dissolution rates are always obtained by the method outlined in Figure 7, or predicted using a more complicated modelling procedure (Christensen and Bjergbakke 1987b, Christensen and Sunder 1989, Christensen et al. 1990a).

4. UO_2 DISSOLUTION IN OXYGENATED SOLUTIONS

Figure 8 shows a set of E_{CORR} measurements made on solutions purged with nitrogen gas containing various percentages of oxygen. As expected, E_{CORR} decreases as the oxygen content of the purge gas decreases, and falls below the threshold for oxidative dissolution as the O_2 content approaches zero, i.e., in a solution purged with pure N_2 gas. Using our electrochemical extrapolation we have determined the corresponding dissolution rates, as shown in Figure 9.

The line drawn through the points represents a first-order relationship. At these high concentrations, the dissolution rate is first order with respect to oxygen concentration, in agreement with the results of Grandstaff (1976), recorded with natural uraninite powders, and with the results of Thomas and Till (1984) recorded with CANDU* fuel pellets similar to those used to construct our electrodes.

In electrochemical experiments we have observed a first-order dependence on concentration for O_2 reduction (Reaction (8)) on UO_2 electrodes prepared

---

* CANada Deuterium Uranium, registered trademark of AECL.

from a standard CANDU fuel pellet (Hocking et al. 1991). Consequently, the first-order dependence for the overall corrosion process in oxygenated solutions (i.e., UO_2 dissolution coupled to O_2 reduction), Figure 9, indicates that oxygen reduction is the rate-controlling step. However, it should be noted that a reaction order of ~0.5 was obtained on a non-standard specimen of UO_2 (Hocking et al. 1991), and Gray has claimed a reaction order, with respect to oxygen concentration, lower than 1.0 for used-fuel dissolution (Gray and Wilson 1990).

In aerated solutions (points marked A in Figure 9), our dissolution rates compare well with the values measured by Thomas and Till (1984) and by Johnson (1982), the latter recorded on irradiated fuel in aerated granite groundwater (Shoesmith et al. 1989). More recent fuel-leaching experiments by Stroes-Gascoyne (unpublished data) also appear to give similar values, although confirmation of this awaits a more rigorous analysis of the fuel-leaching data.

For lower O_2 concentrations, the scatter in the data increases as the oxidative dissolution threshold is approached. The five data points in the hatched area at the bottom of Figure 9 correspond to E_{CORR} values well below our threshold value of -100 mV. A concentration of 10^{-8} mol·L^{-1} represents our best estimate of the residual O_2 concentration in solutions purged with nitrogen (Sunder et al. 1987). Little meaning can be attached to such low rates, since the oxidative dissolution model becomes tenuous for such low O_2 concentrations. At potentials below -100 mV, dissolution is more likely to be either oxidative but chemically controlled (Figure 3(b)), or chemical and not involving oxidation (Figure 3(c)). In other words, as the concentration of oxidants in solution falls, oxidative dissolution should be replaced by chemical dissolution, the rate of which is independent of redox conditions. This situation is depicted schematically in Figure 10 in terms of the redox potential of the solution.

A number of attempts have been made, in particular by Bruno et al. (1988, 1991), to measure the chemical dissolution rate of UO_2 in the absence of oxidants. Such measurements are fraught with problems arising from both the difficulty in maintaining genuinely non-oxidizing conditions and the unavoidable presence of oxidized surface films at the beginning of the experiment. Using a continuous flow-through reactor and maintaining reducing conditions by purging the solutions with hydrogen in the presence of a Pd catalyst, they observed a dissolution rate of $(3.9 \pm 1.6) \times 10^{-3}$ $\mu g \cdot cm^{-2} \cdot d^{-1}$ in the pH range from 7 to 11 (Bruno et al. 1991). This range of values is shown as a horizontal bar (marked B) in

Figure 9. If we reverse our calculation and estimate the E_{CORR} value required to sustain such a corrosion rate, we obtain values ranging from ~15 to ~40 mV. These values of E_{CORR} represent definite oxidizing conditions and suggest little difference between dissolution rates under oxidizing and non-oxidizing conditions. Such a small difference is inconsistent with the results of Gray and Wilson (1990), who observed a decrease in dissolution rate by a factor of 10^2 to 10^3 on switching from aerated to argon-purged conditions. Their experiments were also performed in a flow-through system.

It is possible that the UO_2 used by Bruno et al. was highly surface-defective and non-stoichiometric. The stoichiometry of $UO_{2.001}$, claimed on the basis of X-ray powder diffraction measurements, may be optimistic unless special measures were taken (Klug and Alexander 1974). A more realistic claim might be UO_{2+x} with $x \leq 0.005$. Our preliminary work on the impact of solid-state properties on the reactivity of UO_2 suggests that the degree of non-stoichiometry may exert a significant influence (Hocking et al. 1991).

In an attempt to establish a chemical dissolution rate for UO_2, we have reviewed the dissolution of metal oxides (see Appendix E). On the basis of this review, we have chosen a value of ~2 x 10^{-4} $\mu g \cdot cm^{-2} \cdot d^{-1}$ for the dissolution rate of UO_2, assuming its kinetic behaviour is similar to that of NiO. This dissolution rate value is shown as a horizontal line (marked C) in Figure 9 and corresponds to an anticipated E_{CORR} of -50 mV. A dissolution rate corresponding to an E_{CORR} value of -50 mV can be considered high. At such a potential our experimental evidence indicates that the surface composition is close to $UO_{2.33}$ (Appendices A and B), making the overall dissolution process definitely oxidizing.

Caution must be exercised in trying to interpret the significance of this chemical dissolution rate value. The E_{CORR} value is tantalizingly close to our electrochemically determined threshold of -100 mV, and could be considered as a measure of surface redox condition below which chemically controlled dissolution via Reactions (3) and (4) dominates over oxidative dissolution via Reactions (1) and (2). A fuller discussion of the significance of this rate value is given in Appendix E. Despite the uncertainties surrounding its derivation and interpretation, in subsequent discussions we have used this rate as a threshold value for the onset of oxidative dissolution.

5. UO_2 DISSOLUTION IN HYDROGEN PEROXIDE SOLUTIONS

We have measured the E_{CORR} of UO_2 as a function of time for various concentrations of H_2O_2 over the range $10^{-5} \leq [H_2O_2] \leq 2 \times 10^{-1}$ mol·L^{-1}. Even at the lowest concentrations, E_{CORR} rapidly rises to a steady-state value, demonstrating that the oxidation reaction, Reaction (1) ($UO_2 \longrightarrow UO_{2.33}$), is up to two orders of magnitude faster in H_2O_2 solutions than in O_2 solutions of comparable concentration (Shoesmith et al. 1985). That the oxidation process is the same in the presence of both oxidants is demonstrated by our XPS and cathodic stripping voltammetry (CSV) experiments (Shoesmith et al. 1985, in preparation), which show that the composition and thickness of the surface films present at steady state are the same.

The steady-state dissolution rates obtained by extrapolation of electrochemical data are plotted as a function of H_2O_2 concentration in Figure 11. The values are similar to those obtained in oxygenated solutions of comparable concentration shown in Figure 9. Despite our observation that the oxidation reaction, Reaction (1) ($UO_2 \longrightarrow UO_{2.33}$), is much faster in H_2O_2, the subsequent dissolution step, Reaction (2) ($UO_{2.33} \longrightarrow UO_2^{2+}$), is not.

Three distinct regions of behaviour are apparent in Figure 11:

(1) for $[H_2O_2] > 5 \times 10^{-3}$ mol·L^{-1}, the dissolution rate increases with peroxide concentration with approximately first-order dependence;

(2) for $2 \times 10^{-4} < [H_2O_2] < 5 \times 10^{-3}$ mol·L^{-1}, the dissolution rate is independent of peroxide concentration; and

(3) for $[H_2O_2] < 2 \times 10^{-4}$ mol·L^{-1}, the dissolution rate falls rapidly as the threshold for oxidative dissolution is approached.

We have proposed that, in the intermediate concentration range, peroxide decomposition to oxygen and water competes with the oxidative dissolution reaction (Shoesmith et al. 1985, Sunder et al. 1987). Christensen et al. (1990b) have observed peroxide decomposition on UO_2 in borax buffer solutions (pH ~ 8 ± 0.2): over a 6-d exposure period about half of the H_2O_2 in a 5×10^{-2} mol·L^{-1} solution was decomposed in the presence of UO_2. A more detailed discussion of our evidence for peroxide decomposition is given in Appendix F.

Christensen et al. (1990b) also measured dissolution rates in similar experiments by chemically analyzing the amount of dissolved uranium. In solutions containing 5×10^{-2} mol·L^{-1}, they obtained a rate of 5 ± 3 μg·cm^{-2}·d^{-1}. This rate is shown as a vertical bar in Figure 11, and is somewhat higher than our predicted rates. Since the effect of H_2O_2 on dissolution is very dependent on pH (see Appendix F), this discrepancy between prediction (for pH = 9.5) and measurement (at pH ~ 8.0 ± 0.2) can be attributed to the difference in pH.

6. IMPACT OF GAMMA RADIOLYSIS ON UO_2 DISSOLUTION

We have studied extensively the oxidation and dissolution of UO_2 in solutions subjected to gamma irradiation, and many of our results have been, or are about to be, published (Sunder et al. 1989, 1990a). In experiments in which we measure E_{CORR} as a function of time, the behaviour observed parallels that in solutions containing oxygen or hydrogen peroxide. The rate of the oxidation reaction ($UO_2 \longrightarrow UO_{2.33}$), as measured by the time taken for E_{CORR} to achieve a value of -100 mV, is rapid and dependent on both the gamma dose rate and the nature of the oxidizing radical (Sunder et al. 1990a). Some of our experimental results are discussed in more detail in Appendix B.

Figure 12 shows the predicted dissolution rates as a function of the square root of dose rate for argon-purged solutions. The square root of dose rate was used because it is approximately proportional to the concentration of radiolysis products. The dashed lines in Figure 12 serve only to outline the general trends. The solid line at high dose rates represents a first-order dependence and appears to be a reasonable fit for the points, although the available data is too sparse to be certain. At lower dose rates, the dissolution rates fall rapidly, especially below the threshold value for the transition from oxidative to chemical dissolution. At these low dose rates, the slope suggests a meaninglessly large reaction order with respect to radiolysis product, and can be taken as an indication that an extrapolation based on an oxidative dissolution model is no longer valid.

Electron transfer from the electrode to radical species, such as $OH^{\cdot}$ or O_2^{-}, will almost certainly be fast: certainly, our electrochemical results suggest such a process is fast for H_2O_2 (Shakerinia et al., in preparation). If this is the case, for a constant dose rate, any radical species reaching the surface will be rapidly reduced, its surface concentration

will be close to zero, and dissolution will be controlled by transport of oxidants to the surface. If we assume that the transport layer thickness is independent of dose rate, then we would expect the first-order dependence observed in Figure 12.

Figure 13 compares our predicted dissolution rates in irradiated aerated solutions with the dissolution rates measured under aerated conditions by Gromov (1981) at much higher dose rates. For rates measured in both acidic (pH ~ 1) and alkaline carbonate solutions (pH ~ 10), the dependence of dissolution rate on dose rate is close to what we predict in non-complexing solution at pH ~ 9.5. Not surprisingly, Gromov's values in acidic solutions are higher than our predictions. For comparison, the dashed lines 1 and 2 indicate our dissolution rates measured in unirradiated aerated solutions at pH = 9.5 (from Figure 9) and at pH = 2.5 (Sunder et al. 1991), Gromov's data in carbonate solutions are surprisingly low and inconsistent with our predictions. Also shown in Figure 13 is a rate measured by Christensen et al. (1990b) at a dose rate of 70 000 to 80 000 rad.* This rate is larger than ours, consistent with the fact that it was measured in oxygenated, as opposed to aerated, solutions, and at slightly lower pH.

Using the rates in Figure 12, we can assess the impact of gamma radiolysis on the dissolution of fuel under waste vault conditions. Figure 14 shows the dissolution rates from Figure 12 as a function of the logarithm of the dose rate. A logarithmic scale has no significance except to allow us to expand our analysis over orders of magnitude change in dose rate. Also plotted along the x-axis are the times at which such doses would be achieved at the surface of a CANDU fuel bundle after being discharged from the reactor. This correlation between time and dose rate was taken from calculations of G.B. Wilkin (unpublished data) for the decay of the gamma dose rate at the surface of a Bruce 'A' CANDU fuel bundle with a burnup of 685 GJ/kg U (see Figure 15). The dashed lines in Figure 14 are envelopes for the data and possess no fitting significance. From this plot we predict that the oxidative dissolution rate due to gamma radiolysis would fall below the threshold for oxidative dissolution after, at most, ~200 a. This is not surprising given the shape of the dose-rate curve in Figure 15.

Also shown in Figure 14 are the predicted dissolution rates in irradiated aerated solutions. These rates are substantially higher than, and do not decay as rapidly as, those in argon-purged solutions, because of the much higher concentrations of radicals and H_2O_2 produced by the radiolysis of

---

* 1 rad = 10 mGy

aerated solutions. The dissolution rate expected in unirradiated aerated solutions is also shown in the figure (marked A). Figure 14 shows that the impact of gamma radiolysis in aerated solution could be sustained for up to ~1000 a. Obviously, container failure while vault redox conditions remain oxidizing should be avoided.

It is clear from these results that predicted titanium container lifetimes of >1000 a under Canadian waste vault conditions (Shoesmith et al. 1991) are sufficient to guarantee that the impact of gamma radiolysis on fuel dissolution will be negligible, provided non-oxidizing conditions are established in the meantime.

We have also attempted to assess the impact of beta radiation on oxidative dissolution, since, for fuel from Swedish pressurized-water reactors (PWRs), the dose rate to a water layer in direct contact with nuclear fuel (after a cooling period of 40 a) will be caused mainly by alpha and beta radiation. Detailed calculations of beta dose rates have been performed for PWR fuel with a burnup of 45 MW·d/kg U by Ingemansson and Elkert (1991), assuming all the beta energy is deposited in a layer of water <200 μm in thickness. Such a situation could arise at cracks within the fuel or within the fuel-cladding gap. Assuming the nature and concentration of oxidizing radiolysis species produced by beta radiation are the same as those produced by gamma radiation, we can estimate that oxidative dissolution due to beta radiolysis could be important for 300 to 500 a (see Figure 16). Beyond this period, the rate of oxidative dissolution should become negligible in comparison with that of chemical dissolution.

7. IMPACT OF ALPHA RADIOLYSIS ON UO_2 DISSOLUTION

Of all the forms of radiation likely to produce oxidative dissolution, alpha radiation is the most insidious. The range for alpha particles in water is short. For instance, Garisto (1989) has calculated that >90% of the available alpha-particle energy in CANDU fuel is deposited within a 20-μm layer of water at the fuel surface. Consequently, alpha radiolysis leading to oxidative dissolution in wet cracks within the fuel, or at waterlogged sites within the cladding gap, is likely to be important. Since alpha activity within used fuel decays slowly in comparison with gamma (Figure 15) and beta activity (Figure 17), there is a possibility that oxidative dissolution will be sustained by alpha radiolysis for a long time.

Experimentally, we have measured corrosion potentials in a thin-layer electrochemical cell that allows us to bring an alpha source of known strength within ~25 μm of a UO_2 electrode (Bailey et al. 1985). Using steady-state E_{CORR} values measured for alpha sources of various strengths, we have obtained values for the dissolution rate as a function of alpha source strength in argon-purged solution (Figure 18). Because of the variability in measured values of E_{CORR}, our predicted dissolution rates, at a given source strength, vary by two orders of magnitude and are represented in Figure 18 by bars. A significant portion of this variability appears to arise from problems with our measurement of E_{CORR}. We are repeating these measurements, and our latest data suggest that the lower end of the dissolution rate range may be the more accurate.

Our mechanistic understanding of the impact of alpha radiolysis on UO_2 oxidation and dissolution is incomplete, although we have some evidence to suggest that there is a close similarity between UO_2 oxidation and dissolution in the presence of alpha radiolysis products and in chemically added H_2O_2. This would be consistent with the general understanding of alpha radiolysis, which shows that the production of molecular species, such as H_2O_2 and O_2, is more important than that of radicals (Burns and Sims 1981).

If we are to compare rates arising from alpha radiolysis with rates in H_2O_2 solutions, then it is necessary to calculate the concentration of hydrogen peroxide produced by alpha radiolysis within the thin layer of water between the UO_2 electrode and the alpha source in our cell. This is not straightforward, because the radiolytic production of oxidants will be accompanied by their loss by transport at the edges of the circular disc of water between the alpha source and UO_2 electrode. This situation is illustrated schematically in Figure 19.

In order to compare the results of our experiments using alpha sources with those obtained using H_2O_2, we have used the calculations by Christensen (1990) to calculate H_2O_2 concentrations during alpha radiolysis. In these calculations the G values for alpha radiolysis were taken from the reviews of Christensen and Bjergbakke (1982) and Christensen (1990), and it was assumed that the energy was absorbed in a 30-μm layer of water. Diffusion terms for H_2, O_2 and H_2O_2 were introduced, their relative values being chosen in relation to their diffusion coefficients (Eriksen et al. 1989).

Figure 20 shows the predicted rates in the presence of alpha radiolysis and in H_2O_2. Agreement is reasonable, provided the lower values in the presence of alpha radiolysis are accepted as the more accurate.

Christensen (1990) has also used this model to predict the dissolution rate of UO_2 as a function of alpha source strength. Agreement between calculated and experimentally predicted dissolution rates is reasonable for the highest source strength used (686 μCi*) (within a factor of four), but for the lowest source strength the discrepancy is greater than two orders of magnitude. The source of this increasing discrepancy with decreasing source strength is not totally clear. The most likely explanation appears to be the decreasing importance of oxidative dissolution as E_{CORR} decreases below the oxidative dissolution threshold, accompanied by the increasing importance of the peroxide decomposition process. The change in relative importance of these two processes, as the concentration of H_2O_2 and hence the composition of the UO_2 surface changes, is discussed in some detail in Appendix F. In its present form, the model used by Christensen does not account for such changes in mechanism. Obviously, a more extensive experimental program and a more rigorous modelling procedure is required before a complete understanding of the behaviour of UO_2 in the presence of alpha radiolysis will be achieved.

We can use the predicted dissolution rates in Figure 18 to assess the impact of alpha radiolysis on the dissolution of fuel under waste vault conditions, as we did for gamma radiolysis in Section 6. Figure 21 shows the dissolution rates as a function of alpha source strength. The use of a logarithmic scale for source strength is for convenience only. Since our measurements were made in a 25-μm gap, these rates are equivalent to those predicted by assuming that all the alpha energy is deposited in a 25-μm layer of water on the surface of the fuel. The second axis in Figure 21 relates the source strength used in our experiments to the alpha plus beta activity-time profile in the fuel. The manner in which this relationship was established is described in Appendix G. According to this scale, oxidative dissolution supported by the alpha plus beta radiolysis of water could be important for a period of time somewhere between 500 and 10 000 a for CANDU fuel with a burnup of 685 GJ/kg U. A similar plot is shown relating our dissolution rates to the alpha activity levels in PWR fuel in Figure 22. This relationship is based on the calculations of Ingemansson and Elkert (1991) for fuel with a burnup of 45 MW·d/kg U. Since their calculations were made assuming all alpha energy is deposited within a 50-μm layer, a direct comparison with our results (measured with a 25-μm cell gap) is reasonable. Oxidative dissolution supported by alpha radiolysis for PWR fuel appears possible for a period somewhere between 500 and 30 000 a.

---

* 1 Ci = 37 GBq

These estimates of the impact of alpha radiolysis can only be considered preliminary. They are sufficiently meaningful to demonstrate that the importance of oxidative dissolution will decrease with time. However, the period over which this process will remain significant is uncertain because of the poor quality of the E_{CORR} values obtained so far. Our suspicion, based on a new series of experiments just under way, is that the lower dissolution rates are the most appropriate. If so, then the impact of alpha radiolysis will be small and not as prolonged as suggested by Figures 21 and 22.

The data presented apply only to a single pH of 9.5, a value at which oxidative dissolution appears to be in competition with H_2O_2 decomposition. Although we have yet to demonstrate the fact unequivocally, it seems likely that the behaviour of UO_2 in the presence of alpha radiolysis will be similar to its behaviour in H_2O_2. If so, then the effect of pH on the corrosion potential, and hence on the dissolution rate in the presence of alpha radiolysis, is likely to be large. The E_{CORR} for UO_2 exposed to H_2O_2 shifts to much more positive potentials as the pH decreases (see Figure F-5 in Appendix F). A similar effect in the presence of alpha radiolysis would increase the dissolution rate by about two orders of magnitude for a drop in pH from 9.5 to 7.0. This assumes that the current-potential profile upon which our extrapolation is based (Figure D-1 in Appendix D) does not change significantly with pH. Nicol and Needes (1975) have presented some evidence showing that this profile is indeed independent of pH over the range $6 \leq pH \leq 9$.

Caution should be exercised in the use of such simple estimates, since many factors, not considered in this report and not addressed within our resarch programs to date, may affect the pH. For instance, the impact of pH on E_{CORR} was determined for an H_2O_2 concentration of 10^{-3} mol·L^{-1}, a concentration achievable only for large alpha source strengths (Figure 20), i.e., greater than those anticipated in used fuel. It is unclear whether the impact of pH will be as large at lower H_2O_2 concentrations equivalent to lower source strengths. Also, while water contacting the fuel may be buffered to around pH ~ 8.5 by the bentonite buffer, the pH within cracks in the fuel, where alpha radiolysis is most prevalent, may be different. Our present experimental program is designed to address many of these questions.

8. SUMMARY

Although more experimental data are needed, it is clear that the development of an electrochemistry-based dissolution model is feasible. At present, this development is only partially complete, and mathematical expressions describing the kinetics of the anodic dissolution of UO_2 and the kinetics of reduction of oxidants, such as oxygen and hydrogen peroxide, on UO_{2+x} surfaces remain to be specified. However, predictions of the dissolution rate of UO_2 have been obtained by extrapolating steady-state electrochemical currents for the anodic dissolution of UO_2 to the corrosion potentials measured in solutions containing various concentrations of different oxidants, such as oxygen, hydrogen peroxide and the products of the gamma and alpha radiolysis of water.

As the concentration of oxidant decreases, the rate of oxidative dissolution should eventually fall to a value less than the chemical dissolution rate of UO_2. We have estimated a value for this rate from the dissolution rate of NiO measured in acidic solutions. Once the predicted oxidative dissolution rate falls below this value, we assume that dissolution will be basically chemical in nature and independent of the solution redox conditions. This threshold dissolution rate is estimated to be 2×10^{-4} $\mu g \cdot cm^{-2} \cdot d^{-1}$.

Using this approach, we have tried to define the nature and kinetics of the dissolution process in a number of oxidants.

(1) In the presence of oxygen, the dissolution rate is first order with respect to oxygen concentration, and oxidative dissolution, as defined in Figure 3(a), becomes negligible once the dissolved oxygen concentration falls below $\sim 10^{-6}$ $mol \cdot L^{-1}$.

(2) In hydrogen peroxide solutions, three distinct regions of behaviour are apparent:

(a) For $[H_2O_2] \geq 5 \times 10^{-3}$ $mol \cdot L^{-1}$, the dissolution rate increases with hydrogen peroxide concentration with an approximately first-order dependence.

(b) For $2 \times 10^{-4} \leq [H_2O_2] < 5 \times 10^{-3}$ $mol \cdot L^{-1}$, the dissolution rate is independent of peroxide concentration. In this concentration range oxidative dissolution occurs simultaneously with peroxide decomposition to oxygen and water. Peroxide

decomposition appears to predominate on surfaces of composition UO_{2+x}, where $x \leq 0.33$. On more oxidized surfaces, decomposition appears to be blocked and oxidative dissolution appears to predominate.

(c) For $[H_2O_2] < 2 \times 10^{-4}$ mol·L^{-1}, the dissolution rate falls rapidly as the threshold for oxidative dissolution is approached. The behaviour in H_2O_2 solutions is complicated by a strong pH-dependence, dissolution being promoted as the pH decreases.

(3) In the presence of gamma radiation, oxidative dissolution is rapid because of the fast reaction of UO_2 with radiolytically produced radicals, such as OH and O_2^-. For dose rates of $\geq 1.6 \times 10^3$ rad·h^{-1} (≥ 16 Gy·h^{-1}), the dissolution rate appears to be first order with respect to the concentration of radiolysis products. For dose rates < 6 to 10 Gy·h^{-1}, the oxidative dissolution rate falls below the threshold value. For used CANDU fuel this means that oxidative dissolution of UO_2 due to gamma radiolysis is only important for ~200 a.

(4) In the presence of alpha radiolysis, the dissolution process appears to be similar to that observed in H_2O_2 solutions. Unfortunately, our measured corrosion potentials are not sufficiently accurate to allow us to specify with any certainty the period for which oxidative dissolution will be important. At present, our best estimate of this period for CANDU fuel (burnup 685 GJ/kg U) is between 500 and 10 000 a. For PWR fuel (burnup 45 MW·d/kg U) this period is ~500 to <30 000 a.

Before the development of this model can be considered complete, a number of major improvements are required:

(1) A more complete study of the cathodic reduction of oxidants is necessary in order to specify a mathematical expression for this reaction.

(2) Although a good general mechanistic understanding of the anodic dissolution of UO_2 is available, our present extrapolation relies on only six data points. A more extensive database is required if the reliability of our extrapolation is to be quantified.

(3) So far, all our measurements have been performed on unirradiated specimens cut from CANDU fuel pellets. Since we expect the reactivity of UO_2 to vary after in-reactor irradiation, we need to make a much more extensive series of measurements on electrodes with different properties (i.e., conductivities, conductivity types (p- or n-type), grain size, densities, etc.). The impact of many of these parameters on the dissolution process are amenable to study by electrochemical methods, and we are in the process of studying the electrochemistry of a number of SIMFUEL (unirradiated UO_2 containing stable fission products simulating a 6% fuel burnup) specimens.

(4) In H_2O_2 solutions the dissolution behaviour of UO_2 is complicated by the simultaneous occurrence of H_2O_2 decomposition. Our present mechanistic understanding of this latter process is poor, as is our understanding of the major impact of pH on oxidative dissolution in hydrogen peroxide solutions.

(5) The oxidative dissolution of UO_2 in the presence of gamma irradiation appears to be first order with respect to the concentration of oxidizing radiolysis products. This claim is based on only four data points.

(6) Our understanding of oxidative dissolution in the presence of alpha radiolysis is poor. A much more extensive experimental program coupled to a more rigorous modelling procedure is required if we are to use our electrochemistry-based model to predict the impact of alpha radiolysis on used-fuel dissolution.

(7) The effects of a number of other parameters on the oxidative dissolution of UO_2 in radiolytically decomposed solutions remain to be investigated. In particular, some understanding of the impact of temperature and the presence of scavengers is required. Our own unpublished electrochemical studies on the oxidation and dissolution of UO_2 at 55°C show that the increase in temperature (from 25°C) does not alter the threshold potential for oxidative dissolution. The expected increase in dissolution rate with temperature appears to be largely offset by a thickening of the surface layer of $UO_{2.33}$. Many species likely to be present in groundwater (e.g., Fe^{2+}/Fe^{3+} from mineral dissolution, hydrogen from container corrosion) are likely to scavenge radiolytically produced oxidants, especially at low dose rates. Thus, Sunder et

al. (1990b) have demonstrated that, in the presence of dissolved H_2, the extent of oxidation of UO_2 arising from alpha radiolysis is reduced. Such effects are likely to shorten the period for which oxidative dissolution can be sustained.

ACKNOWLEDGEMENTS

The preparation of this report was funded by SKB Stockholm.
We are grateful to W.H. Hocking and L.H. Johnson for reviewing the manuscript.

REFERENCES

Bailey, M.G., L.H. Johnson and D.W. Shoesmith. 1985. The effects of alpha-radiolysis of water on the corrosion of UO_2. Corrosion Science 25, 233-238. Also Atomic Energy of Canada Limited Reprint, AECL-8430.

Bruno, J., I. Casas and I. Puigdomènech. 1988. The kinetics of dissolution of UO_2 (s) under reducing conditions. Radiochimica Acta, 44/45, 11-16.

Bruno, J., I. Casas and I. Puigdomènech. 1991. The kinetics of dissolution of UO_2 under reducing conditions and the influence of an oxidized surface layer (UO_{2+x}): Application of a continuous flow-through reactor. Geochimica et Cosmochimica Acta 55, 647-658.

Burns, W.G. and H.E. Sims. 1981. Effect of radiation type in water radiolysis. Journal of the Chemical Society, Faraday Transactions 1 77, 2803-2813.

Christensen, H. 1990. Calculation of the effect of α-Radiolysis on UO_2 oxidation. Studsvik Report NS-90/72, Studsvik Energiteknik AB, Nykoping, Sweden.

Christensen, H. and E. Bjergbakke. 1982. Radiolysis of groundwater from spent fuel. Swedish Nuclear Fuel Supply Co. Report, SKBF/KBS-TR-82-18.

Christensen, H. and E. Bjergbakke. 1987a. Radiolysis of groundwater from spent fuel. Studsvik Report NS-87/161, Studsvik Energiteknik AB, Nykoping, Sweden.

Christensen, H. and E. Bjergbakke. 1987b. Radiation-induced dissolution of UO_2. In Materials Research Society Symposium Proceedings 84 (Scientific Basis for Nuclear Waste Management X), 115-122.

Christensen, H. and S. Sunder. 1989. Calculations of radiolysis in connection with UO_2 oxidation studies. Studsvik Report NS-89/117, Studsvik Energiteknik AB, Nykoping, Sweden.

Christensen, H., S. Sunder and D.W. Shoesmith. 1990a. Calculations of radiolysis in connection with UO_2 oxidation studies; adjustment of the final stage of oxidation. Studsvik Report NS-90/99, Studsvik Energiteknik AB, Nykoping, Sweden.

Christensen, H., R. Forsyth, R. Lundqvist and L.O. Werme. 1990b. Radiation induced dissolution of UO_2. Studsvik Report NS-90/85, Studsvik Energiteknik AB, Nykoping, Sweden.

Eriksen, T.E., P. Ndalamba, H. Christensen and E. Bjergbakke. 1989. Radiolysis of groundwater: Influence of carbonate and chloride on hydrogen peroxide production. Journal of Radioanalytical and Nuclear Chemistry 132 (1), 19-35.

Garisto, F. 1986. Solid dissolution: Effect of mass transport-precipitation coupling. Chemical Engineering Science 41, 3219-3222. Also Atomic Energy of Canada Limited Reprint, AECL-9032.

Garisto, F. 1989. The energy spectrum of α-particles emitted from used CANDU™ fuel. Annals of Nuclear Energy 16, 33-38. Also Atomic Energy of Canada Limited Reprint, AECL-9822.

Garisto, F. and N.C. Garisto. 1985. A UO_2 solubility function for the assessment of used nuclear fuel disposal. Nuclear Science and Engineering 90, 103-110. Also Atomic Energy of Canada Limited Reprint, AECL-8515.

Garisto, F. and N.C. Garisto. 1990. Source term models for the release of radionuclides from used nuclear fuel. Presented at the Technical Workshop on Near-Field Performance Assessment for High-Level Waste, Madrid, Spain, 1990.

Garisto, N.C. and F. Garisto. 1988. Mass transport-precipitation coupling in finite systems. Atomic Energy of Canada Limited Report, AECL-9562.

Garisto, N.C. and D.M. LeNeveu. 1989. The Vault Model for the disposal of used CANDU fuel: Documentation and analysis of scoping calculations. Atomic Energy of Canada Limited Report, AECL-9578.

Grandstaff, D.E. 1976. A kinetic study of the dissolution of uraninite. Economic Geology 71 (8), 1493-1506.

Gray, W. and C. Wilson. 1990. Effects of water composition and temperature variables on the dissolution rate of UO_2. Presented at the 1990 Spent Fuel Workshop, Gull Harbour, MB.

Gromov, V. 1981. Dissolution of uranium oxides in the gamma-radiation field. Radiation Physics and Chemistry 18 (1-2), 135-146.

Hocking, W.H., J.S. Betteridge and D.W. Shoesmith. 1991. The cathodic reduction of dioxygen on uranium oxide in dilute alkaline aqueous solution. Atomic Energy of Canada Limited Report, AECL-10402.

Hocking, W.H., J.S. Betteridge and D.W. Shoesmith. In preparation. Reactivity effects in the oxidative dissolution of UO_2 nuclear fuel. To be published in the Journal of Nuclear Materials.

Ingemansson, T. and J. Elkert. 1991. Model for calculation of absorbed alpha and beta radiation dose to water in contact with highly burnt up nuclear fuel. ABB Atom Report, RM-91-23, Asea Brown Boveri, Sweden.

Johnson, L.H. 1982. The dissolution of irradiated UO_2 fuel in groundwater. Atomic Energy of Canada Limited Report, AECL-6837.

Johnson, L.H. and D.W. Shoesmith. 1988. Spent fuel. In Radioactive Waste Forms for the Future (W. Lutze and R.C. Ewing, editors), Elsevier Publishers, 635-698. Also Atomic Energy of Canada Limited Reprint, AECL-9583.

Johnson, L.H., D.W. Shoesmith and S. Stroes-Gascoyne. 1988. Spent fuel: Characterization studies and dissolution behaviour under disposal conditions. In Materials Research Society Symposium Proceedings 112 (Scientific Basis for Nuclear Waste Management XI), 99-113. Also Atomic Energy of Canada Limited Reprint, AECL-9651.

Klug, H.P. and L.E. Alexander. 1974. X-ray Diffraction Procedures for Polycrystalline and Amorphous Materials. Second edition, John Wiley, New York, Chapter 8.

Lemire, R.J. and P.R. Tremaine. 1980. Uranium and plutonium equilibria in aqueous solutions to 200°C. Journal of Chemical Engineering Data 25, 361-370. Also Atomic Energy of Canada Limited Reprint, AECL-6655.

Lemire, R.J. and F. Garisto. 1989. The solubility of U, Np, Pu, Th and Tc in a geological disposal vault for used nuclear fuel. Atomic Energy of Canada Limited Report, AECL-10009.

Marsh, G.P. and K.J. Taylor. 1988. An assessment of carbon steel containers for radioactive waste disposal. Corrosion Science, 28 (3), 289-320.

Needes, C.R.S., M.J. Nicol and N.P. Finkelstein. 1975. Electrochemical model for the leaching of uranium dioxide: 2 - Alkaline carbonate media. In Leaching and Reduction in Hydrometallurgy (A.R. Burkin, editor), 12-19.

Nicol, M.J. and C.R.S. Needes. 1975. The anodic dissolution of uranium dioxide - 1. In perchlorate solutions. Electrochimica Acta 20, 585-589.

Nicol, M.J., C.R.S. Needes and N.P. Finkelstein. 1975. Electrochemical model for the leaching of uranium dioxide: 1 - Acid media. In Leaching and Reduction in Hydrometallurgy (A.R. Burkin, editor), 1-11.

Paquette, J. and R.J. Lemire. 1981. A description of the chemistry of aqueous solutions of uranium and plutonium at 200°C using potential-pH diagrams. Nuclear Science and Engineering 79, 26-48. Also Atomic Energy of Canada Limited Reprint, AECL-7037.

Segall, R.L., R. St.C. Smart and P.S. Turner. 1988. Oxide surfaces in solution. In Surface and Near-Surface Chemistry of Oxide Materials (J. Nowotny and L.-C. Dufour, editors), Elsevier Science Publishers, Amsterdam, Chapter 13, 527-576.

Shakerinia, S., W.H. Hocking, J.S. Betteridge and D.W. Shoesmith. In preparation. Cathodic reduction of hydrogen peroxide on uranium oxide.

Shoesmith, D.W., S. Sunder, L.H. Johnson and M.G. Bailey. 1985. Oxidation of CANDU UO_2 fuel by the alpha-radiolysis products of water. In Materials Research Society Symposium Proceedings 50 (Scientific Basis for Nuclear Waste Management IX), 309-316. Also Atomic Energy of Canada Limited Reprint, AECL-8888.

Shoesmith, D.W., S. Sunder, M.G. Bailey and G.J. Wallace. 1989. The corrosion of nuclear fuel (UO_2) in oxygenated solutions. Corrosion Science 29 (9), 1115-1128. Also Atomic Energy of Canada Limited Reprint, AECL-9887.

Shoesmith, D.W., B.M. Ikeda and D.M. LeNeveu. 1991. Lifetime predictions for titanium nuclear waste containers. Presented at the International Conference on Life Prediction of Corrodible Structures, Cambridge, U.K., 1991. Proceedings to be published by NACE, Houston, TX, U.S.A.

Shoesmith, D.W., S. Sunder, M.G. Bailey, G.J. Wallace and N.H. Miller. In preparation. Electrochemical and XPS studies of the corrosion of nuclear fuel (UO_2) in hydrogen peroxide solutions.

Smith, H.J., J.C. Tait and R.E. Von Massow. 1987. Radioactive decay properties of Bruce "A" CANDU UO_2 fuel and fuel recycle waste. Atomic Energy of Canada Limited Report, AECL-9072.

Sunder, S. and D.W. Shoesmith. 1991. Chemistry of UO_2 fuel dissolution in relation to the disposal of used nuclear fuel. Atomic Energy of Canada Limited Report, AECL-10395.

Sunder, S., D.W. Shoesmith, L.H. Johnson, G.J. Wallace, M.G. Bailey and A.P. Snaglewski. 1987. Oxidation of CANDU™ fuel by the products of alpha-radiolysis of groudwater. In Materials Research Society Symposium Proceedings 84 (Scientific Basis for Nuclear Waste Management X), 103-113. Also Atomic Energy of Canada Limited Reprint, AECL-9296.

Sunder, S., D.W. Shoesmith, H. Christensen, M.G. Bailey and N.H. Miller. 1989. Electrochemical and X-ray photoelectron spectroscopic studies of UO_2 fuel oxidation by specific radicals formed during radiolysis of groundwater. In Materials Research Society Symposium Proceedings 127 (Scientific Basis for Nuclear Waste Management XII), 317-324. Also Atomic Energy of Canada Limited Reprint, AECL-9597.

Sunder, S., D.W. Shoesmith, H. Christensen, N.H. Miller and M.G Bailey. 1990a. Oxidation of UO_2 fuel by radicals formed during radiolysis of water. In Materials Research Society Symposium Proceedings 176 (Scientific Basis for Nuclear Waste Management XIII), 457-464.

Sunder, S., G.D. Boyer and N.H. Miller. 1990b. XPS studies of UO_2 oxidation by alpha radiolysis of water at 100°C. Journal of Nuclear Materials 175, 163-169.

Sunder, S., D.W. Shoesmith, R.J. Lemire, M.G. Bailey and G.J. Wallace. 1991. The effect of pH on the corrosion of nuclear fuel (UO_2) in oxygenated solutions. Corrosion Science 32 (4), 373-386.

Thomas, G.F. and G. Till. 1984. The dissolution of unirradiated UO_2 fuel pellets under simulated disposal conditions. Nuclear and Chemical Waste Management 5, 141-147.

Werme, L., P. Sellin and R. Forsyth. 1990. Radiolytically induced oxidative dissolution of spent nuclear fuel. Swedish Nuclear Fuel and Waste Management Company Report, SKB-TR-90-08.

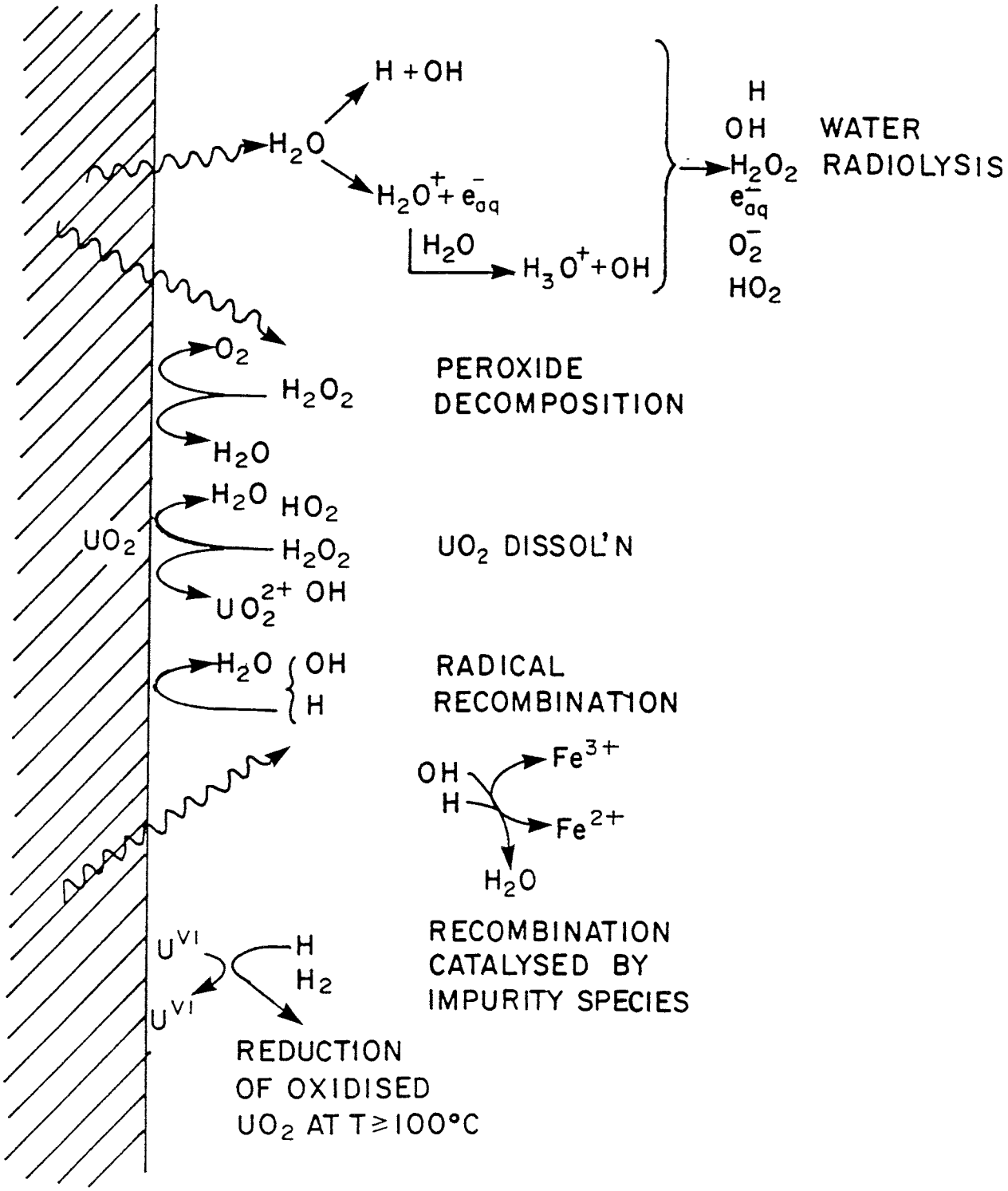

FIGURE 1: Possible Reactions on a UO_2 Surface in the Presence of Radiolytically Decomposed Water

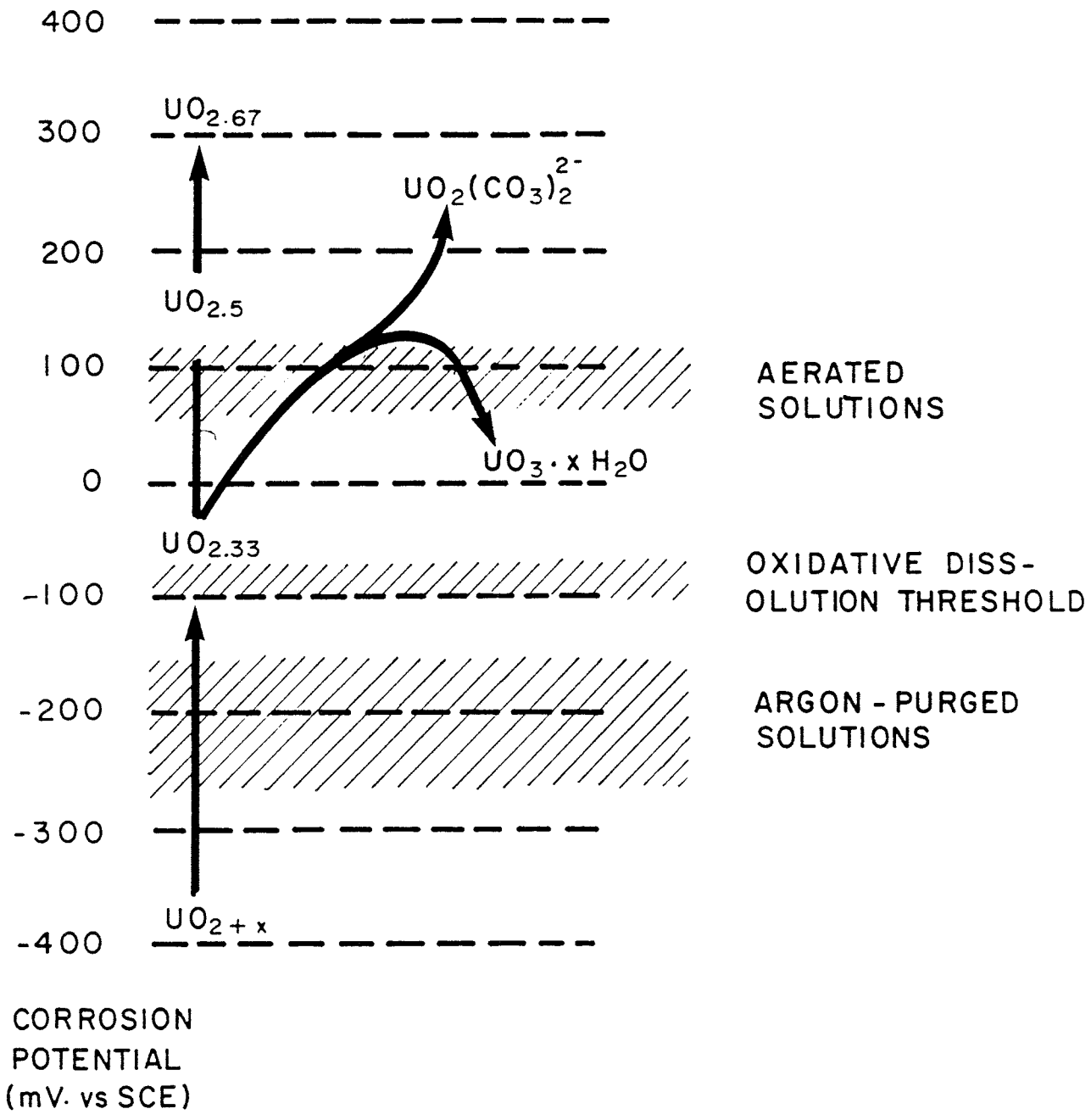

FIGURE 2: Surface Chemistry of UO_2 Oxidation/Dissolution as a Function of Surface Redox Conditions

A. OXIDATIVE DISSOLUTION

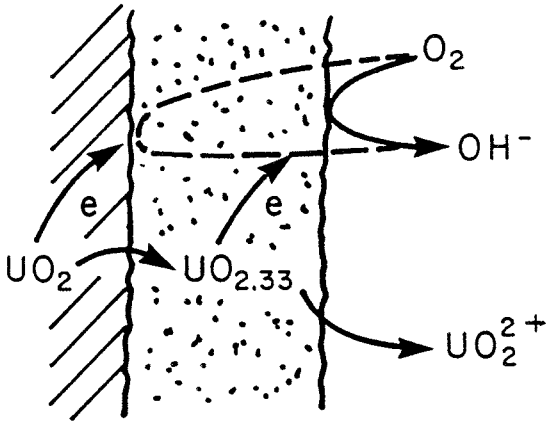

B. CHEMICALLY-CONTROLLED OXIDATIVE DISSOLUTION

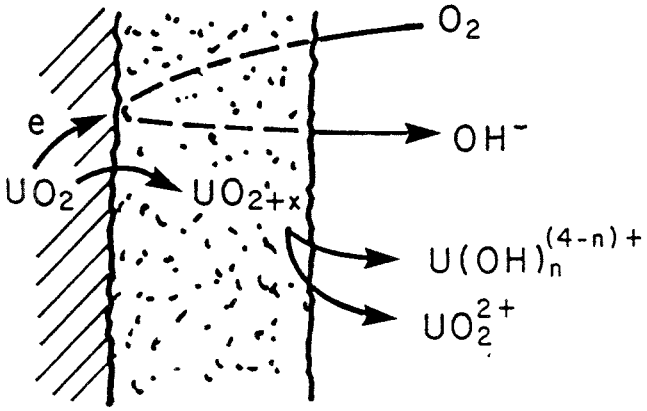

C. NON-OXIDATIVE CHEMICAL DISSOLUTION

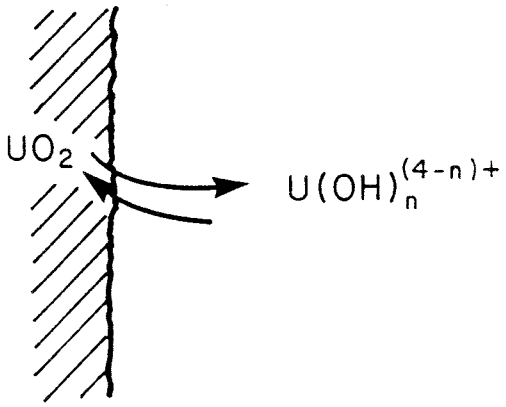

FIGURE 3: Possible Modes of Dissolution on UO_{2+x} Surfaces

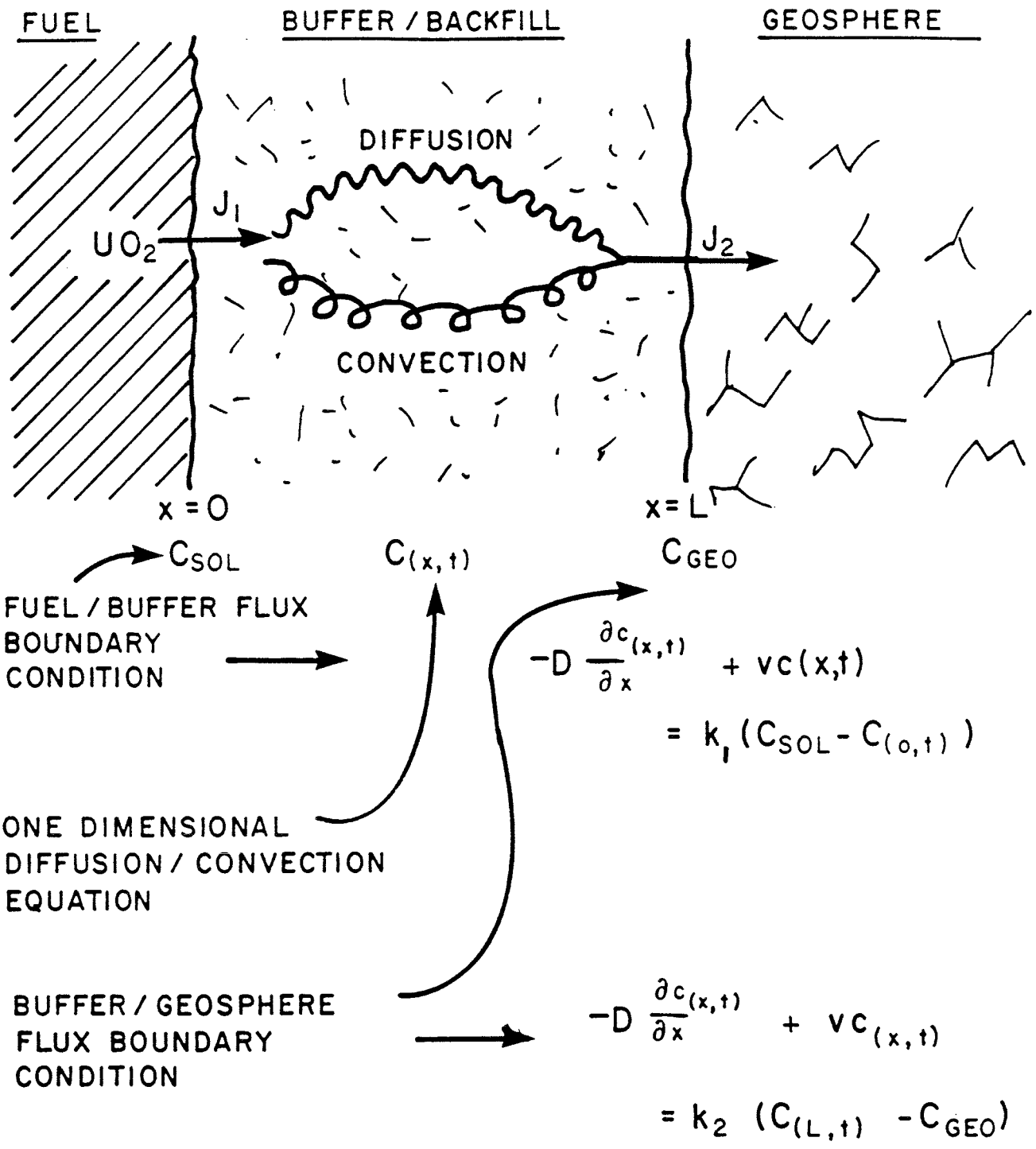

FIGURE 4: Schematic Illustration of the Form of the Solubility-Based Dissolution Model Used in the Canadian NFWMP. J_1 and J_2 are fluxes at the respective interfaces, c is the concentration of dissolved uranium, x is the distance from the fuel surface, D is the diffusion coefficient of dissolved uranium, v is the velocity of groundwater flow in the x direction; k_1 and k_2 are constants

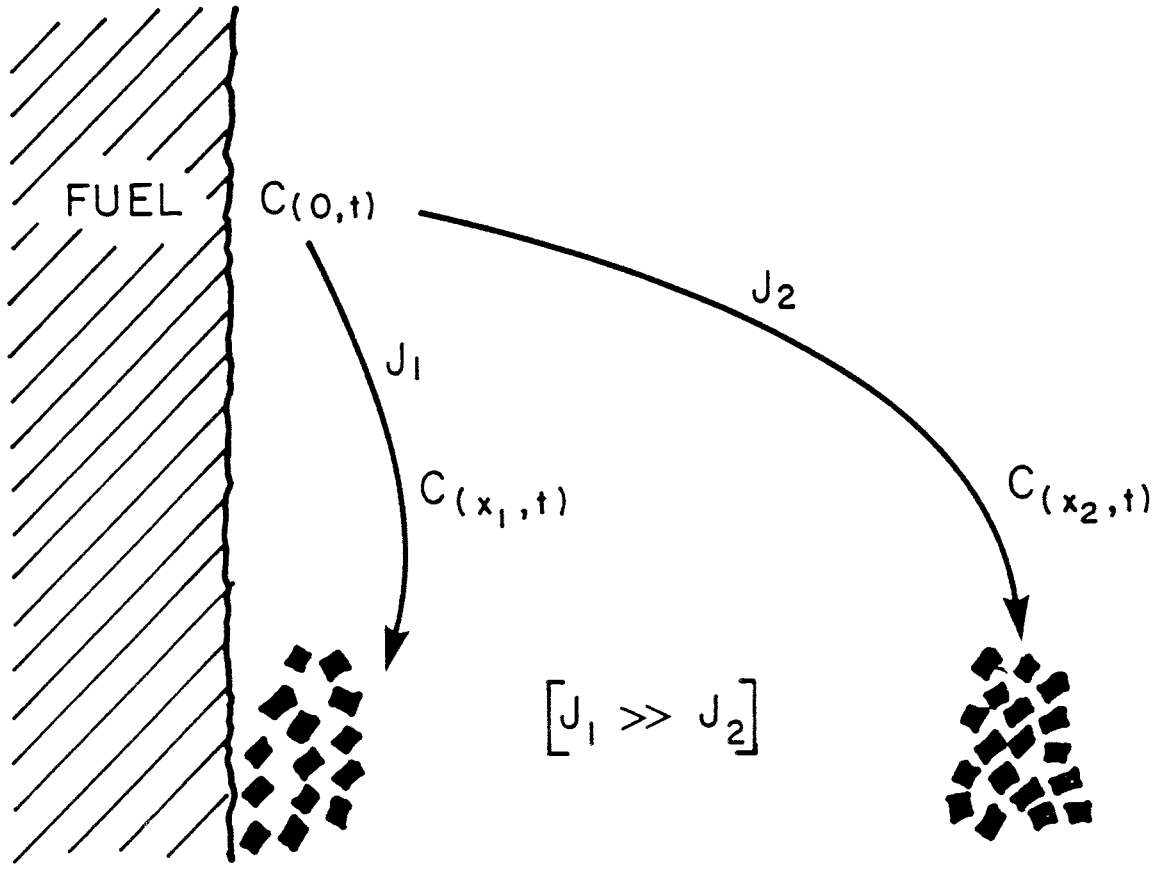

FIGURE 5: Schematic Illustration of the Implications of Coupling Precipitation Processes with a Mass Transport Model for Dissolution Involving a Reversible Interfacial Step. The symbols have the significance defined in Figure 4.

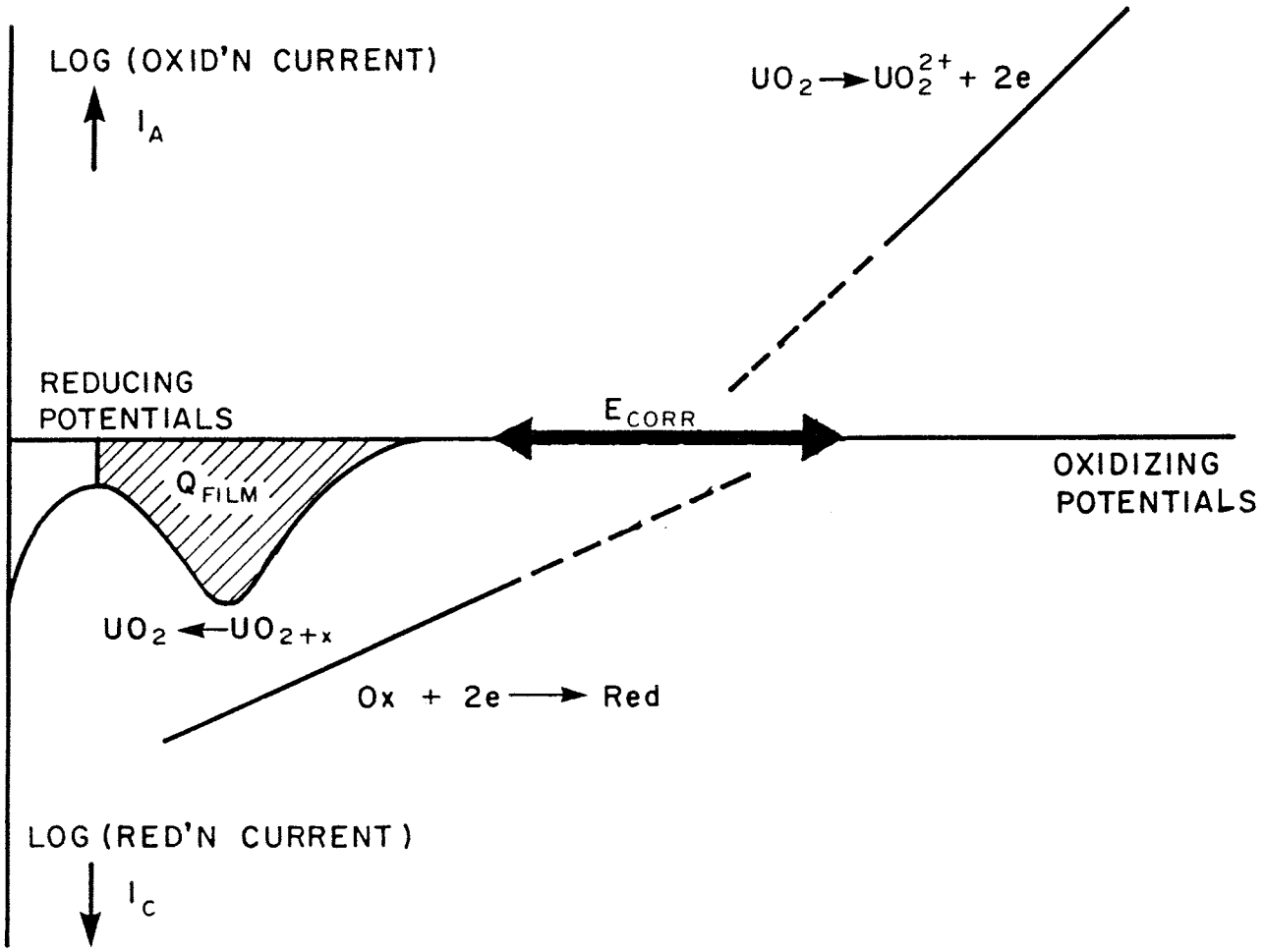

FIGURE 6: Schematic Illustration of the log Current vs. Applied Potential (Tafel) Relationships for the Anodic Dissolution of UO_2 and the Cathodic Reduction of Oxidant (Ox) on a UO_2 Surface. The dashed lines represent extrapolations of the measured relationships (full lines) to the corrosion potential (E_{CORR}) to obtain the corrosion current for that particular set of conditions. The arrow along the potential axis represents the range of E_{CORR} values measured in the presence of various oxidants. The line labelled $UO_{2+x} \longrightarrow UO_2$ represents the current for film reduction measured during a cathodic stripping voltammogram. Integration of the shaded area yields the charge, Q_{FILM}, for film reduction, which is a measure of film thickness.

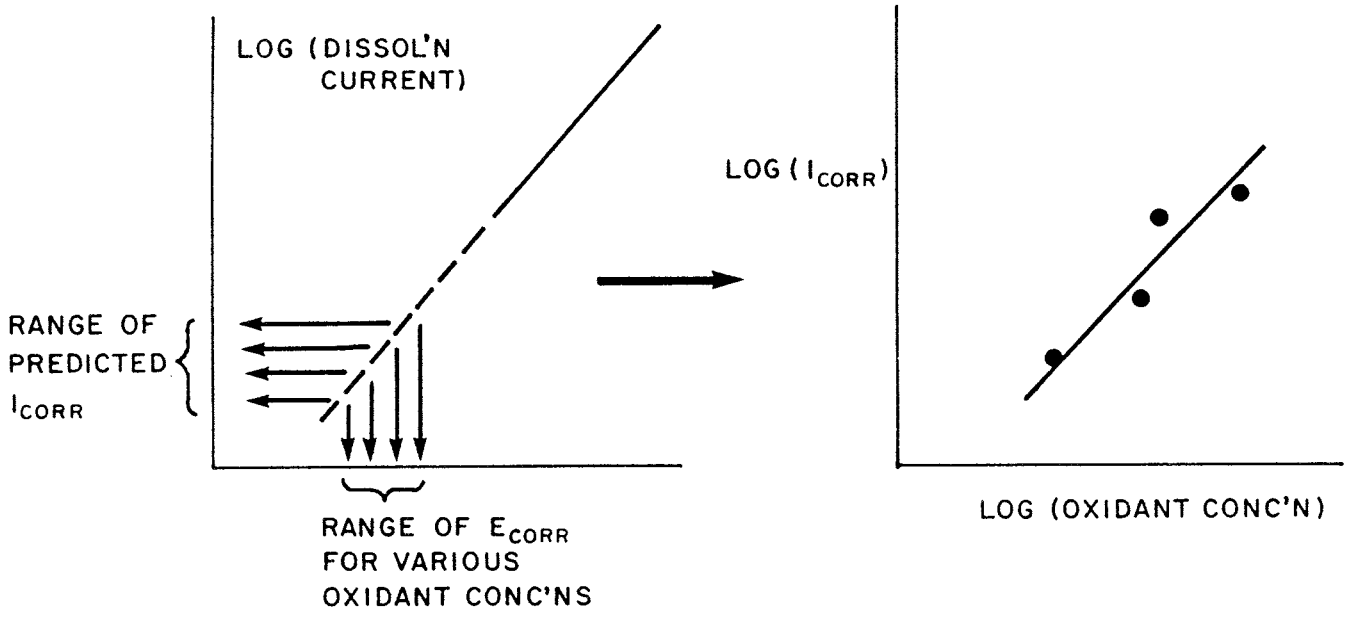

FIGURE 7: Illustration of the Procedure to Obtain Values of Corrosion Current (I_{CORR} ≡ Dissolution Rate) for the Oxidative Dissolution of UO_2 by Extrapolation of the Tafel Relationship to the Measured Corrosion Potential (E_{CORR})

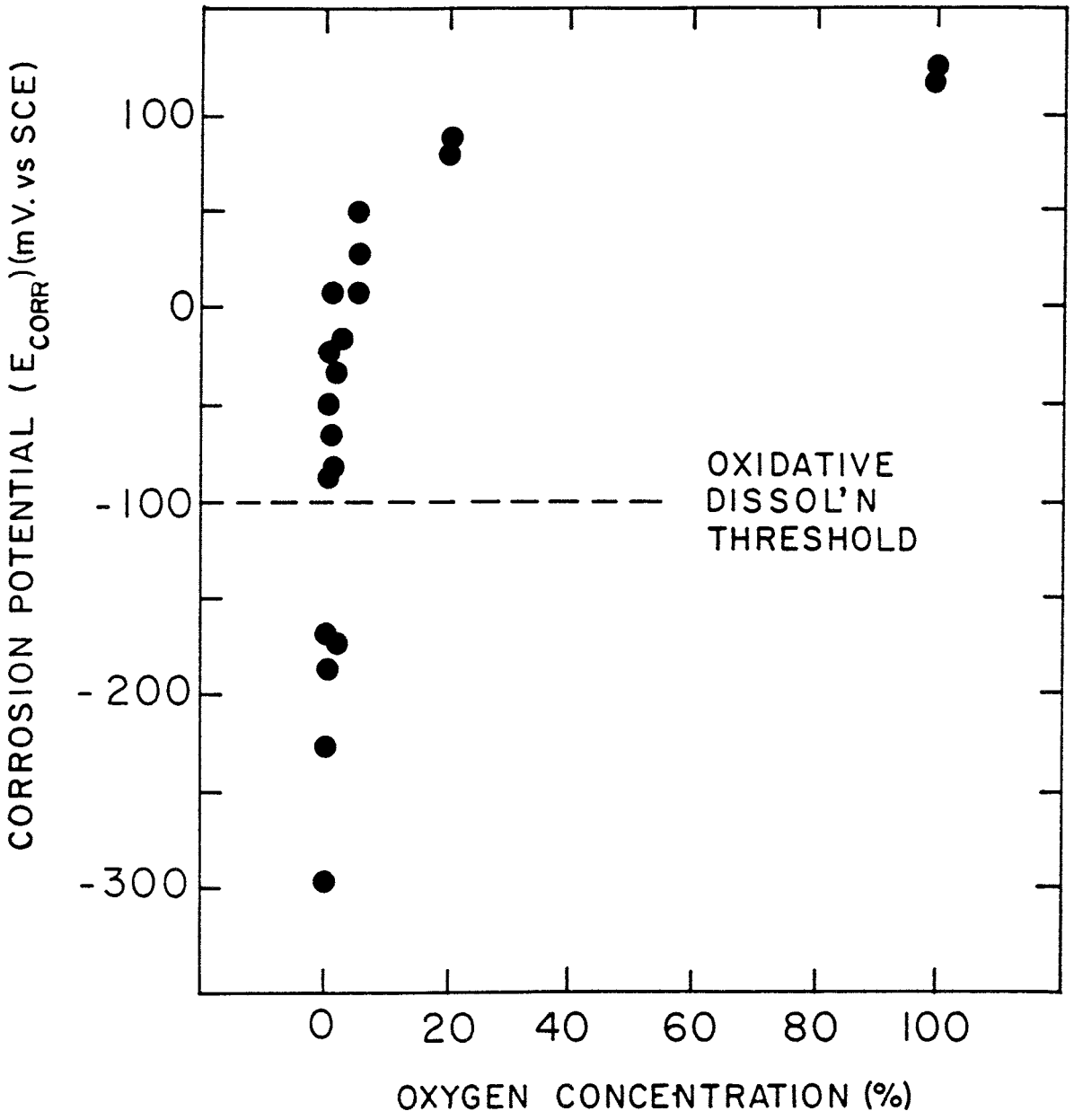

FIGURE 8: E_{CORR} Measurements on a UO_2 Electrode in 0.1 mol·L^{-1} $NaClO_4$ (pH = 9.5) Purged with Nitrogen Gas Containing Various Percentages of Oxygen. The level of the oxidative dissolution threshold is determined from the electrochemical and XPS experiments described in Appendix A.

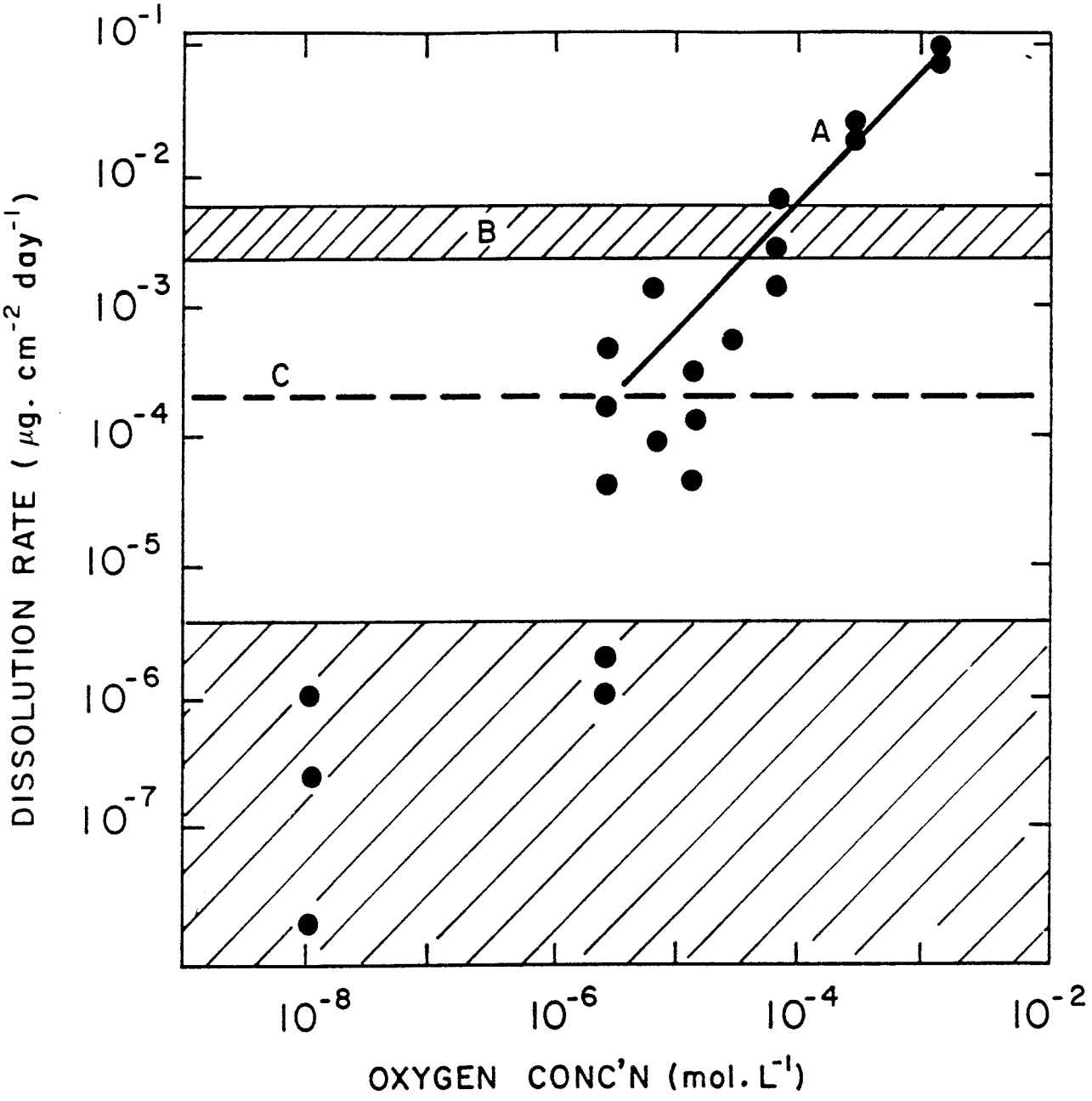

FIGURE 9: Dissolution Rates for UO_2 as a Function of Dissolved Oxygen Concentration in 0.1 mol·L^{-1} $NaClO_4$ (pH = 9.5). The data points marked A were obtained in aerated solutions. The shaded range of values, marked B, are taken from Bruno et al. (1991). The dashed line C represents our estimate for the chemical dissolution rate of UO_2, obtained by assuming the behaviour of UO_2 will be similar to that of NiO (Appendix E).

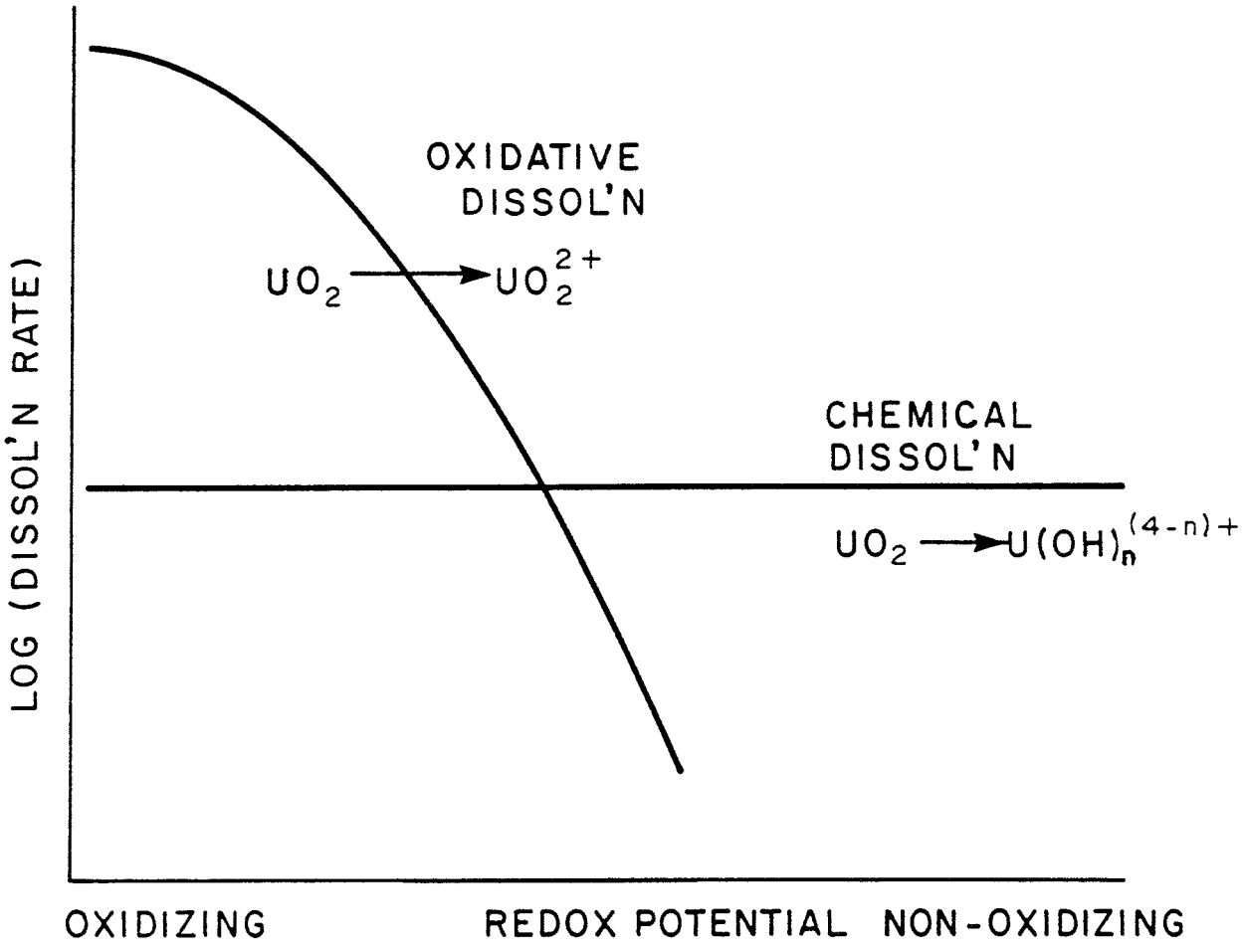

FIGURE 10: Schematic Illustration of the Expected Decrease in Importance of Oxidative Dissolution Compared with Chemical Dissolution as Vault Redox Conditions Become Less Oxidizing

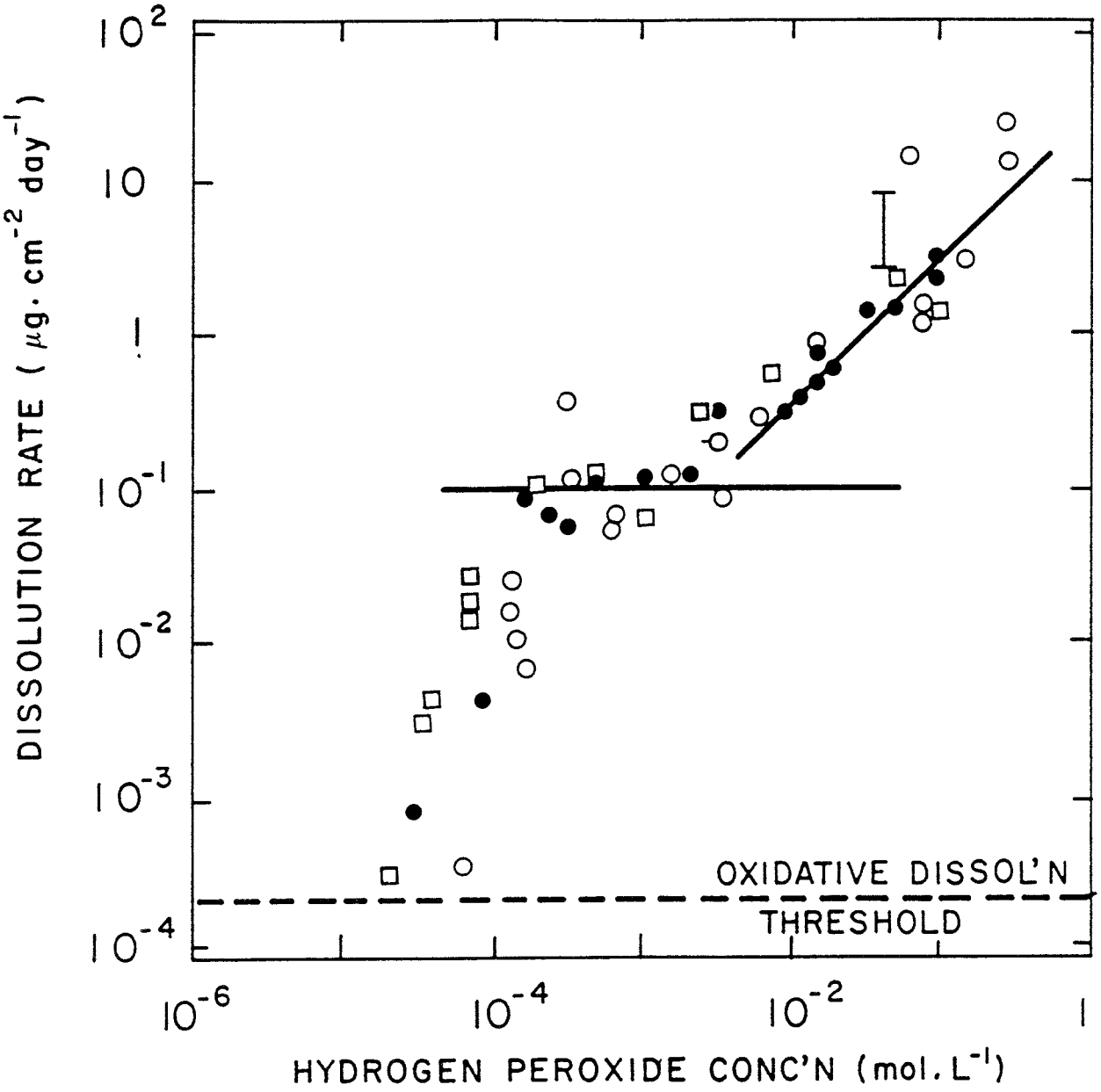

FIGURE 11: Dissolution Rates for UO_2 as a Function of H_2O_2 Concentration in 0.1 mol·L^{-1} $NaClO_4$ (pH ≃ 9.5). The line at high concentrations represents a first-order dependence but is not a fit to the data. The vertical bar shows the dissolution rates measured chemically by Christensen et al. (1990b) at a pH of 8.0 ± 0.2. The different data points represent individual experimental series.

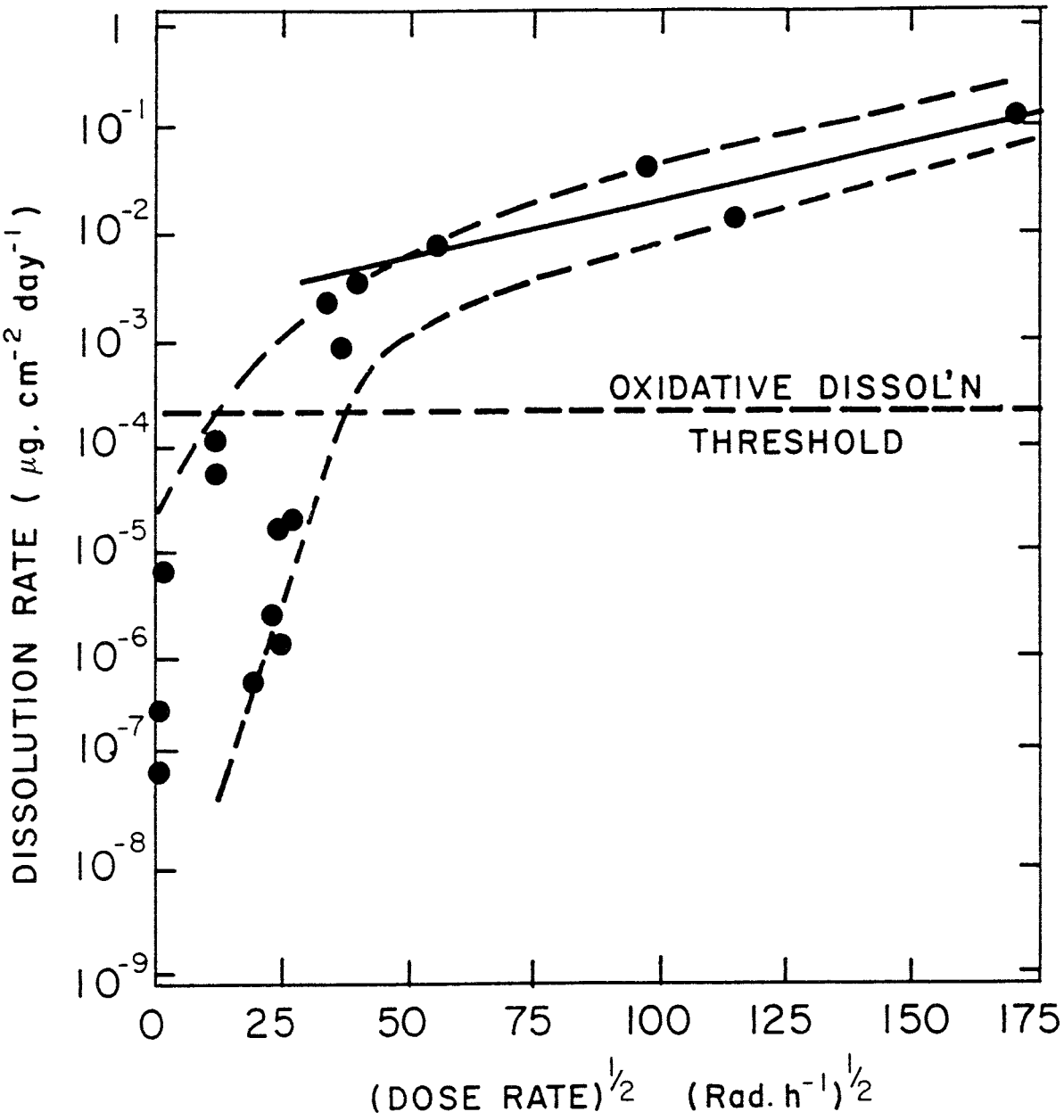

FIGURE 12: Dissolution Rates for UO_2 as a Function of the Square Root of Gamma Dose Rate in Argon-Purged 0.1 mol·L^{-1} $NaClO_4$ (pH = 9.5) Solutions (1 rad = 10 mGy)

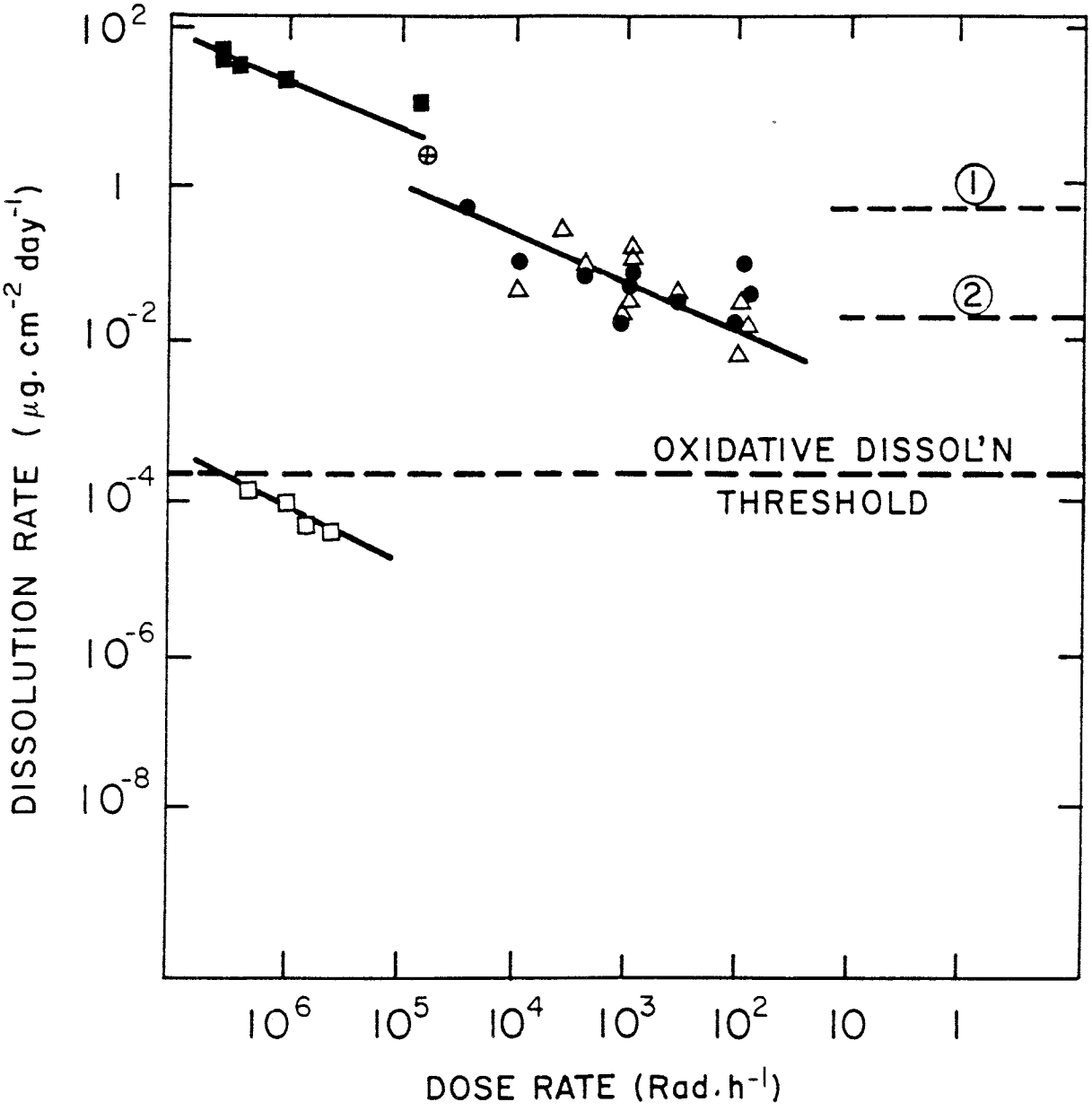

FIGURE 13: Dissolution Rates for UO_2 as a Function of the Logarithm of Gamma Dose Rate in Aerated 0.1 mol·L^{-1} $NaClO_4$ (pH = 9.5) Solutions (o,Δ). Dissolution rates for UO_2 measured by Gromov (1981) in acidic sulphate (pH ~1, []) and alkaline carbonate (pH ~10; []). The data point (⊕) shows the dissolution rate measured by Christensen et al. (1990b) in oxygenated solution irradiated at a dose rate of 70 000-80 000 rad·h^{-1} (1 rad = 10 mGy).

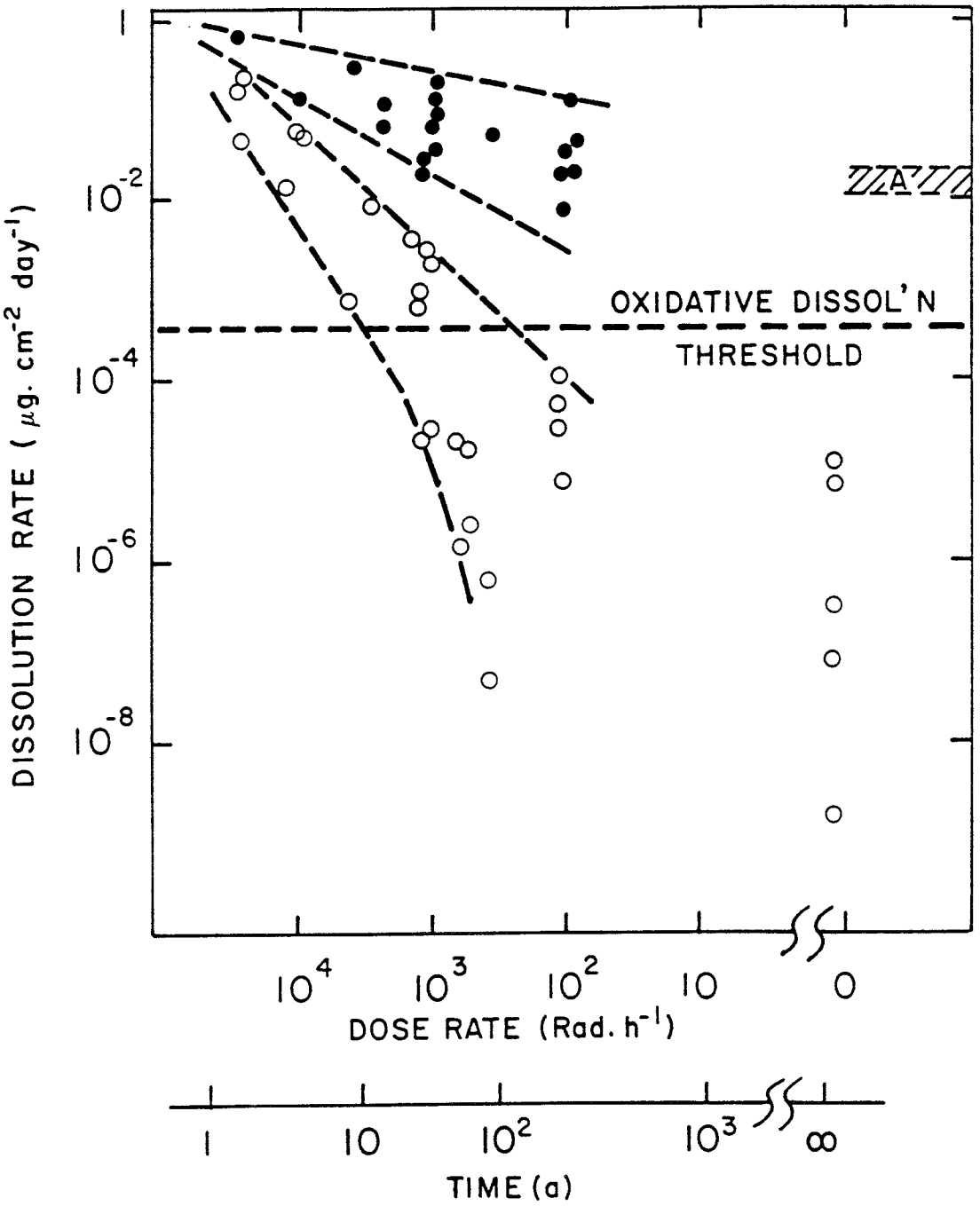

FIGURE 14: Dissolution Rates for UO_2 (from Figures 12 and 13) as a Function of the Logarithm of Gamma Dose Rate; o - Argon-Purged Solutions; o - Aerated Solutions. A is the range of dissolution rates measured in unirradiated but aerated solutions (Shoesmith et al. 1989). The time axis represents the times at which such dose rates would be achieved at the surface of a CANDU fuel bundle after being discharged from reactor (G.B. Wilkin, unpublished data). (1 rad = 10 mGy.)

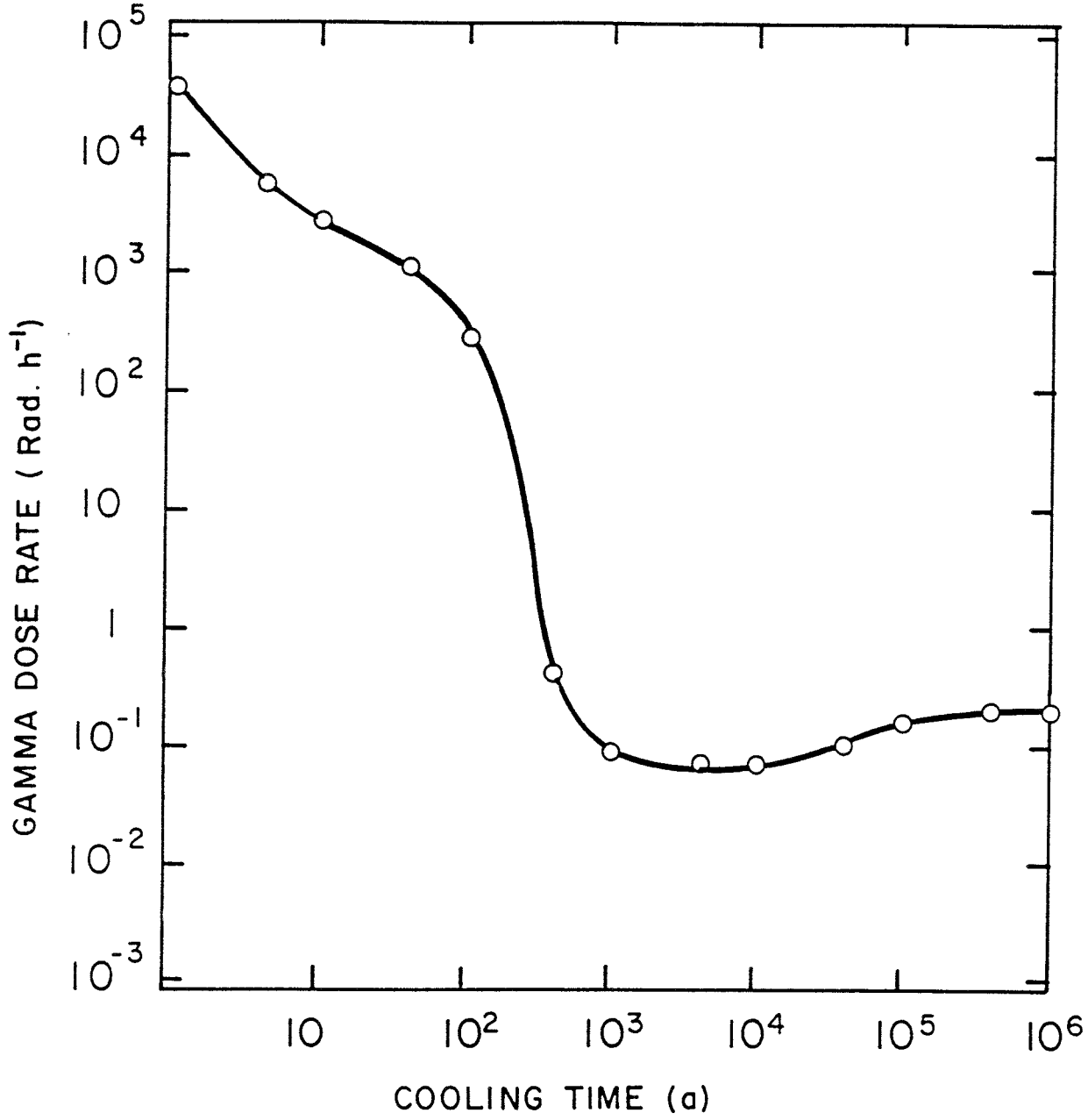

FIGURE 15: Decay in Gamma Dose Rate at the Surface of a Bruce 'A' CANDU Fuel Bundle with a Burnup of 685 $GJ \cdot kg^{-1}$ U (G.B. Wilkin, unpublished data). (1 rad = 10 mGy.)

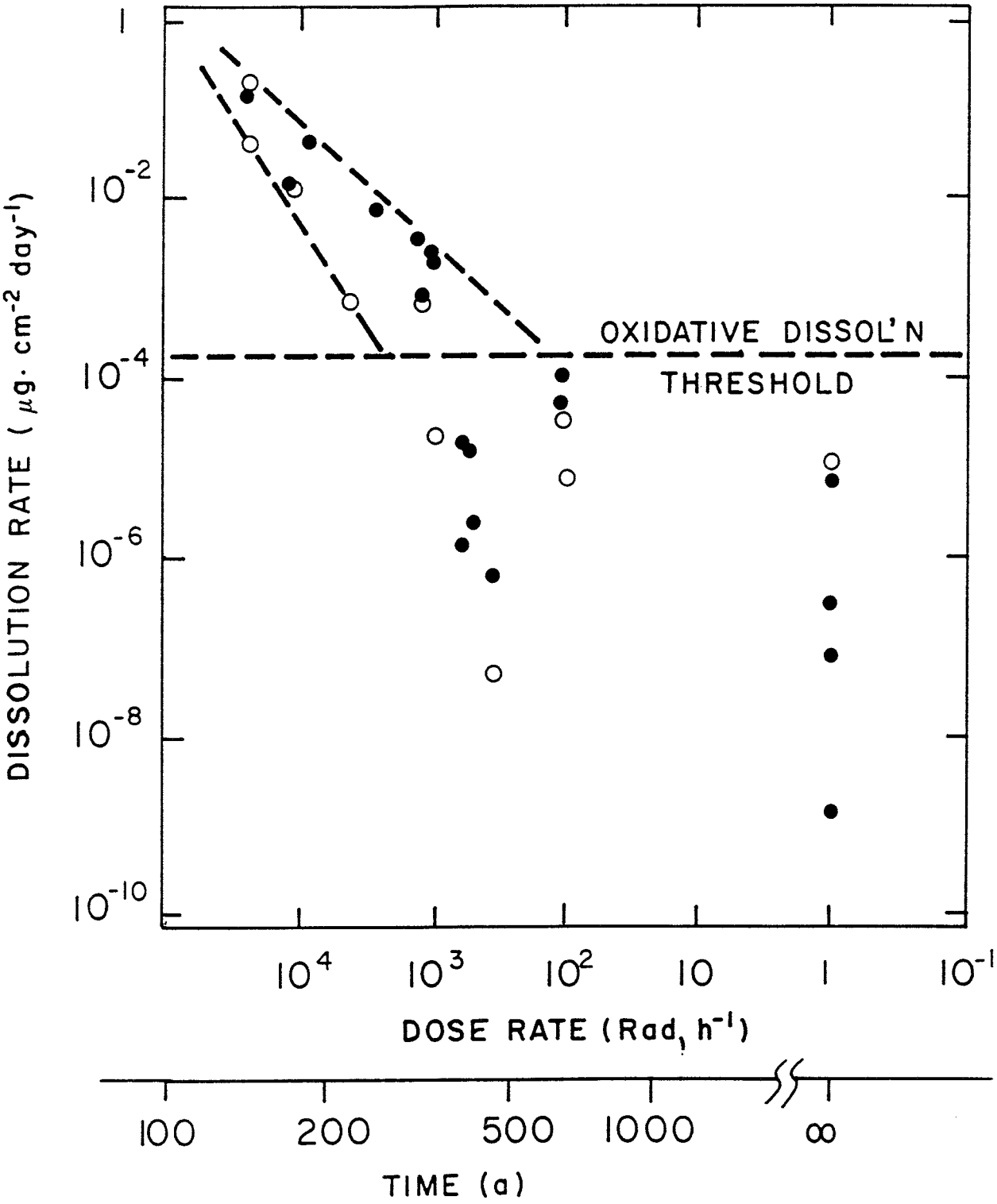

FIGURE 16: Dissolution Rates for UO_2 as a Function of the Logarithm of Beta Dose Rates for PWR Fuel with a Burnup of 45 MW·d/kg U on Discharge from the Reactor (Ingemansson and Elkert 1991). Full and closed data points indicate two independent sets of data. (i rad = 10 mGy.)

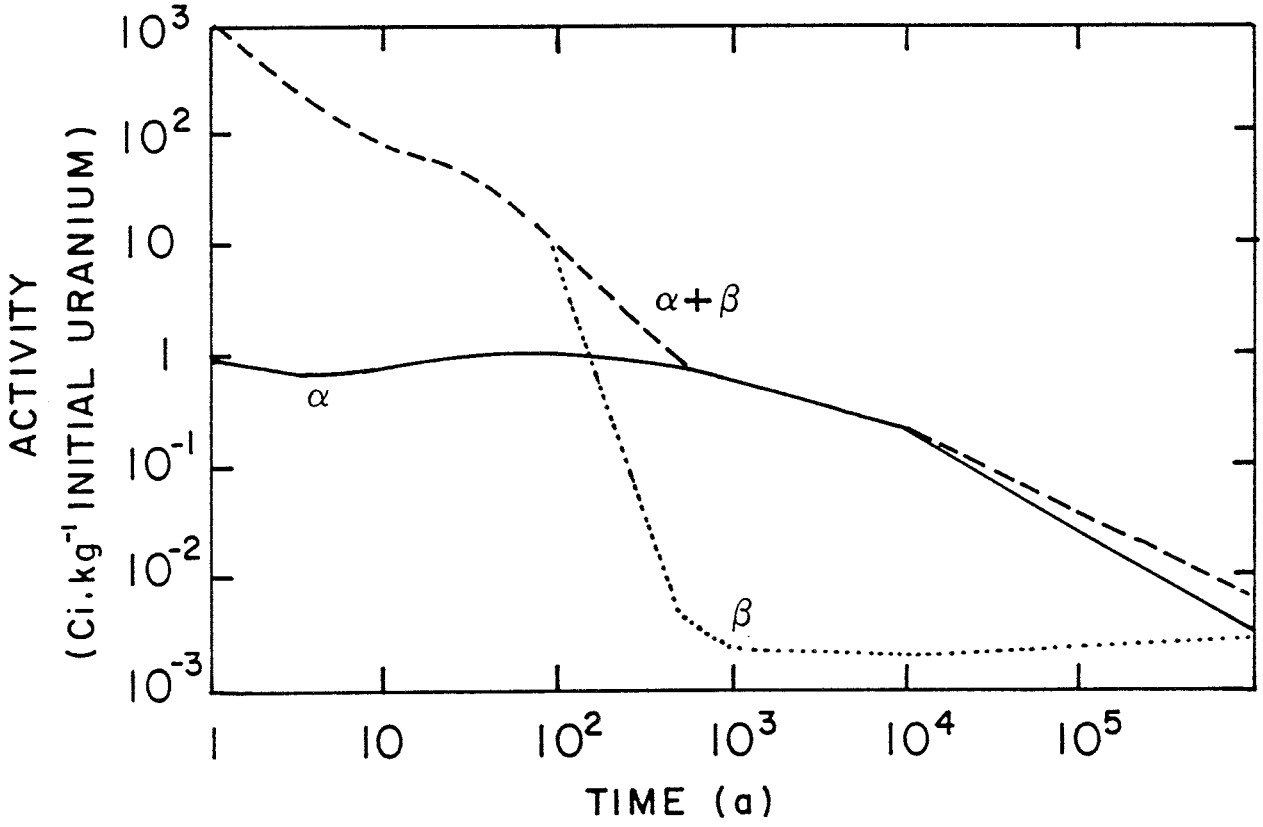

FIGURE 17: The Alpha and Beta Activity as a Function of Time in Terms of Kilograms of Uranium in Irradiated CANDU Fuel with a Burnup of 685 GJ.kg^{-1} U (Appendix G) (1 Ci = 37 GBq) (Smith et al. 1987)

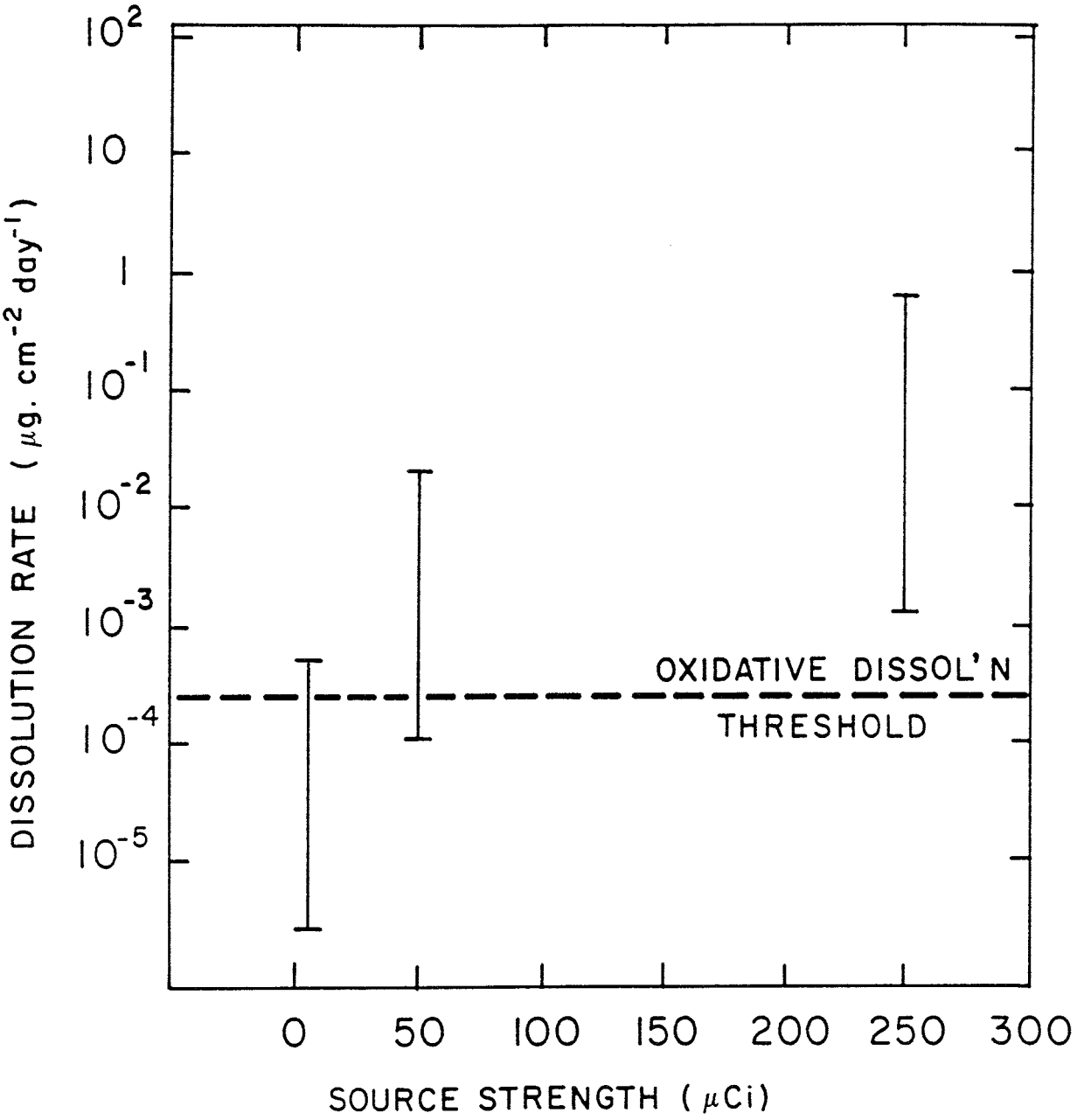

FIGURE 18: Dissolution Rates of UO_2 in Argon-Purged 0.1 mol·L^{-1} $NaClO_4$ (pH = 9.5) as a Function of the Alpha Source Strength Used in our Thin-Layer Electrochemical Cell (Bailey et al. 1985). Each vertical bar includes 3 to 5 individual measurements (1 Ci = 37 GBq).

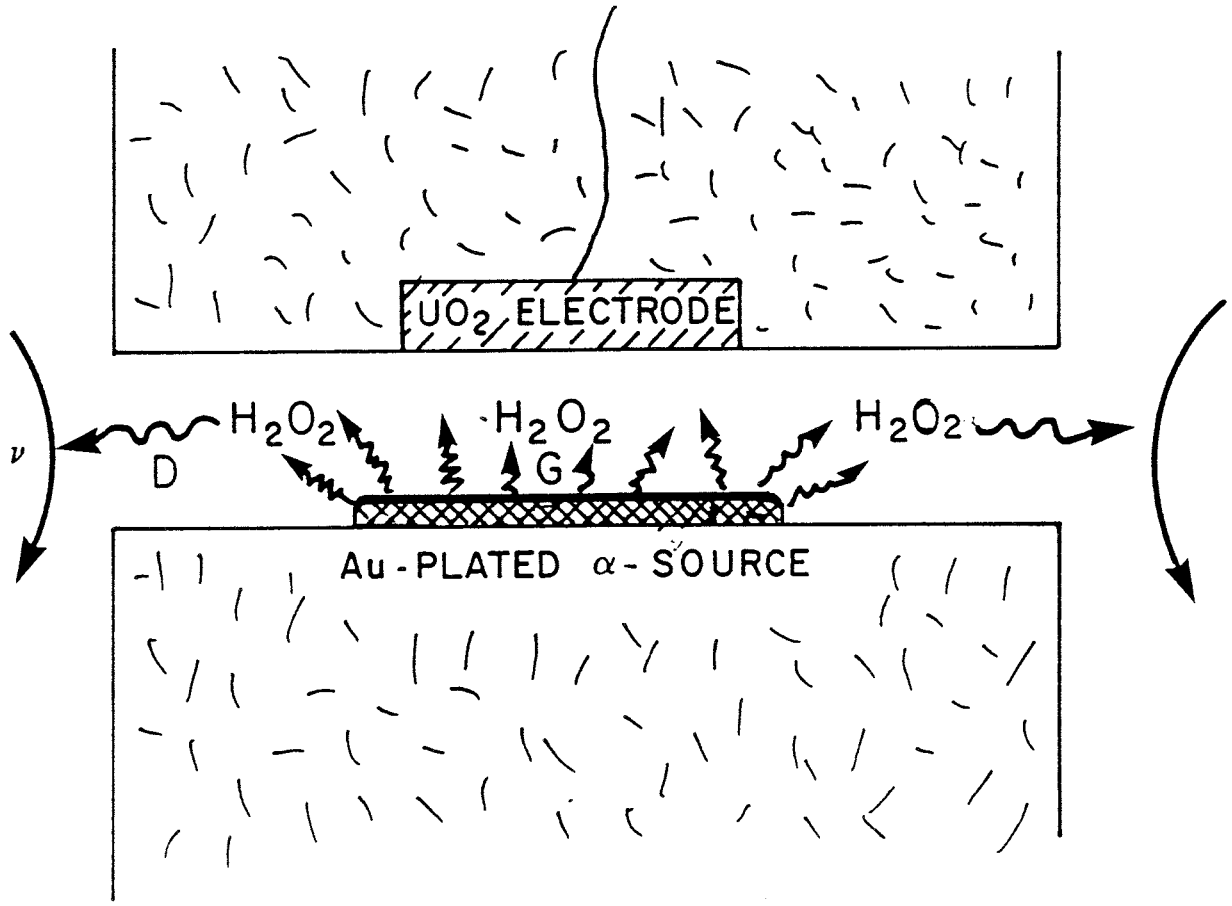

FIGURE 19: Schematic Illustration of the Chemical Conditions Within our Thin-Layer Electrochemical Cell Including the Effects of Alpha Radiolysis (G) and the Effects of Diffusive (D) and Convective (ν) Transport

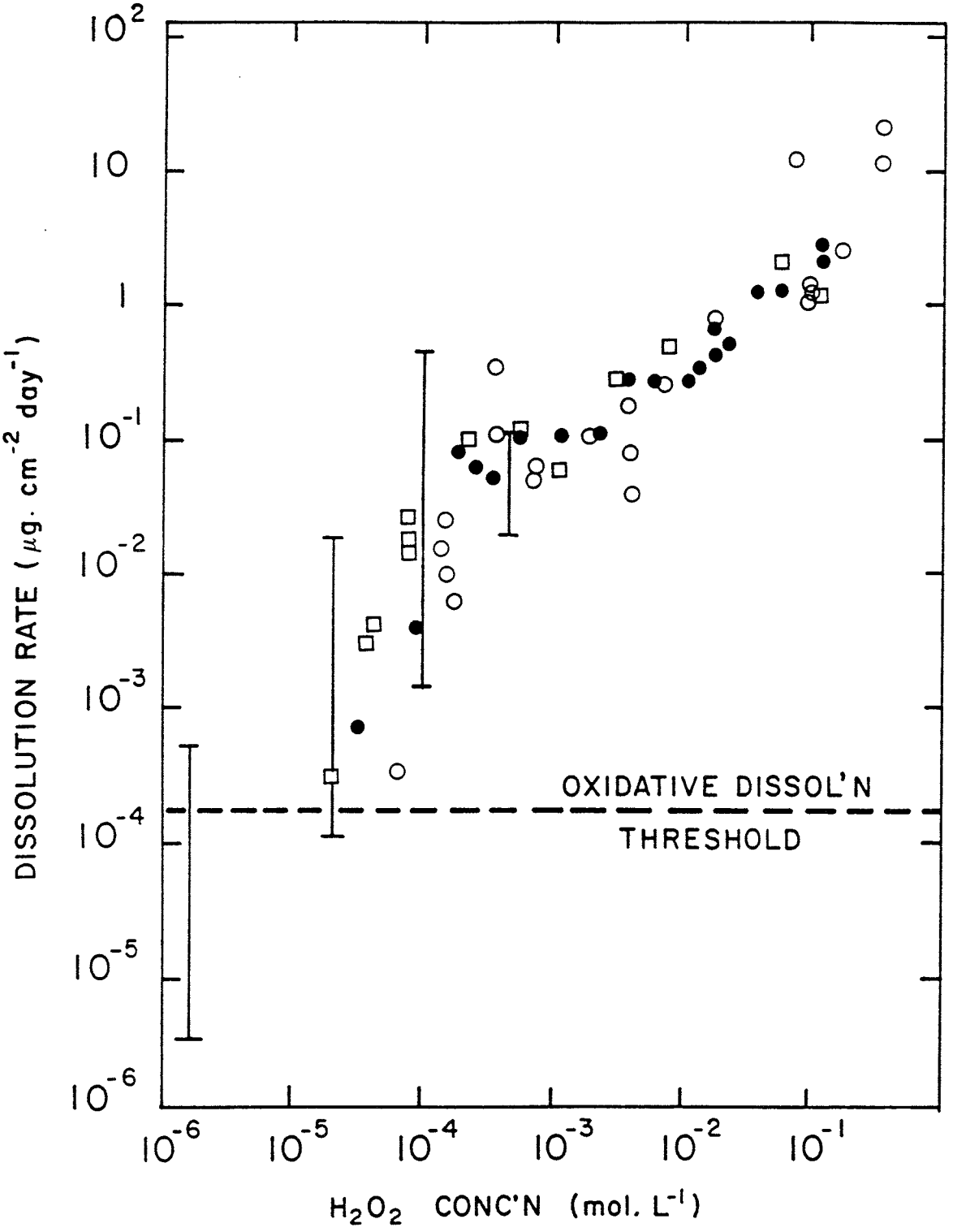

FIGURE 20: Dissolution Rates as a Function of H_2O_2 Concentration from Figure 11 ([], o and o) and for Alpha Radiolysis Within our Thin-Layer Electrochemical Cell (vertical bars) from Figure 18. The H_2O_2 concentrations corresponding to the alpha source strengths (Figure 18) were estimated by Christensen (1990).

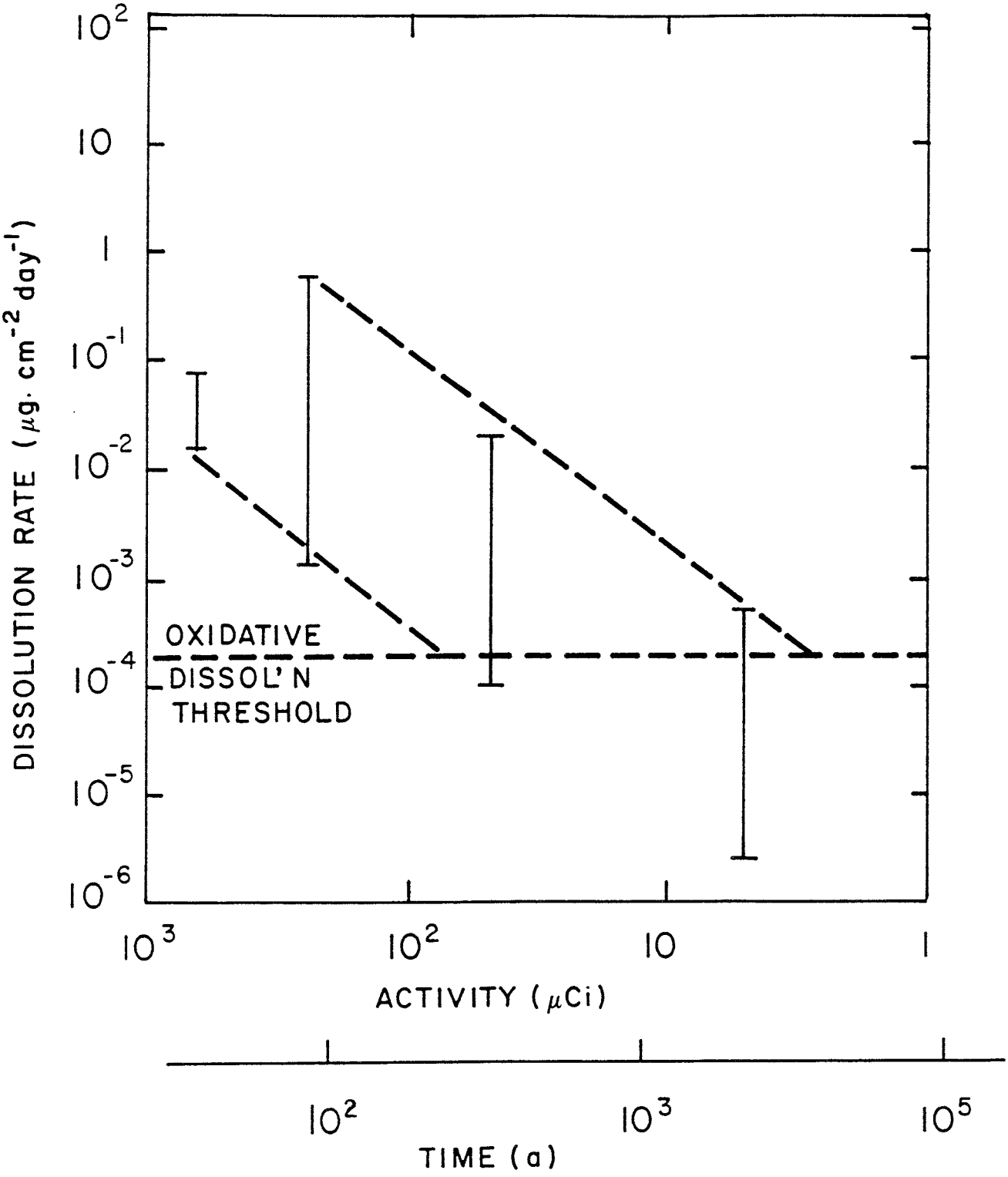

FIGURE 21: Dissolution Rates as a Function of the Logarithm of Alpha Source Strength (from Figure 18). The time axis shows the time at which such activity levels are achieved on the surface of CANDU fuel with a burnup of 685 GJ·kg^{-1} U (Appendix G). (1 Ci = 37 GBq.)

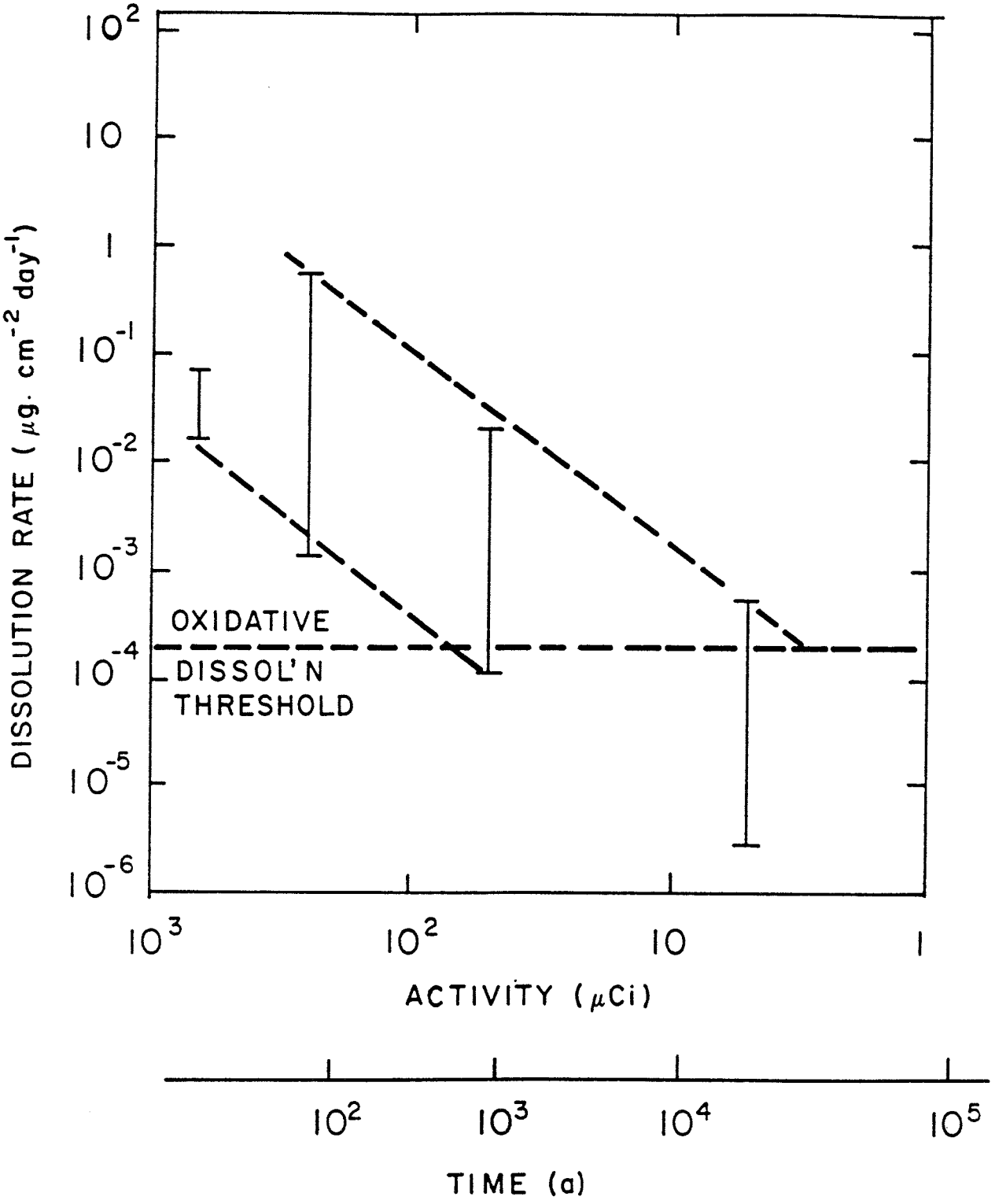

FIGURE 22: Dissolution Rates as a Function of the Logarithm of Alpha Source Strength (from Figure 18). The time axis shows the time at which such activity levels are achieved on the surface of PWR fuel with a burnup of 45 MW·d/kg U on discharge from the reactor. (1 Ci = 37 GBq.)

APPENDIX A

EVIDENCE FOR A THRESHOLD FOR OXIDATIVE DISSOLUTION

Our claim that a potential of ~-100 mV vs. SCE can be considered an approximate dividing line between definitely oxidizing and nominally reducing conditions can be justified from a combination of electrochemical and X-ray photoelectron spectroscopy (XPS) experiments. Figure A-1 shows the charge in coulombs obtained by integrating the electrochemical current flowing through a UO_2 electrode controlled at constant potentials within the range from -150 to 0 mV (vs. SCE) for a 24-h period in argon-purged solution (Sunder et al. 1982). If we assume that all of this accumulated charge can be attributed to the overall dissolution reaction,

$$UO_2 \rightarrow UO_2^{2+} + 2e \qquad (A.1)$$

these values represent the total amount of uranium dissolved in 24 h. Since current flow was transitory and complete after ~12 h at -100 and -150 mV, these values of charge cannot be used to calculate a meaningful dissolution rate. However, they clearly indicate that a threshold for oxidative dissolution exists in the region between -150 and -100 mV (vs. SCE). In these experiments, the limit of detection for a meaningful electrochemical current density appears to be ~3 x 10^{-3} $\mu A \cdot cm^{-2}$, corresponding to a minimum measurable dissolution rate of ~0.5 $\mu g \cdot cm^{-2} \cdot d^{-1}$. Because anticipated dissolution rates are expected to be below this value, the direct electrochemical measurement of UO_2 dissolution rates under meaningful conditions is not feasible.

Figure A-2 shows the results of two series of potentiostatic experiments in argon-purged solution, one for 10 min and one for 1000 min, followed by XPS analysis of the oxidized surface. For short oxidations, the surface is never more oxidized than $UO_{2.33}$ (U_3O_7), a composition achieved for potentials $\geq$+100 mV. For longer oxidations, a composition of $UO_{2.33}$ is achieved around -100 mV. The vertical dashed zone outlines the potential range (-150 to -100 mV) claimed from Figure A-1 as a threshold for oxidative dissolution.

REFERENCE

Sunder, S., D.W. Shoesmith, M.G. Bailey and G.J. Wallace. 1982. Mechanism of oxidative dissolution of UO_2 under waste disposal vault conditions. In Proceedings of the Canadian Nuclear Society International Conference on Radioactive Waste Management, Winnipeg, 1982, 398-405.

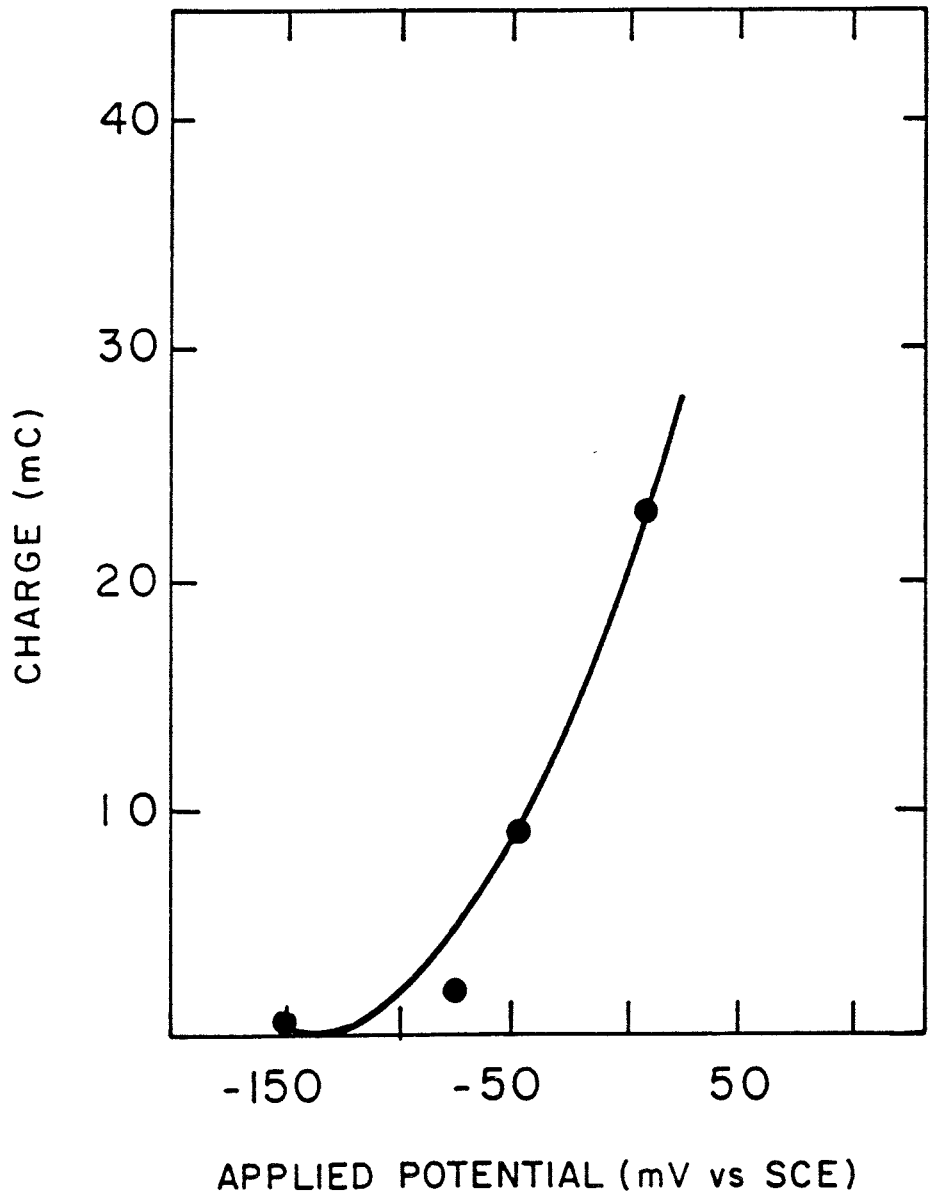

FIGURE A-1: Amount of Dissolved Uranium, Expressed as an Electrochemical Charge, after 24 h of Electrolysis on a UO_2 Electrode at a Constant Applied Potential in 0.5 $mol \cdot L^{-1}$ Na_2SO_4

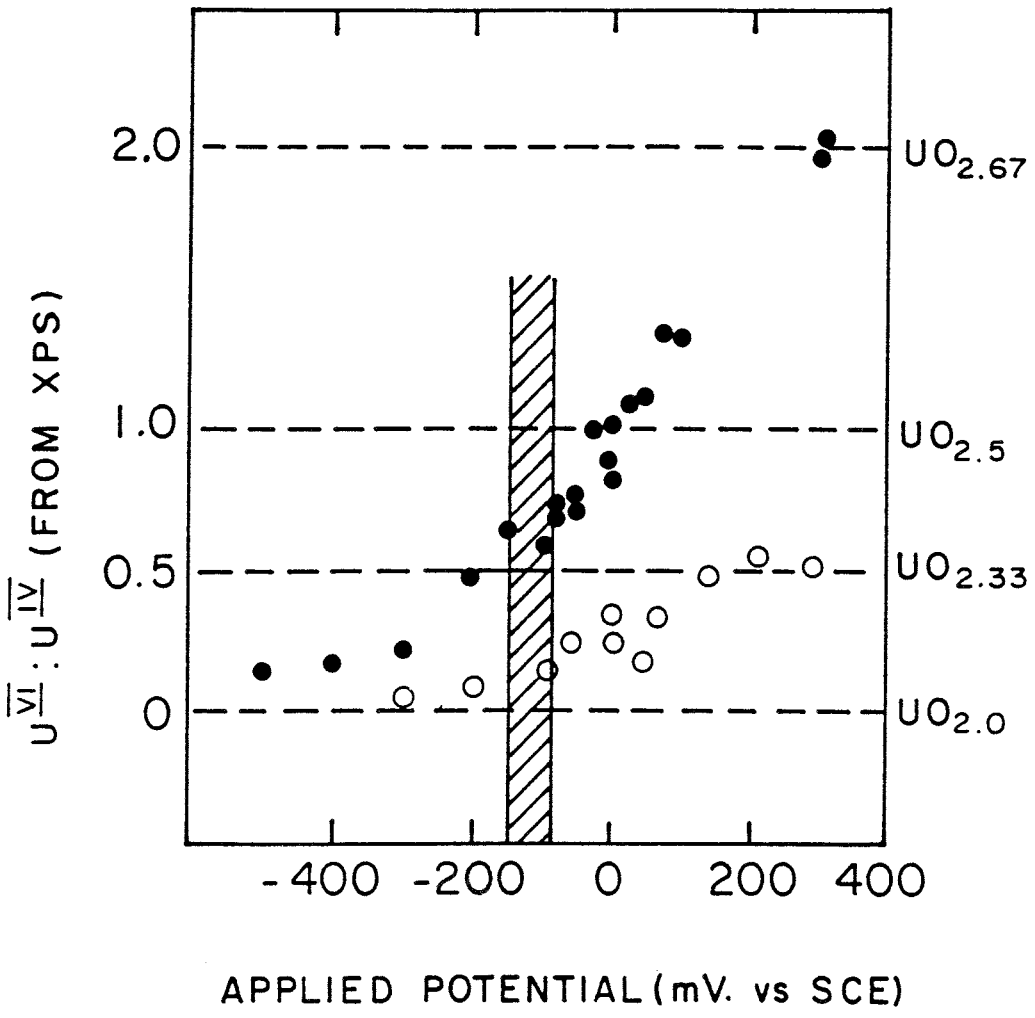

FIGURE A-2: $U^{VI}:U^{IV}$ Ratio (from XPS Measurements) in the Surface of a UO_2 Electrode after Potentiostatic Oxidation in 0.1 mol·L^{-1} $NaClO_4$ (pH = 9.5) for Either 10 min (o) or 1000 min (o)

APPENDIX B

UO_2 OXIDATION AND DISSOLUTION DURING GAMMA RADIOLYSIS

Prior to the onset of oxidative dissolution in neutral to basic solutions not containing significant amounts of complexing anions, a cathodically cleaned UO_2 surface undergoes oxidation to the $UO_{2.33}$ (U_3O_7) stage. This oxidation process is the same whether the oxidant is dissolved oxygen, hydrogen peroxide, or radiolytically decomposed water. Here, we discuss briefly this oxidation process in gamma-irradiated $NaClO_4$ (pH = 9.5) solutions. We have followed the corrosion potential (E_{CORR}) of UO_2 electrodes for various lengths of time in solutions containing a variety of scavengers added to them to maximize the concentration of various radicals (e.g., $OH^{\cdot}$, O_2^{-}). A wide range of gamma dose rates was used (~1 to 300 $Gy \cdot h^{-1}$). The details of this work will be published elsewhere (Sunder et al., in preparation).

Figure B-1 shows the cathodic charge measured by cathodic stripping voltammetry (CSV, see Appendix D) as a function of E_{CORR} achieved under natural corrosion conditions by the time the experiment was terminated. The length of these experiments varied from a few minutes at large dose rates to a few hours at small dose rates. The cathodic charge is a direct measure of the thickness of the film of UO_{2+x} grown on the UO_2 surface during corrosion (Shoesmith et al. 1984). This thickness is directly related to E_{CORR} up to ~100 mV, irrespective of whether oxidation is slow or fast. A steady-state E_{CORR} is established around 100 mV, but the surface film continues to thicken.

Figure B-2 shows the $U^{VI}:U^{IV}$ ratio obtained by XPS analysis of an identical UO_2 specimen exposed for the same length of time to the same solution as the electrode. Consequently, we expect the surface composition of this specimen to reflect that of the electrode itself. This ratio increases slowly over the E_{CORR} range from -400 to 0 mV, during which the film thickness is increasing linearly with potential (Figure B-1). Once steady-state is achieved around 100 mV, the film thickening indicated by the results in Figure B-1 is accompanied by a large increase in the $U^{VI}:U^{IV}$ ratio.

Figure B-3 plots the $U^{VI}:U^{IV}$ ratio against the cathodic charge. The horizontal bar shows that the surface film thickens without a change in

composition over the potential range from -200 to +100 mV. The U^{VI} to U^{IV} ratio is ~0.7 within this range. The thicker films that build up under steady-state conditions are much more oxidized.

These data demonstrate that oxidation of UO_2 occurs in two distinct stages. Between -400 and ~0 mV, oxidation leads to the growth of a film that achieves a composition of ~$UO_{2.33}$ in the range from -200 to -100 mV, i.e., as our threshold for oxidative dissolution is approached (see Appendix A). The thickness and composition of this film are directly related to the E_{CORR} achieved, irrespective of the rate of oxidation. This suggests that oxidation is rapid and that the composition and film thickness are steady-state values at potentials within this range.

If dissolution were to occur within the potential range (-400 to -100 mV), it would likely proceed via Reactions (B.1) and (B.2):

$$UO_2 + xH_2O \longrightarrow UO_{2+x} + 2xH^+ + 2xe \qquad (B.1)$$

$$UO_{2+x} + n(1 - x)OH^- + (x - 2)H_2O \longrightarrow (1 - x)U(OH)_n^{(4-n)+} + xUO_2^{2+} + (2x - 4)H^+ \qquad (B.2)$$

i.e., by rapid oxidation followed by the slow ion transfer of U^{IV} and U^{VI} species to solution (see Figure 3(b) in main report). Once steady state is achieved, film growth leads to the formation of highly oxidized films, indicating the occurrence of an oxidative process via Reactions (B.3) and (B.4) (see Figure 3(a) of main report):

$$UO_2 + 0.33H_2O \longrightarrow UO_{2.33} + 0.66H^+ + 0.66e \qquad (B.3)$$

$$UO_{2.33} + 0.66H^+ \longrightarrow UO_2^{2+} + 0.33H_2O + 1.34e \qquad (B.4)$$

followed by the formation of a U^{VI}-containing secondary phase. In the "non-complexing" electrolyte solutions employed in these experiments, this phase is likely to be $UO_3 \cdot zH_2O$. This oxidative transformation occurs at a constant potential. The fact that the formation of $UO_3 \cdot zH_2O$ does not appear to occur until E_{CORR} is well beyond the oxidative dissolution threshold of -100 mV (Appendix A) is a reflection of the dynamic nature of the experiment and of the difficulties of removing the specimen for analysis by XPS without redissolution of the small amounts of $UO_3 \cdot zH_2O$ on the surface.

REFERENCES

Shoesmith, D.W., S. Sunder, M.G. Bailey, G.J. Wallace and F.W. Stanchell. 1984. Anodic oxidation of UO_2. IV - X-ray photoelectron spectroscopic and electrochemical studies of film growth in carbonate-containing solutions. Applications of Surface Science 20, 39-57. Also Atomic Energy of Canada Limited Reprint, AECL-8174.

Sunder,S., D.W. Shoesmith, H. Christensen and N.H. Miller. In preparation. Oxidation of UO_2 fuel by specific radicals formed during radiolysis of groundwater.

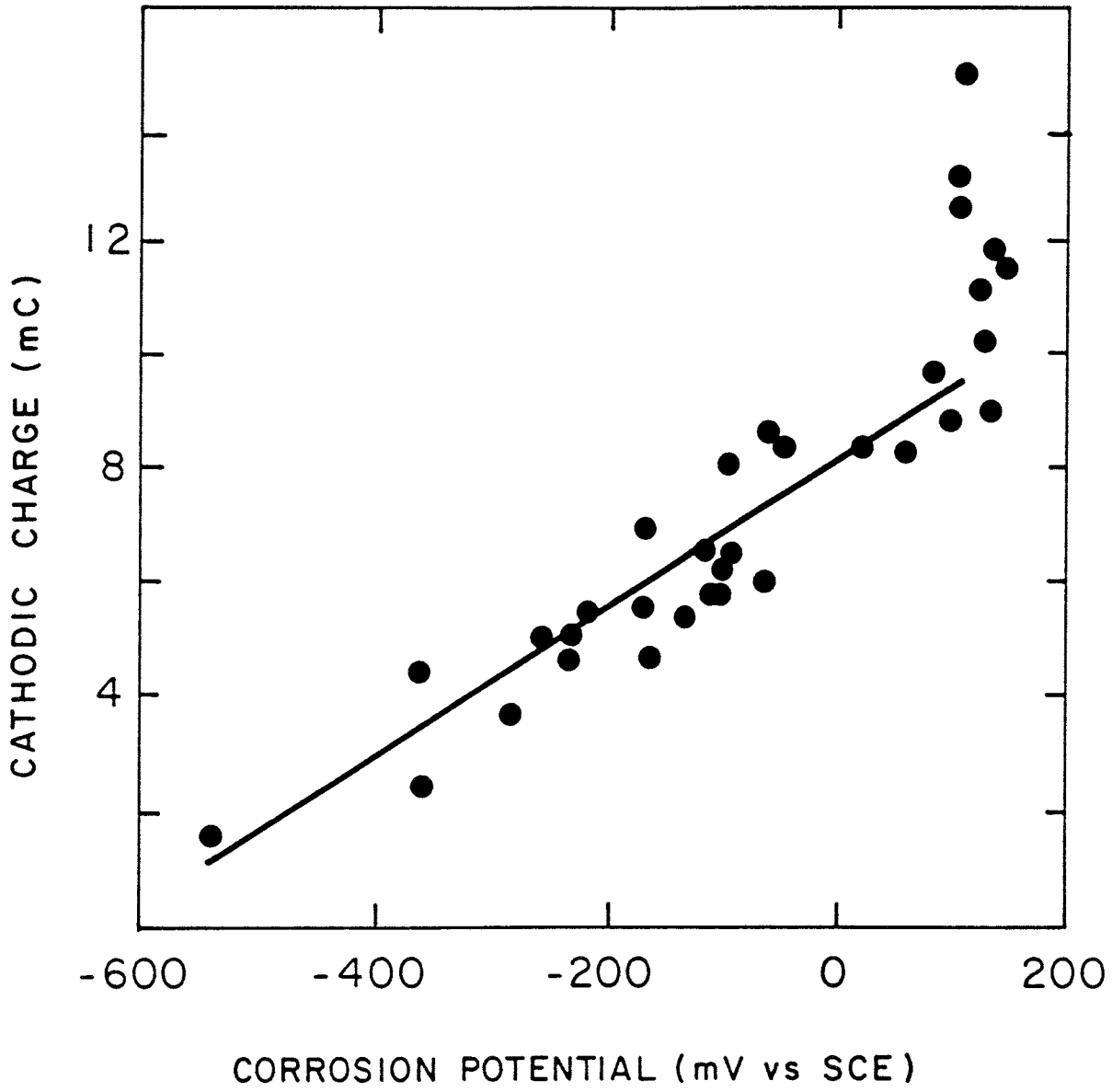

FIGURE B-1: Cathodic Charge Measured by Cathodic Stripping Voltammetry (Q_{FILM}) as a Function of the Corrosion Potential (E_{CORR}) Achieved under Natural Corrosion Conditions in 0.1 mol·L^{-1} $NaClO_4$ (pH = 9.5) Containing Various Additives and Gamma-Irradiated at Various Dose Rates for Various Times

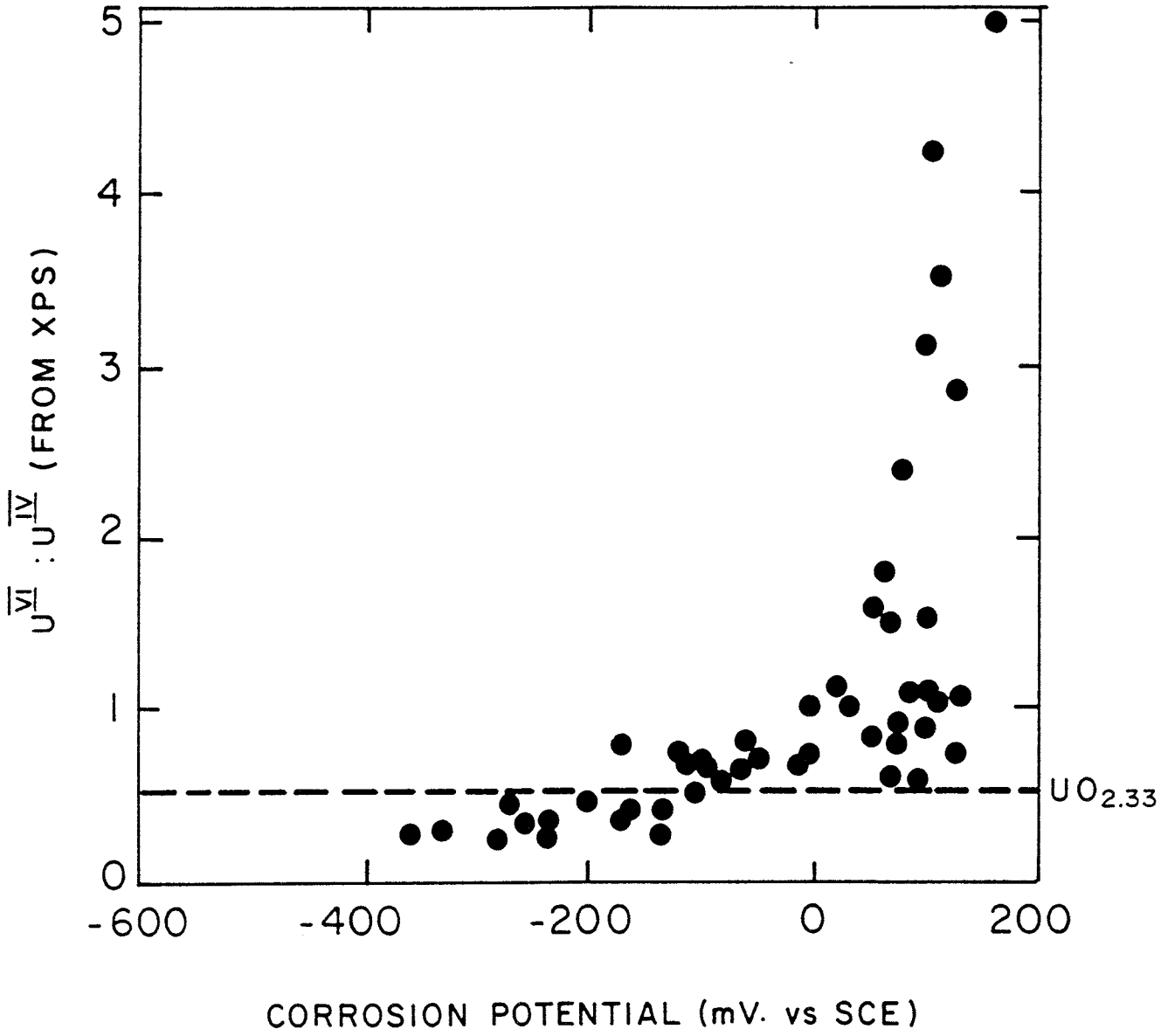

FIGURE B-2: $U^{VI}:U^{IV}$ Ratio in the Surface of a UO_2 Specimen after Exposure to Gamma-Irradiated Solutions under the Conditions Noted in Figure B-1

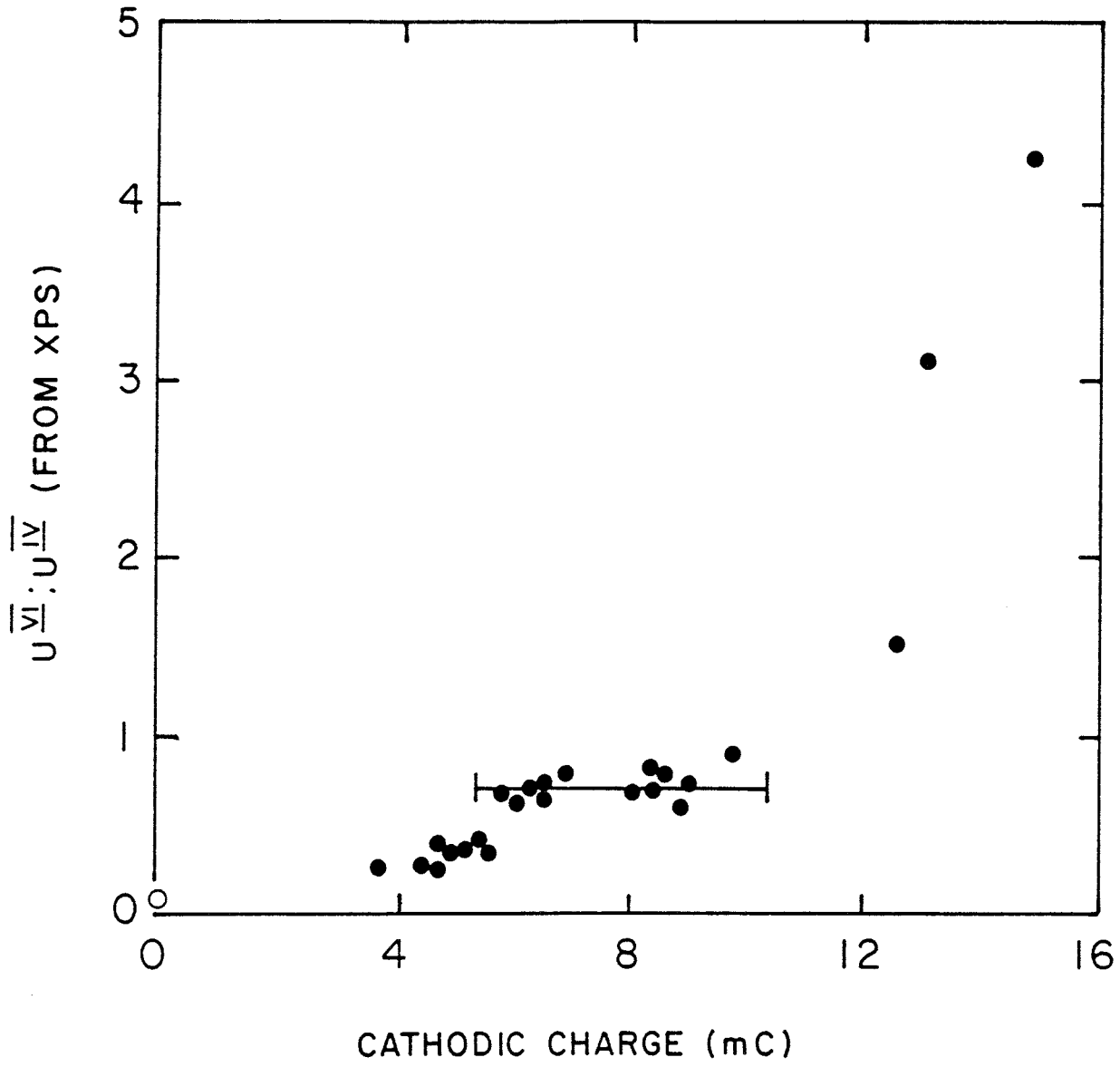

FIGURE B-3: $U^{VI}:U^{IV}$ Ratios (from Figure B-2) as a Function of Cathodic Charge (from Figure B-1)

APPENDIX C

REDOX CONDITIONS FOR WHICH THE SOLUBILITY-BASED MODEL FOR FUEL DISSOLUTION IS APPROPRIATE

In the solubility-based model, the dissolution rate of the used fuel is limited by the solubility of UO_{2+x}, provided the groundwater flow is slow enough for local saturation to occur. For $x = 0$, dissolution can be envisaged as proceeding via the chemical dissolution reaction,

$$UO_2 + (n - 2)H_2O \longrightarrow U(OH)_n^{(4-n)+} + (n - 4)H^+ \qquad (C.1)$$

in the absence of oxidant. For $0 < x \leq 0.25$ (the composition range over which the model is applied (Lemire and Garisto 1989)), dissolution requires a continuous source of oxidant, is oxidative and proceeds by the following reactions:

$$UO_2 + xH_2O \longrightarrow UO_{2+x} + 2xH^+ + 2xe \qquad (C.2)$$

$$UO_{2+x} + n(1 - x)OH^- + (x - 2)H_2O \longrightarrow (1 - x)U(OH)_n^{(4-n)+} + xUO_2^{2+} + (2x - 4)H^+ \qquad (C.3)$$

In both cases, it is assumed that the dissolution reaction is reversible, and therefore capable of approaching equilibrium. Such a situation is achievable if the overall rate of dissolution is controlled not by interfacial rate parameters but by transport in the surrounding clay/sand mixtures.

In terms of the redox conditions within the vault, this sequence of assumptions requires that the composition of the fuel surface be that which is in equilibrium with the surrounding redox environment. For the electrochemical kinetics of the oxidative dissolution process to be negligible (i.e., infinitely fast compared to the rate-controlling transport step) the redox potential at the UO_{2+x} surface must equal the redox potential in the surrounding environment (often termed Eh). If we were to succeed in measuring the potential at the solid/environment interface, the corrosion potential, then we would obtain the single value representative of these redox conditions. Furthermore, this potential could only be achieved for

that single surface composition in equilibrium with its surroundings for that single redox condition. This situation is shown in Figure C-1(a). Since no potential difference exists across the solid/environment interface, the rate of ion transfer ($U_{solid} \rightarrow U_{sol,n}$) cannot be controlled by electrochemical parameters.

The results presented in Appendix B for the oxidation of UO_2 in water decomposed by gamma radiolysis showed that for potentials $\leq$-100 mV, the composition of the surface did dictate the value of the corrosion potential and vice versa. This correlation suggests that the conditions required for the solubility-based model may be achieved in this potential range ($E \leq -100$ mV). Our results do not, however, demonstrate that the required reversibility is achieved.

When testing the solubility-based model, Lemire and Garisto (1989) calculated the impact of various parameters and combinations of parameters on the solubility of fuel. Based on calculations for 40 000 sampled contact waters, whose properties represented the range of conditions expected in a disposal vault, they found that the highest uranium solubilities represented oxidative dissolution of $UO_{2.25}$ at potentials approaching that for the $UO_{2.25}/UO_{2.33}$ stability line (Figure C-2). Our own experimental results (Appendices A and B) show that, once $UO_{2.33}$ is the stable phase, oxidative dissolution becomes irreversible in character and leads to the transformation of $UO_{2.33}$, by dissolution and precipitation processes, to secondary phases such as $UO_3 \cdot zH_2O$; i.e., dissolution is proceeding via Reactions (C.4) and (C.5):

$$UO_2 + 0.33H_2O \longrightarrow UO_{2.33} + 0.66H^+ + 0.66e \qquad (C.4)$$

$$UO_{2.33} + 0.66H^+ \longrightarrow UO_2^{2+} + 0.33H_2O + 1.34e \qquad (C.5)$$

Under these conditions, use of the solubility-based model is no longer warranted, since the redox potential at the UO_{2+x} surface will not be equal to the redox potential in the surrounding environment. This situation is depicted in Figure C-1(b). Since a potential difference exists across the interface, electrochemical parameters will be important in determining the dissolution/transformation rate. The corrosion potential is determined by the balance between the kinetics of the overall UO_2 dissolution reaction,

$$UO_2 \rightarrow UO_2^{2+} + 2e \qquad (C.6)$$

and the corresponding oxidant reduction reaction,

$$Ox + 2e \rightarrow Red \qquad (C.7)$$

REFERENCE

Lemire, R.J. and F. Garisto. 1989. The solubility of U, Np, Pu, Th and Tc in a geological disposal vault for used nuclear fuel. Atomic Energy of Canada Limited Report, AECL-10009.

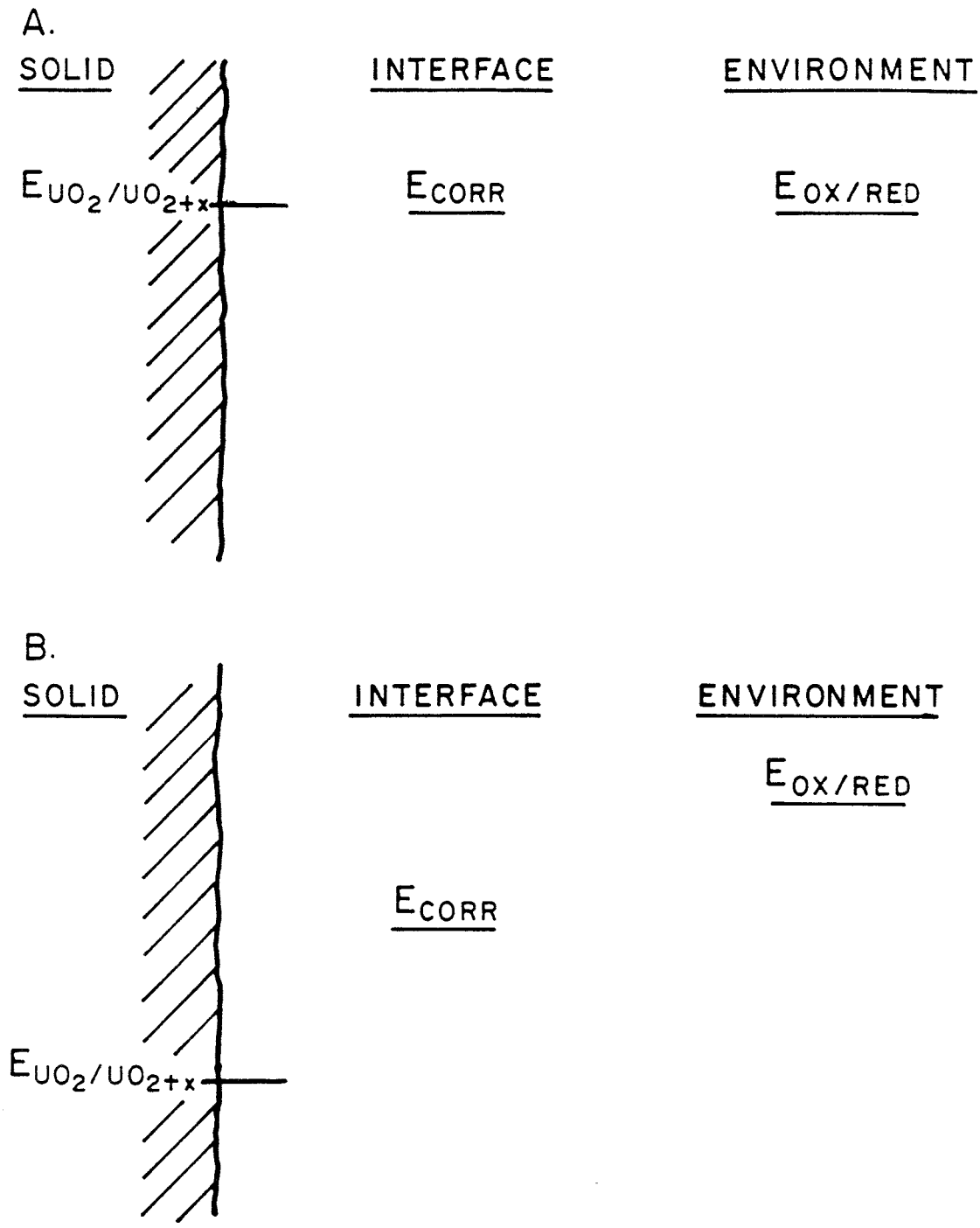

FIGURE C-1: (a) Relationship Between Potentials when the Surface Composition of a Solid Is in Equilibrium with Its Environment and No Electrochemical Driving Force Exists

(b) Relationship Between Potentials when the Surface Composition Is not in Equilibrium with Its Environment and an Electrochemical Driving Force for Oxidative Dissolution Exists

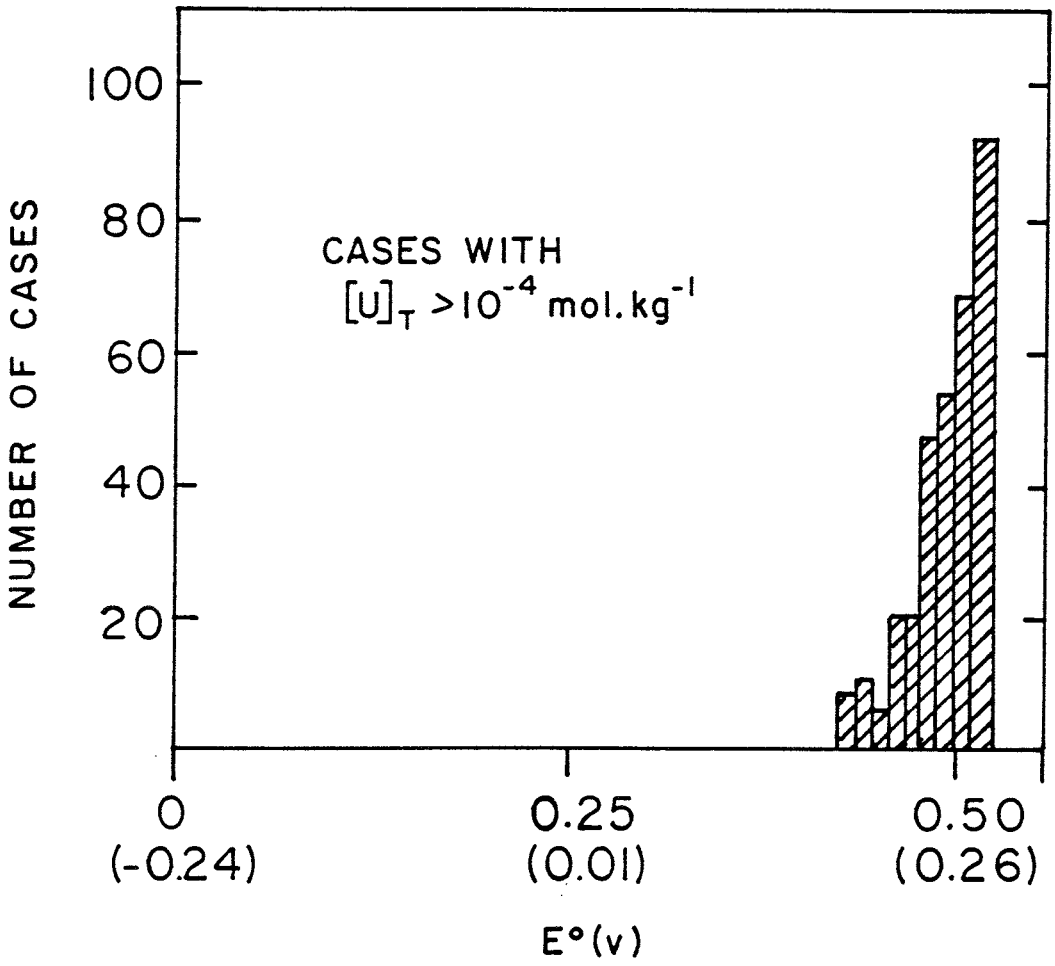

FIGURE C-2: Distribution of Uranium Solubilities at 25°C as a Function of Redox Potential for Those Contact Waters (of a Set of 40 000 Sampled Contact Waters) in Which the Total Uranium Solution Concentration is $>10^{-4}$ mol.kg^{-1} (from Lemire and Garisto 1989). The potential plotted is the E° value unadjusted for differences in solution composition and pH within the set of sampled contact waters. Consequently, these potentials cannot be directly compared with the electrochemical or corrosion potentials given elsewhere. The potential values in brackets are quoted against SCE.

APPENDIX D

BASIS FOR AN ELECTROCHEMISTRY-BASED DISSOLUTION MODEL

CONTENTS

		Page
D.1.	ANODIC DISSOLUTION OF UO_2	68
D.2.	CATHODIC REDUCTION OF OXIDANTS	69
D.3.	CORROSION OF UO_2 UNDER OPEN-CIRCUIT CONDITIONS	71
D.4.	CATHODIC STRIPPING VOLTAMMETRY OF SURFACE OXIDE FILMS	72
	REFERENCES	72
	FIGURES	74

D.1 ANODIC DISSOLUTION OF UO_2

Extensive studies of the anodic oxidation and dissolution of UO_2, generally coupled with X-ray photoelectron spectroscopy (XPS) analyses of the oxidized surfaces, have been published. A good mechanistic understanding is available and has recently been reviewed (Johnson and Shoesmith 1988, Sunder and Shoesmith 1991). This mechanism can be stated in the simple reaction step,

$$UO_2 \rightarrow UO_2^{2+} + 2e \qquad (D.1)$$

Figure D-1 shows the steady-state dissolution currents recorded at 0.1 $mol \cdot L^{-1}$ $NaClO_4$ (pH = 9.5) and used in our extrapolations to determine dissolution rates under natural corrosion conditions. Graphs such as these, which plot the logarithm of the current against the applied potential, are known as Tafel plots. Also shown as a horizontal bar in Figure D-1 is the range of E_{CORR} values measured in the presence of various oxidants in this work. Obviously, the extrapolation involved is long (up to ~500 mV), yielding corrosion currents ranging over many orders of magnitude. Such long extrapolations on such sparse data lead to corrosion currents (dissolution rates) with significant uncertainties. A more extensive series of measurements is required if these uncertainties are to be removed, or at least quantified.

Also indicated in Figure D-1 are the potential ranges for various surface compositions ($UO_{2+x} \rightarrow UO_{2.33} \rightarrow UO_{2.67}$) and the potential threshold for oxidative dissolution (see Appendix A). Our electrochemical data are recorded on a surface different in composition to that on which natural corrosion occurs. Unfortunately, if we extend our electrochemical measurements to lower potentials, it is very difficult to establish steady state and hence obtain reliable dissolution currents. However, similar experiments in carbonate solution exhibit the same relationship between current and potential, despite the fact that bicarbonate/carbonate prevents the formation of surface phases beyond $UO_{2.33}$ (Shoesmith et al. 1984,1989). This similarity in Tafel slopes indicates that the kinetics of anodic dissolution are not particularly dependent on surface composition in this potential range.

Some justification for our electrochemical approach was gained when the rate obtained by extrapolating the data in Figure D-1 to E_{CORR} measured in aerated solution was found to be within an order of magnitude of the rate

obtained from fuel leaching studies under similar conditions (Shoesmith et al. 1989). We also attempted to use the same extrapolation to obtain a corrosion rate under argon-purged conditions (Figure D-1). The rate obtained was extremely low, between three and five orders of magnitude lower than that under aerated conditions (Shoesmith et al. 1989). It is doubtful that this value is quantitatively significant.

The possibility of secondary phase formation (e.g., as $UO_3 \cdot zH_2O$) was minimized in recording the data plotted in Figure D-1 by using an electrode of small surface area in a large volume of stirred solution. Consequently, the current measured is the maximum sustainable dissolution rate for Reaction (D.1),

$$UO_2 \longrightarrow UO_2^{2+} + 2e \qquad (D.1)$$

at the potential applied, and is unattenuated by the presence of films of corrosion product. The presence of precipitated secondary phases cannot accelerate oxidative dissolution beyond this rate (current), since the reaction is irreversible. However, the buildup of substantial layers of corrosion product (secondary phases) could inhibit dissolution, because of their low permeability, and the actual dissolution current may be lower than that measured in our electrochemical experiment. If measurements were made in the presence of corrosion product films, a meaningful extrapolation to natural corrosion conditions would be unobtainable. The log I-E plot would likely not remain linear with applied potential, as illustrated in Figure D-2.

By extrapolating electrochemical data measured as described here, we obtain maximum values of corrosion current for the oxidative dissolution of $UO_2/UO_{2.33}$. The real rates would be expected to decrease as corrosion product layers thicken. In natural groundwaters, Lahalle et al. (1989) have shown that dissolution is strongly inhibited by the formation of Mg/Si hydrous oxides on UO_2.

D.2. CATHODIC REDUCTION OF OXIDANTS

We have recently reported our detailed studies of the cathodic reduction of oxygen on UO_2 electrodes (Hocking et al. 1991). A preliminary study of the reduction of hydrogen peroxide on UO_2 has also been performed (Shakerinia et al., in preparation). Here we confine our discussion to the reduction of O_2 for which we possess a good, but not complete, mechanistic understanding.

The kinetics of oxygen reduction are dependent on the composition and electronic properties of the electrode surface. Figure D-3 shows two steady-state log I-E plots for oxygen reduction in aerated solution: one recorded on a cathodically reduced electrode as the potential is made more positive; and one recorded on an electrode allowed to naturally corrode in aerated solution for up to 6 d before the reduction curve is recorded as the potential is made more negative.

On the reduced electrode, a linear Tafel region (A in Figure D-3) is obtained between ~-0.4 and -0.6 V. The deviations from linearity at higher and lower applied potentials coincide with changes in the surface composition of the electrode. This dependence on surface composition is important since O_2 reduction appears to require the adjacent donor/acceptor properties of uranium in two oxidation states (U^{IV}/U^{V} or U^{IV}/U^{VI}). On the naturally corroded electrode, there appears to be two distinct Tafel regions (B and C in Figure D-3), the switch from one to the other again coinciding with a change in composition of the surface. The increased current for O_2 reduction has been attributed to an increase in density of donor/acceptor sites on the naturally corroded surface.

Only an extrapolation from region B yields a corrosion current in the same range as that obtained by the extrapolation of the anodic currents in Figure D-1. Extrapolation from regions A and C yields corrosion currents up to two orders of magnitude greater than that obtained by the anodic extrapolation. This behaviour confirms that anodic dissolution is coupled to oxygen reduction on an oxidized surface, and that any mathematical expressions used to represent oxygen reduction must be determined by experimentation in the narrow potential region B.

The Tafel slope in region B is close to 120 mV^{-1}, the theoretical value expected for an electrochemical process involving one electron in the rate-determining step. Since our results indicate that the rate of the oxygen reduction reaction is controlled by the first electron transfer (Hocking et al. 1991), such a slope indicates that the number of donor/acceptor sites is effectively unlimited in this potential region; i.e., the parameter N' in Equation (11) of the main report ($I_c = k_{ox}N'[Ox]^q \exp(-b'E)$) can be taken as one.

Also shown in Figure D-3 is the same range of measured corrosion potentials as that shown in Figure D-1. The two plots are for aerated solutions and will extrapolate to the positive potential end of this range. By recording similar plots at different oxygen concentrations, we have shown that, for

standard unirradiated CANDU fuel, the reaction order with respect to oxygen is first order in the Tafel region; i.e., the parameter, q, in the above Equation (11) is equal to one. So far, the oxygen dependence has only been determined on cathodically reduced electrodes.

D.3. CORROSION OF UO_2 UNDER OPEN-CIRCUIT CONDITIONS

We have followed the corrosion potential (E_{CORR}) of cathodically reduced UO_2 electrodes in the presence of a number of chemical and radiolytically produced oxidants (Sunder and Shoesmith 1991). In all cases, the form of the curve of E_{CORR} with time is the same as shown schematically in Figure D-4, the potential rising exponentially to a steady-state value. The rate of potential rise and the final steady-state E_{CORR} depend on the nature and concentration of the particular oxidant. The horizontal hatched area indicates our threshold for oxidative dissolution (Appendix A).

During the potential rise, the UO_2 is undergoing solid-state surface oxidation to UO_{2+x}, and a surface film of $UO_{2.33}$ approximately 5 to 7 nm in thickness is achieved by the time E_{CORR} passes the threshold for oxidative dissolution. The oxidation process in this region is fast, the value of E_{CORR} being determined by a combination of surface composition and film thickness, as described in Appendix B for oxidation in gamma-irradiated solutions. We have used the time taken to reach the threshold as a measure of the rate of the oxidation process and demonstrated the differences in oxidation rates for a number of radiolytic oxidants (Sunder et al. 1990).

From the threshold for oxidative dissolution to the final steady state, further oxidation and dissolution to produce the secondary phase $UO_3 \cdot zH_2O$ occurs, with some evidence that the process may be concentrated at grain boundaries (Shoesmith et al. 1989, Sunder et al. 1991). At steady state, the predominant process occurring is oxidative dissolution. Our experiments were terminated before substantial buildup of secondary phases occurred on the electrode surface. The steady-state E_{CORR} value is determined by the redox potential of the solution, and the kinetics of the oxidative-dissolution and oxidant-reductant reactions occurring on the surface. This steady-state value of E_{CORR} is the one at which the corrosion current (oxidative dissolution rate) is determined.

D.4. CATHODIC STRIPPING VOLTAMMETRY OF SURFACE OXIDE FILMS

The consequences of surface oxidation of UO_2 during corrosion can be determined by electrochemically reducing the surface films formed using a cathodic potential sweep at a constant sweep rate, $v = dE/dt$. A series of such stripping voltammograms is shown in Figure D-5 for UO_2 exposed for various times on O_2-saturated 0.1 $mol \cdot L^{-1}$ $NaClO_4$ (pH = 9.5) (Shoesmith et al. 1989). Similar experiments have been performed on UO_2 electrodes corroded (oxidized) in H_2O_2 and in water decomposed by gamma radiolysis.

The cathodic sweep was started from the E_{CORR} achieved by the electrode during the corrosion period. By integrating these current profiles (over the potential range shaded in Figure D-5), the charge (Q_{FILM}) from the reduction of oxide films can be determined as a function of exposure time to the oxidizing solution. This charge is directly related to film thickness. From the known unit cell dimensions for $UO_{2.33}$ (Shoesmith et al. 1984), we estimate the thickness of these films to be only 5 to 7 nm. In this manner, we can show that by the time steady state is achieved, the $UO_{2.33}$ layer (reduced at peak b in Figure D-5) has reached a constant thickness, and that only small amounts of $UO_3 \cdot zH_2O$ (reduced at peak a) are present on the surface.

We have weak evidence, from electrochemical experiments, suggesting that dissolution and the formation of secondary phases (e.g., $UO_3 \cdot zH_2O$) were occurring predominantly at grain boundaries (Shoesmith et al. 1989). A stronger indication that the oxidative dissolution process is enhanced at grain boundaries is provided by the secondary ion mass spectrometry (SIMS) and Rutherford backscattering spectroscopy (RBS) analyses of Christensen et al. (1990), made on UO_2 specimens exposed to strongly irradiated aqueous solutions (700 to 800 $Gy \cdot h^{-1}$) (7×10^4 to 8×10^4 $rad \cdot h^{-1}$). An oxidized surface layer up to 200 nm in depth was observed. The variation of SIMS and RBS signals are consistent with a decreasing degree of oxidation with depth, suggesting penetration down grain boundaries.

REFERENCES

Christensen, H., R. Forsyth, R. Lundqvist and L.O. Werme. 1990. Radiation induced dissolution of UO_2. Studsvik Report NS-90/85, Studsvik Energiteknik AB, Nykoping, Sweden.

Hocking, W.H., J.S. Betteridge and D.W. Shoesmith. 1991. The cathodic reduction of dioxygen on uranium oxide in dilute alkaline aqueous solution. Atomic Energy of Canada Limited Report, AECL-10402.

Johnson, L.H. and D.W. Shoesmith. 1988. Spent fuel. In Radioactive Waste Forms for the Future (W. Lutze and R.C. Ewing, editors), Elsevier Publishers, 635-698. Also Atomic Energy of Canada Limited Reprint, AECL-9583.

Lahalle, M.P., J.C. Krupa, R. Guillaumont, G. Genet, G.C. Allen and N.R. Holmes. 1989. Surface analysis of UO_2 leached in mineral water studied by X-ray photoelectron spectroscopy. In Materials Research Society Symposium Proceedings 127 (Scientific Basis for Nuclear Waste Managemant XII), 351-356.

Shakerinia, S., W.H. Hocking, J.S. Betteridge and D.W. Shoesmith. In preparation. Cathodic reduction of hydrogen peroxide on uranium oxide.

Shoesmith, D.W., S. Sunder, M.G. Bailey, G.J. Wallace and F.W. Stanchell. 1984. Anodic oxidation of UO_2. IV - X-ray photoelectron spectroscopic and electrochemical studies of film growth in carbonate-containing solutions. Applications of Surface Science 20, 39-57. Also Atomic Energy of Canada Limited Reprint, AECL-8174.

Shoesmith, D.W., S. Sunder, M.G. Bailey and G.J. Wallace. 1989. The corrosion of nuclear fuel (UO_2) in oxygenated solutions. Corrosion Science 29 (9), 1115-1128. Also Atomic Energy of Canada Limited Reprint, AECL-9887.

Sunder, S. and D.W. Shoesmith. 1991. Chemistry of UO_2 fuel dissolution in relation to the disposal of used nuclear fuel. Atomic Energy of Canada Limited Report, AECL-10395.

Sunder, S., D.W. Shoesmith, H. Christensen, N.H. Miller and M.G Bailey. 1990. Oxidation of UO_2 fuel by radicals formed during radiolysis of water. In Materials Research Society Symposium Proceedings 176 (Scientific Basis for Nuclear Waste Management XIII), 457-464.

Sunder, S., D.W. Shoesmith, R.J. Lemire, M.G. Bailey and G.J. Wallace. 1991. The effect of pH on the corrosion of nuclear fuel (UO_2) in oxygenated solutions. Corrosion Science 32 (4), 373-386.

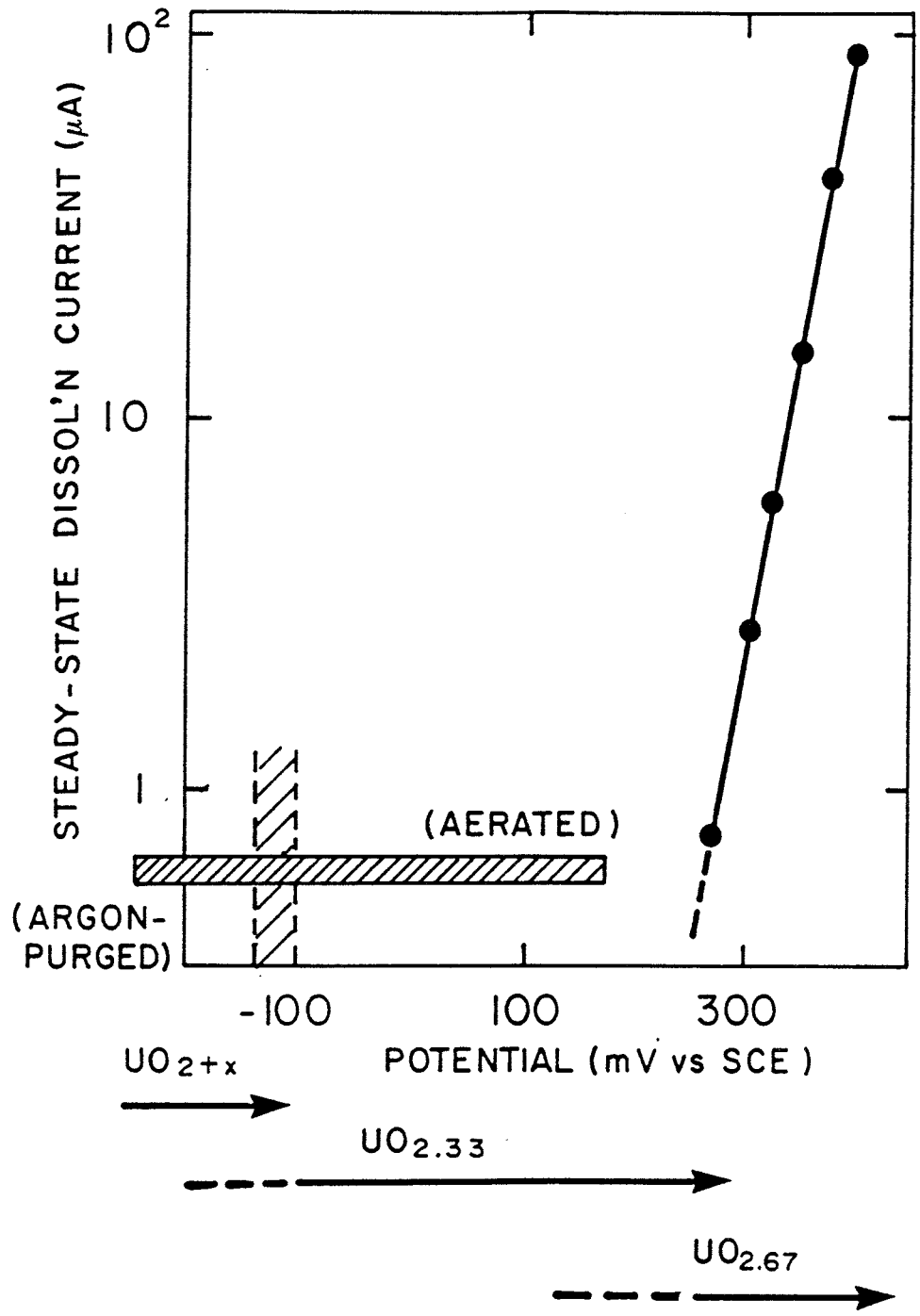

FIGURE D-1: Steady-State Currents as a Function of Applied Potential for the Anodic Dissolution of a UO_2 Electrode in 0.1 mol·L^{-1} $NaClO_4$ (pH = 9.5) (from Shoesmith et al 1989). The horizontal bar shows the range of E_{CORR} values measured in the same solution in the presence of the various oxidants considered in this work. The horizontal arrows indicate the potential ranges for various surface compositions.

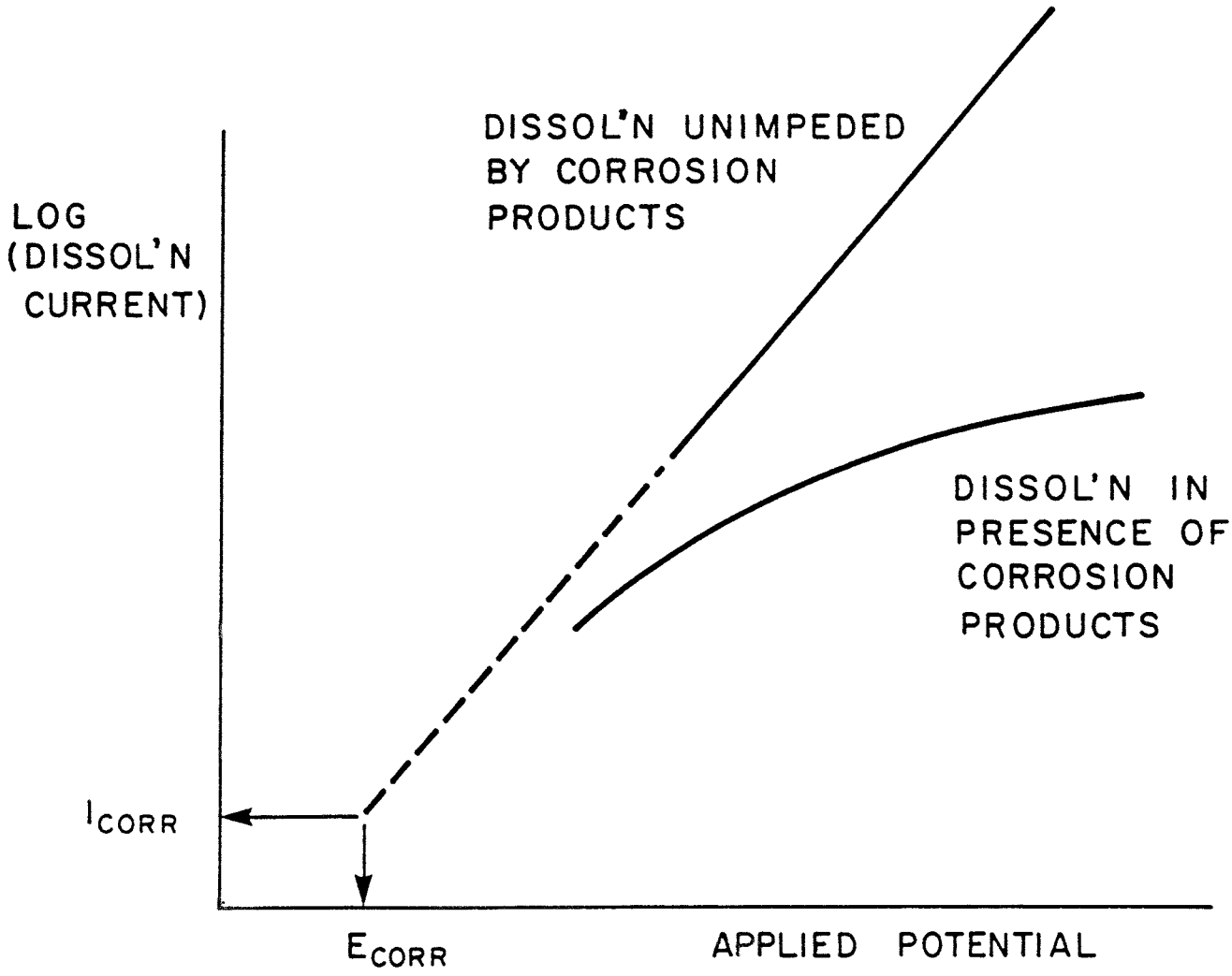

FIGURE D-2: Illustration of the Form of the Current Potential Relationship in the Presence of Corrosion Products Deposited on the Surface of the UO_2 Electrode

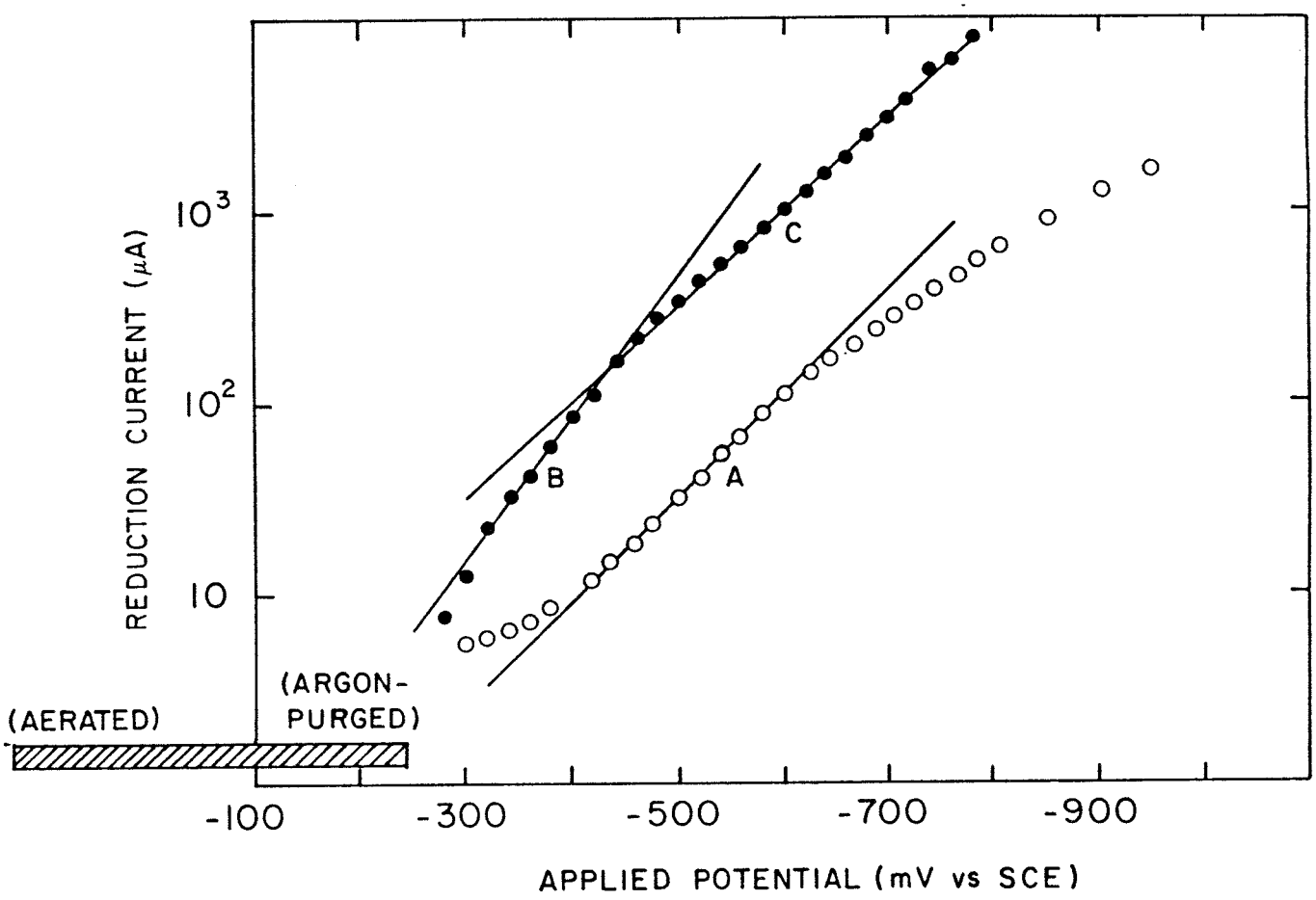

FIGURE D-3: Steady-State Currents as a Function of Applied Potential for Oxygen Reduction on a UO_2 Electrode in Aerated 0.1 mol·L^{-1} $NaClO_4$ (pH = 9.5). Open circle data points recorded on a cathodically reduced electrode as the potential is systematically made more positive. Full data points recorded on an electrode allowed to corrode naturally in the same solution for up to 6 d before the data were recorded as the potential was made more negative. A, B and C indicate linear Tafel regions.

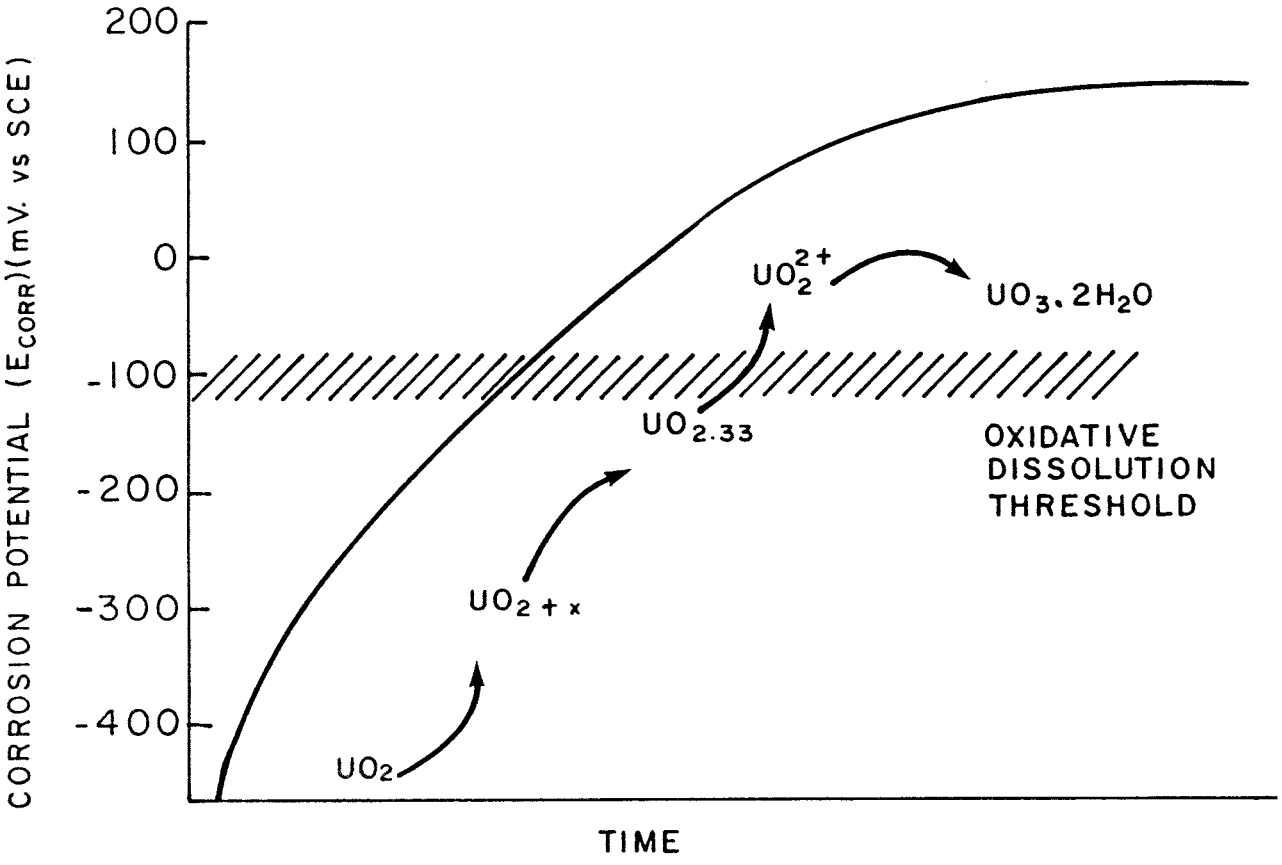

FIGURE D-4: Form of the Corrosion Potential as a Function of Time for Corrosion of UO_2 in the Presence of Dissolved Oxidants

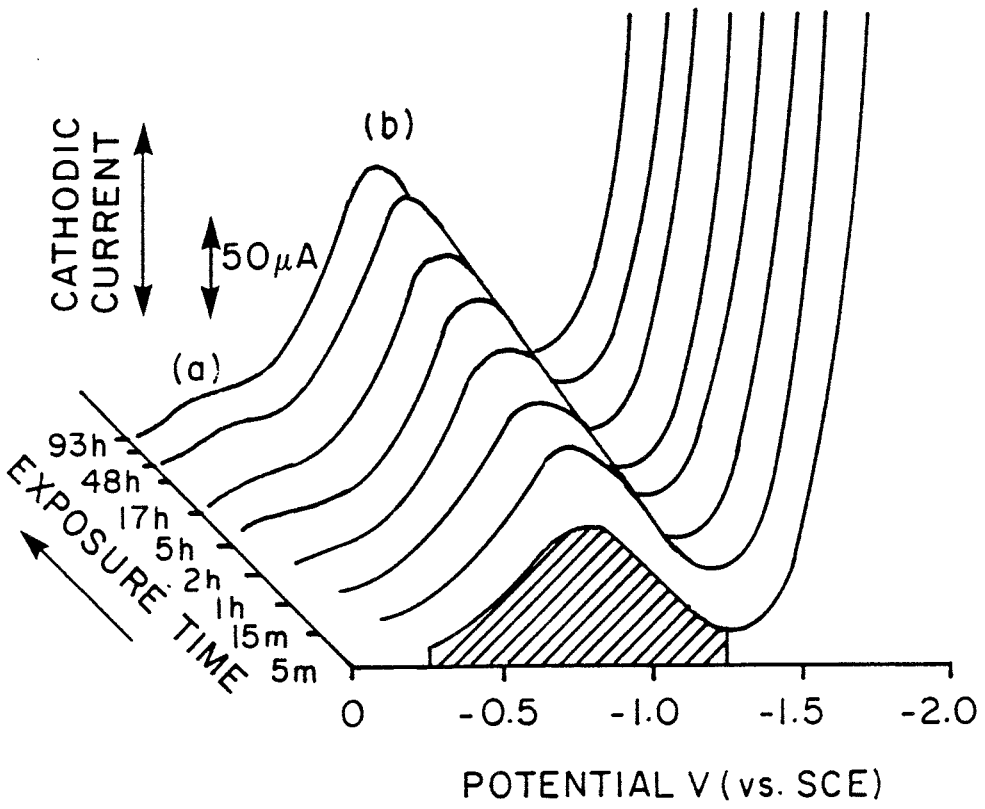

FIGURE D-5: Cathodic Stripping Voltammograms Recorded on a UO_2 Electrode Exposed for Various Times in Oxygen-Saturated 0.1 mol·L^{-1} $NaClO_4$ (pH = 9.5)

APPENDIX E

CHEMICAL DISSOLUTION OF METAL OXIDES

The parameters controlling the dissolution rates of oxides have been reviewed by Segall et al. (1988). A characteristic of oxide dissolution processes is the wide range of dissolution rates, generally measured in acidic solutions, which can vary by many orders of magnitude even for the same oxide.

According to Segall et al., the slowly dissolving semiconducting oxides generally possess dissolution rates in the range 10^{-4} to 10^{-1} $\mu mol \cdot cm^{-2} \cdot d^{-1}$. The rate-controlling process is either charge transfer to the surface to form surface ionic species (M^{n+}, O^{2-}) before interfacial ion transfer to the solution, or surface alterations to produce these surface ionic species. Thus, properties such as solid-state conductivity, ion formation at surface defect sites, and the solution redox potential are major factors that determine the kinetics of dissolution. The dissolution rates are found to vary substantially with the conditions of preparation and subsequent treatment, which can affect both the degree of non-stoichiometry, hence the conductivity, and the concentration of reactive sites in the surface.

Since UO_2 is generally a p-type semiconductor (Hocking et al. 1991), its chemical dissolution behaviour would be expected to parallel that of other p-type oxides, which range from the "fast-dissolving" MnO and CoO to the slow-dissolving NiO. Segall et al. (1988) have categorized these oxides according to their conductivity (see Figure E-1), and include UO_2 with the slowly dissolving oxides, such as NiO.

The major difference between the slow- and fast-dissolving oxides appears to be the intrinsic conductivity, which makes solid-state charge transfer rate-limiting for slowly dissolving oxides, such as NiO, but not for the more rapidly dissolving oxides like CoO. This difference is apparent in the effect of annealing temperature and the presence of dopants on the dissolution rates of both oxides. For NiO an increase in annealing temperature (700 to 1450°C), which decreases the extent of non-stoichiometry and hence the conductivity, decreases the dissolution rate by up to three orders of magnitude. That charge transfer in the solid is rate-determining is confirmed by the impact of donor or acceptor defects that increase and

decrease the dissolution rate respectively (Pease et al. 1980). By contrast, the impact of annealing conditions and dopants exerts a relatively small influence on the dissolution rate of CoO.

If the kinetics of UO_2 dissolution parallel those of NiO, then we can use a rate of $\sim 10^{-3}$ $\mu mol \cdot cm^{-2} \cdot d^{-1}$ (pH = 2, 30°C). Virtually all p-type oxides show a linear dependence of log(rate) on pH with a slope of approximately -0.5. Provided this pH dependence holds into the neutral to alkaline pH range (8 to 10), we obtain a dissolution rate ranging from $\sim 2 \times 10^{-4}$ to $\sim 2 \times 10^{-5}$ $\mu g \cdot cm^{-2} \cdot d^{-1}$. These rates are compared with our predicted rates of oxidative dissolution and the results of Bruno et al. (1991) in Figure E-2.

Extrapolation of our electrochemical current-potential relationship suggests that such dissolution rates should be established over the corrosion potential range from -50 to -150 mV, a range which straddles our threshold potential for the onset of oxidative dissolution. Such a coincidence may be fortuitous considering the approximations involved in determining this range of chemical dissolution rates. However, the procedure does establish a criterion, consistent with our observations, for determining the corrosion potential range of validity for our oxidative model, and to determine when it becomes more appropriate to consider dissolution as purely chemical. We have taken the upper value of this range of rates as an appropriate value for the chemical dissolution rate of UO_2, making a corrosion potential of ~-50 mV the threshold value above which oxidative, as opposed to chemical, dissolution dominates. In mechanistic terms this is equivalent to a switch from dissolution by Reactions (E.1) and (E.2) at $E_{CORR} < -50$ mV,

$$UO_2 + xH_2O \longrightarrow UO_{2+x} + 2xH^+ + 2xe \qquad (E.1)$$

$$UO_{2+x} + n(1 - x)OH^- + (x - 2)H_2O \longrightarrow (1 - x)U(OH)_n^{(4-n)+} + xUO_2^{2+} + (2x - 4)H^+ \qquad (E.2)$$

to dissolution by Reactions (E.3) and (E.4) at $E_{CORR} < -50$ mV,

$$UO_2 + 0.33H_2O \longrightarrow UO_{2.33} + 0.66H^+ + 0.66e \qquad (E.3)$$

$$UO_{2.33} + 0.66H^+ \longrightarrow UO_2^{2+} + 0.33H_2O + 1.34e \qquad (E.4)$$

Such an interpretation suggests that the dissolution of UO_{2+x} will always be oxidative in nature, and that in the absence of external oxidants the

rate of the dissolution process will be controlled by the transport of defects from the bulk of the solid. These defects will be in the form of O^{2-} interstitial ions with accompanying lattice uranium atoms in the oxidation states U^{V} or U^{VI}. The elimination of such defects at the oxide/solution interface will involve the transfer to solution of uranium atoms in oxidation states above +4. The rate of dissolution according to this scheme will be very dependent on the non-stoichiometry of UO_{2+x}. Since this non-stoichiometry can vary over a very wide range for UO_{2+x} ($0 < x \leq 0.33$), the rate of dissolution is likely to vary drastically, depending on the treatment of the oxide. Chemical dissolution exclusively in the form of U^{4+},

$$UO_2 + (n - 2)H_2O \longrightarrow U(OH)_n^{(4-n)+} + (n - 4)H^+ \qquad (E.5)$$

(see Figure 3(c) of main text), will only occur for UO_{2+x} with x close to zero in the complete absence of oxidants, and should have an extremely low rate.

REFERENCES

Bruno, J., I Casas and I. Puigdomenech. 1991. The kinetics of dissolution of UO_2 under reducing conditions and the influence of an oxidized surface layer (UO_{2+x}): Application of a continuous flow-through reactor. Geochimica et Cosmochimica Acta 55, 647-658.

Hocking, W.H., J.S. Betteridge and D.W. Shoesmith. 1991. The cathodic reduction of dioxygen on uranium oxide in dilute alkaline aqueous solution. Atomic Energy of Canada Limited Report, AECL-10402.

Pease, W.R., R.L. Segall, R. St. C. Smart and P.S. Turner. 1980. Evidence for modification of nickel oxide by silica: Infrared, electron microscopy and dissolution rate studies. Journal of the Chemical Society Faraday Transactions 1, 76, 1510-1519.

Segall, R.L., R. St.C. Smart and P. S. Turner. 1988. Oxide surfaces in solution. In Surface and Near-Surface Chemistry of Oxide Materials (J. Nowotny and L.-C. Dufour, editors), Elsevier Science Publishers, Amsterdam, 527-576.

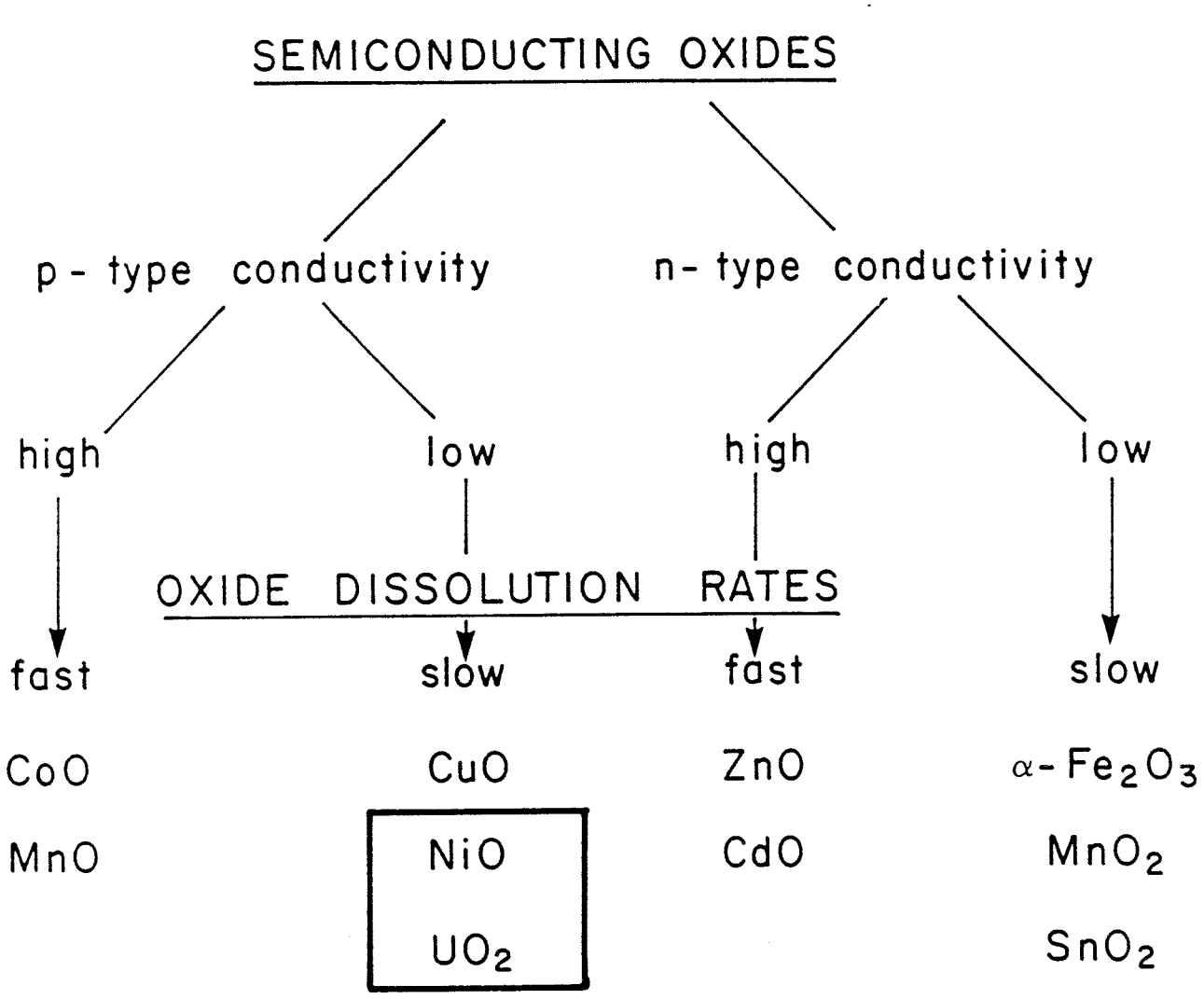

FIGURE E-1: Categorization of Oxides According to their Conductivity Type and Dissolution Behaviour (from Segall et al. 1988)

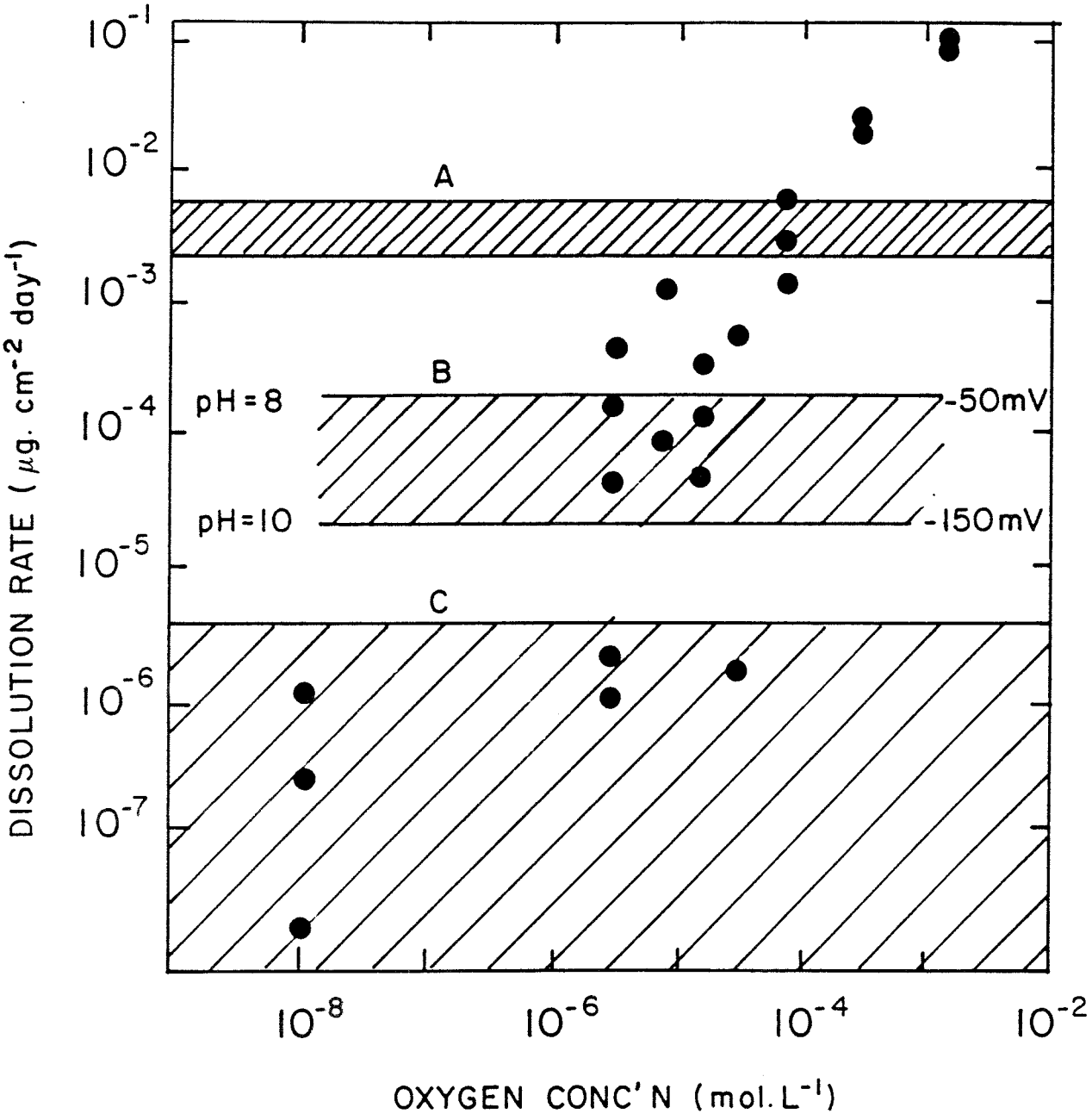

Figure E-2: Dissolution Rates for UO_2 as a Function of Dissolved Oxygen Concentration in 0.1 mol·L^{-1} $NaClO_4$ (pH = 9.5). The shaded range of values marked A are taken from Bruno et al. (1991). The shaded range marked B are our estimated range for the chemical dissolution rate of UO_2 by analogy with NiO. The line marked C represents an arbitrary meaningful lower limit for dissolution rate values.

APPENDIX F

PEROXIDE DECOMPOSITION AND OXIDATIVE DISSOLUTION IN H_2O_2-CONTAINING SOLUTIONS

For intermediate hydrogen peroxide concentrations (2×10^{-4} to 5×10^{-3} mol·L^{-1}) at pH = 9.5, we have interpreted the independence of UO_2 corrosion potential (Figure 11 of the main text) to be a result of the predominance of peroxide decomposition over uranium oxide dissolution. Instead of the reduction process,

$$H_2O_2 + 2e \longrightarrow 2OH^- \qquad (F.1)$$

coupling with the oxidative dissolution reaction,

$$UO_{2.33} + 0.66H^+ \longrightarrow UO_2^{2+} + 0.33H_2O + 1.33e \qquad (F.2)$$

it is coupled to the peroxide oxidation reaction

$$H_2O_2 \longrightarrow O_2 + 2H^+ + 2e \qquad (F.3)$$

to yield the overall decomposition process,

$$2H_2O_2 \longrightarrow O_2 + 2H_2O \qquad (F.4)$$

In previous publications we have speculated on the nature of the intermediates involved in this decomposition process (Sunder et al. 1987, Shoesmith et al. 1985). The shift in potential with H_2O_2 concentration for the two half reactions (F.1 and F.3) will be equal but opposite in sign, and the value of E_{CORR} would not be expected to shift with peroxide concentration, as observed, if these two reactions were coupled.

The kinetics of the peroxide decomposition reaction are very dependent on the composition and defect structure of the electrode surface. Our X-ray photoelectron spectroscopy (XPS) results show that the behaviour of H_2O_2 appears to change from predominantly H_2O_2 decomposition on $UO_{2.33}$ to predominantly causing uranium dissolution on $UO_{2.33}/UO_3 \cdot 2H_2O$. This is apparent when we compare the compositions of Figure F-1 with the dissolution rates in Figure 11 (main text). These results are consistent with those of Needes and Nicol (1973), who showed electrochemically that

H_2O_2 oxidation to O_2 predominates at low applied potentials, but was blocked as oxidative dissolution took over on more oxidized surfaces (Figure F-2).

It is possible that H_2O_2 decomposition is catalyzed by the presence of adjacent U^{4+} and U^{6+} sites on the electrode surface, as shown schematically in Figure F-3, and inhibited when these sites are blocked by the formation of secondary phases, such as $UO_3 \cdot 2H_2O$. Evidence in support of this mechanism comes from experiments in carbonate solutions when the solubilization of U^{6+} species by complexation with carbonate prevents secondary phase formation. In these solutions E_{CORR} does not shift to more positive values at higher H_2O_2 concentrations (Figure F-4). This behaviour suggests that decomposition may still predominate over dissolution even at high H_2O_2 concentrations.

The kinetics of electron transfer reactions involving H_2O_2 on UO_2 are very dependent on the defect structure of the surface. Whether or not hydrogen peroxide is observed during rotating Au-ring UO_2-disc experiments on the electrochemical reduction of oxygen,

$$O_2 + 2H_2O + 2e \longrightarrow 2H_2O_2 \qquad (F.5)$$

$$2H_2O_2 + 2e \longrightarrow 4OH^- \qquad (F.6)$$

depends on the fineness of polish on the UO_2 surface (Hocking et al. 1991). On rough electrodes (polished to a 600-grit finish), no peroxide is released to solution, presumably because its subsequent reduction via Reaction (F.6) is facilitated when a high density of defects is present on the surface. By contrast, significant amounts of peroxide are released from smooth electrodes (polished to a 1-μm finish).

For UO_2 oxidation by H_2O_2, a matter of more immediate importance is the impact of a decrease in pH. Figure F-5 shows the dependence of corrosion potential on pH in 0.1 $mol \cdot L^{-1}$ $NaClO_4$ containing 10^{-3} $mol \cdot L^{-1}$ H_2O_2. As the pH decreases, E_{CORR} increases rapidly, suggesting that the rate of oxidative dissolution is accelerated significantly at lower values of pH. A similar increase of E_{CORR} with pH is not observed in oxygen-containing solutions (Figure F-6).

REFERENCES

Hocking, W.H., J.S. Betteridge and D.W. Shoesmith. 1991. The cathodic reduction of dioxygen on uranium oxide in dilute alkaline aqueous solution. Atomic Energy of Canada Limited Report, AECL-10402.

Needes, C.R.S. and M.J. Nicol. 1973. A study of some redox reactions at a UO_2 surface. National Institute for Metallurgy, Republic of South Africa, Report No. 7073.

Shoesmith, D.W., S. Sunder, L.H. Johnson and M.G. Bailey. 1985. Oxidation of CANDU UO_2 fuel by the alpha-radiolysis products of water. In Materials Research Society Symposium Proceedings 50 (Scientific Basis for Nuclear Waste Management IX), 309-316. Also Atomic Energy of Canada Limited Reprint, AECL-8888.

Sunder, S., D.W. Shoesmith, L.H. Johnson, G.J. Wallace, M.G. Bailey and A.P. Snaglewski. 1987. Oxidation of CANDU™ fuel by the products of alpha-radiolysis of groudwater. In Materials Research Society Symposium Proceedings 84 (Scientific Basis for Nuclear Waste Management X), 103-113. Also Atomic Energy of Canada Limited Reprint, AECL-9296.

Sunder, S., D.W. Shoesmith, R.J. Lemire, M.G. Bailey and G.J. Wallace. 1991. The effect of pH on the corrosion of nuclear fuel (UO_2) in oxygenated solutions. Corrosion Science 32 (4), 373-386.

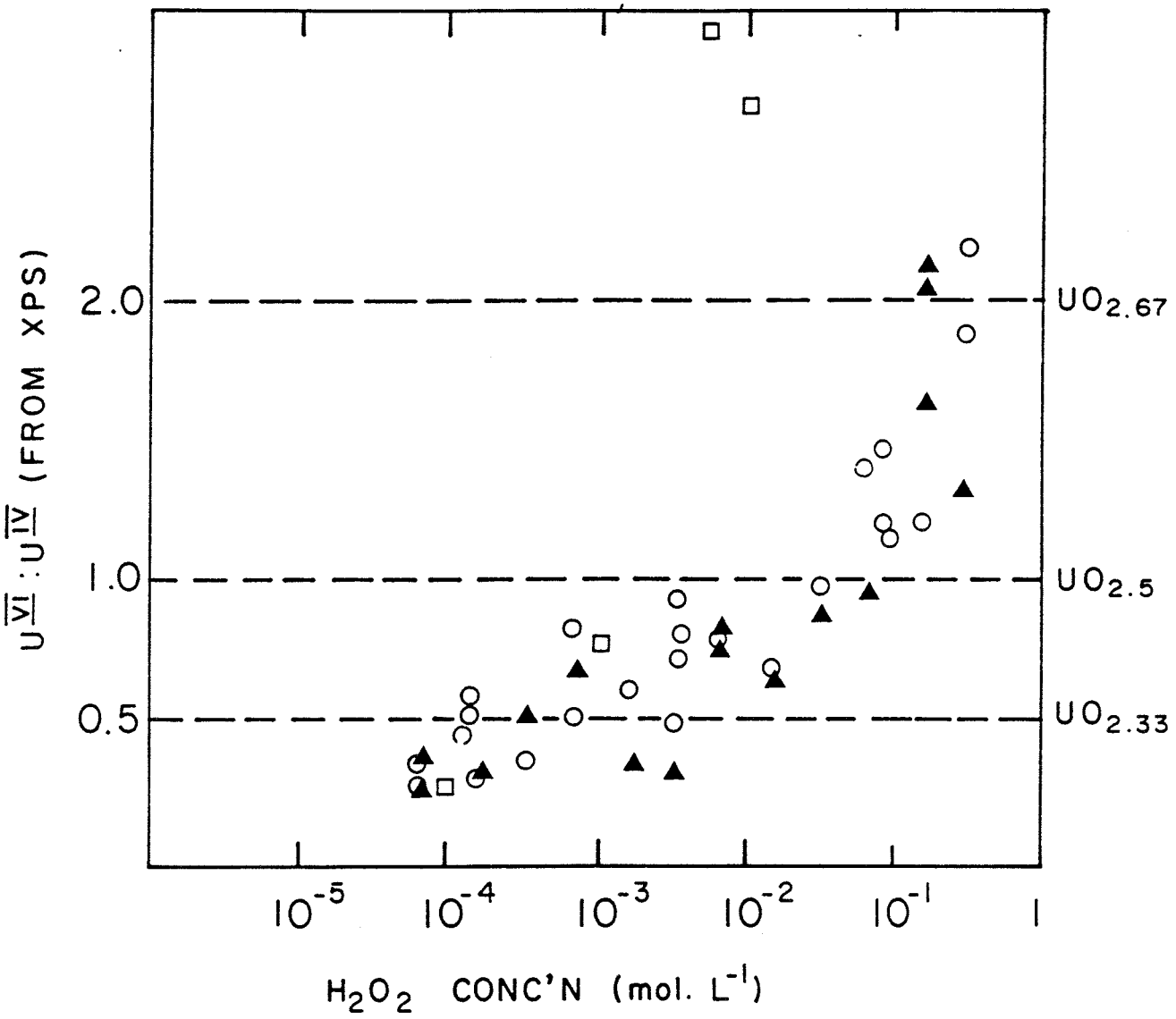

FIGURE F-1: $U^{VI}:U^{IV}$ Ratio (from XPS Measurements) in the Surface of a UO_2 Electrode Exposed to 0.1 mol·L^{-1} $NaClO_4$ (pH = 9.5) Containing Various Concentrations of H_2O_2. The different data points are from different sets of experiments.

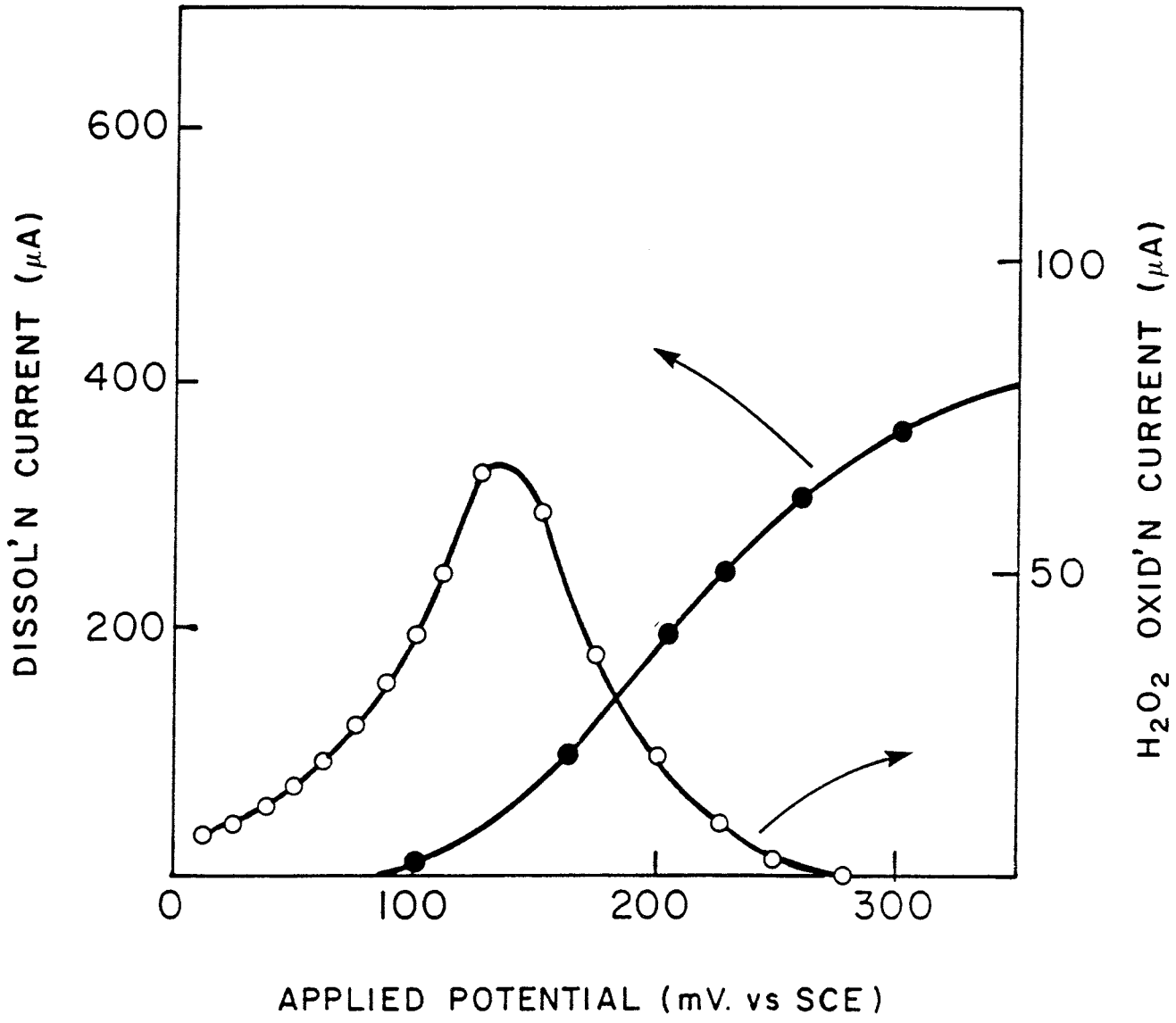

FIGURE F-2: Currents Due to the Anodic Oxidation of H_2O_2 and the Dissolution of UO_2 Recorded in 0.5 mol·L^{-1} Na_2CO_3 (pH = 11.3) Using a Rotating Au Ring-UO_2 Disc Electrode (from Needes and Nicol 1973)

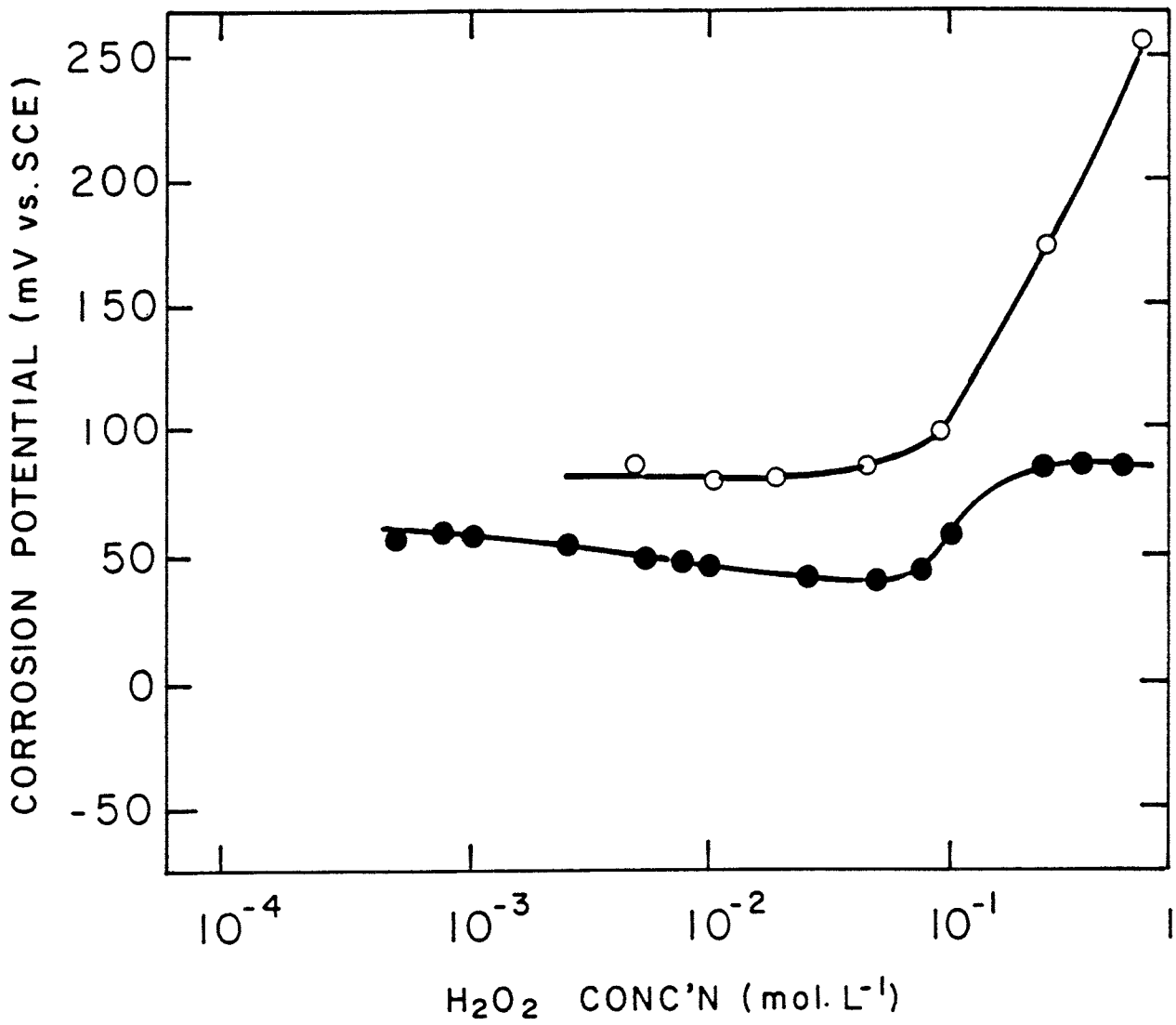

FIGURE F-3: Schematic Showing the Surface-Catalyzed Decomposition of H_2O_2 on UO_{2+x} Surfaces

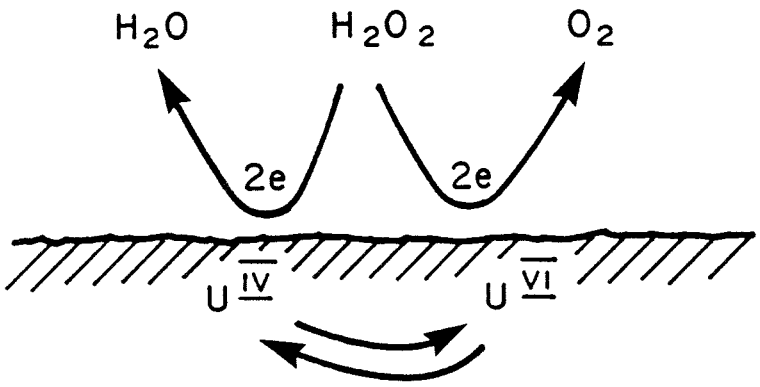

FIGURE F-4: Corrosion Potential of a UO_2 Electrode as a Function of H_2O_2 Concentration in 0.1 mol·L^{-1} $NaClO_4$ (pH = 9.5) (o) and in the Same Solution Containing 0.1 mol·L^{-1} Na_2CO_3 (o)

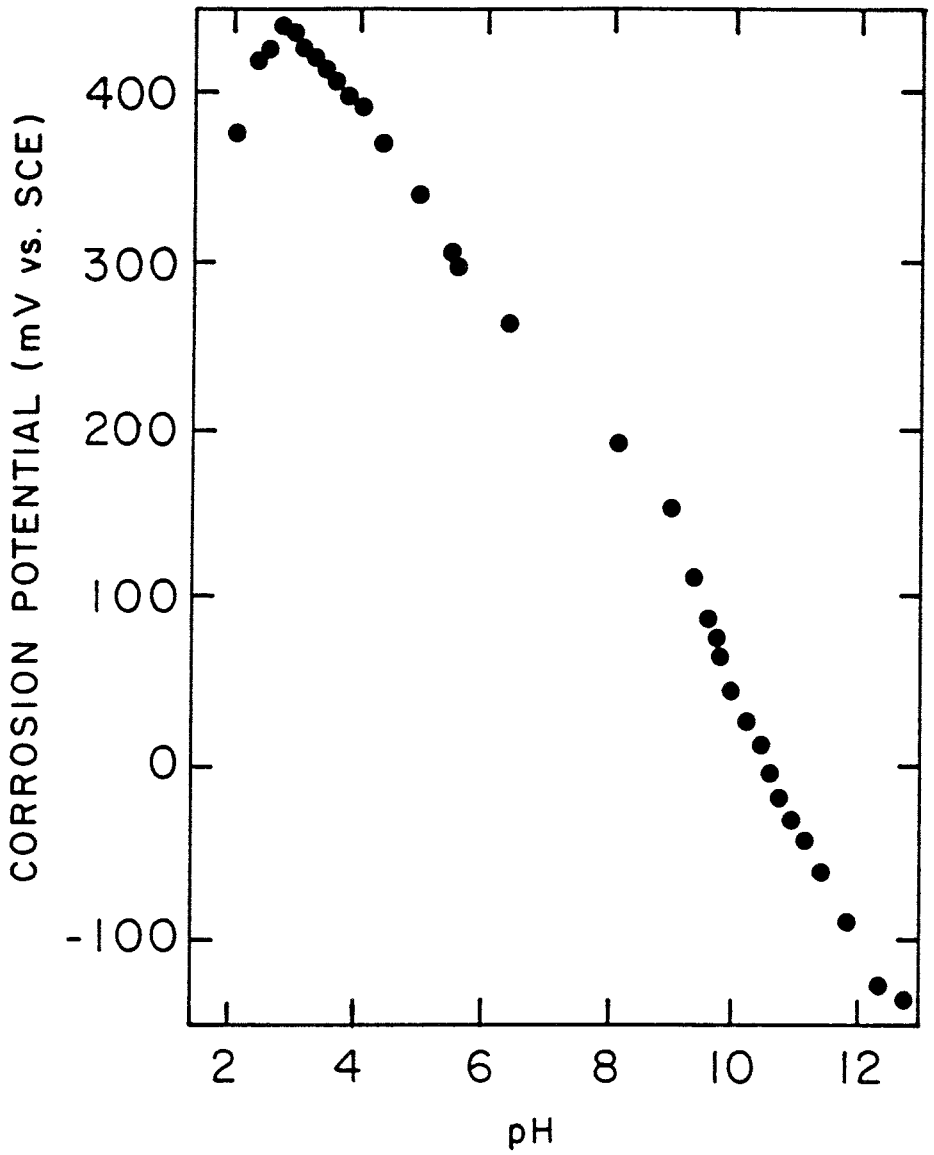

FIGURE F-5: Steady-State Corrosion Potential of UO_2 as a Function of pH for 0.1 mol·L^{-1} H_2O_2 (from Sunder et al. 1987)

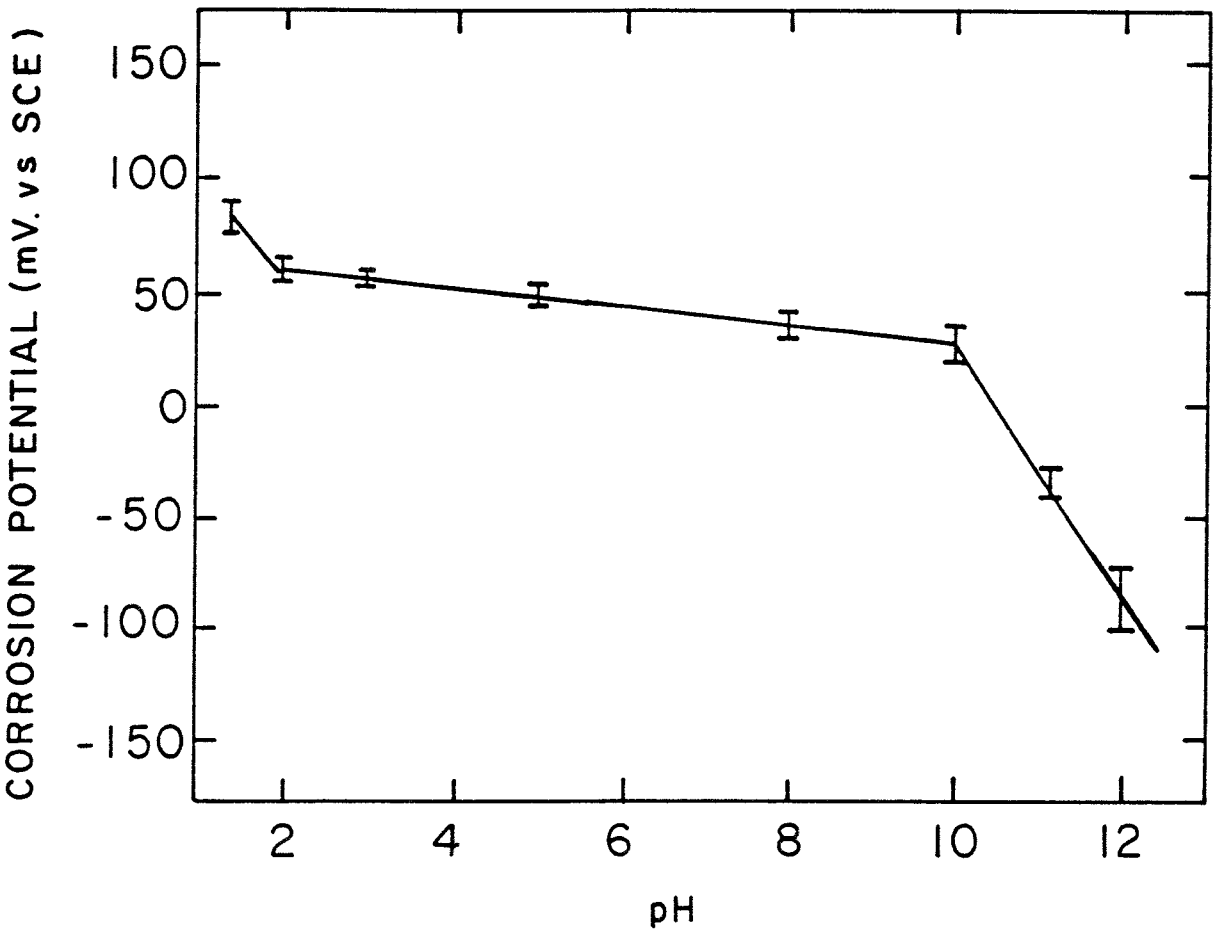

FIGURE F-6: Steady-State Corrosion Potential of a UO_2 Electrode as a Function of pH in Aerated 0.1 mol·L^{-1} $NaClO_4$ (from Sunder et al. 1991)

APPENDIX G

RELATIONSHIP BETWEEN ALPHA SOURCE STRENGTH USED IN EXPERIMENTS AND THE ALPHA PLUS BETA ACTIVITY-TIME PROFILE FOR IRRADIATED CANDU FUEL

The relationship between the time profile of the alpha plus beta activity of the irradiated fuel and the alpha source strength used in the experiments was derived using the data given in Figure 2.1 of Smith et al. (1987) (Figure 17 in the main text). This figure gives the activity, as a function of time in terms of kilograms of uranium in irradiated CANDU fuel with a burnup of 685 GJ/kg U in the Bruce nuclear reactors.

The diameter of alpha sources used in the experiments was 1.6 cm, and therefore the area of the source was ~2 cm^2. To relate activity of the irradiated fuel, as given in Smith et al. (1987), with that of the sources used in the experiment, one has to calculate the activity from an equivalent surface area of the irradiated fuel (Sunder et al. 1990).

Water at the surface of the used fuel will experience an alpha flux, mainly from the top 11 μm of the fuel, as a result of the limited mean free path of the alpha particles in solid UO_2 (Nitzki and Matzke 1973). The density of the used CANDU fuel is reported to be ~10.36 g/cm^3 (Tait et al. 1989). Therefore, the mass of an 11-μm-thick layer of the used fuel, of surface area 2 cm^2, is ~0.0228 g. This corresponds to ~0.02 g of uranium. Thus, to relate the alpha source strength used in the experiments with the predicted alpha plus beta activity of the irradiated fuel, one has to calculate the activity in 0.02 g of uranium as a function of time from the data in Smith et al. (1987).

If the activity of the irradiated fuel, in Smith et al. (1987), at time t is Z Ci/kg, then the equivalent source strength in the experiments is

$$\frac{Z \times 10^6}{10^3} \times 0.02 = 20Z \ \mu Ci \qquad (G.1)$$

A derivation of the relationship between the time profile of the alpha plus beta activity of the used-fuel surface and alpha strength of the sources used in the experiments should include a discussion of two other factors that have an important bearing on the radiolysis of water in contact with the used fuel.

(a) First, the decrease in the number and energy of alpha particles formed in the top 11 μm of used fuel and reaching the water layer in contact with the fuel. Not all the alpha particles formed in the used-fuel surface will escape into the solution as assumed above in Equation (G.1). Johnson has suggested that the fraction of the alpha particles reaching the solution in contact with the used fuel is only ~0.25 of the total number generated in the surface layer, because of geometric constraints (Johnson 1982). This suggestion is supported by the later calculations of Hosoe et al. (1984) and Garisto (1989). Also, there is some decrease in the energy of the alpha particles because of inelastic collisions within the fuel matrix before they reach the water in contact with fuel (Garisto 1989).

(b) Second, the real surface area of the fuel is about three times greater than the apparent geometric surface area used for Equation (G.1) (Johnson and Shoesmith 1988). CANDU fuel is fabricated from UO_2 particles with a typical grain size of 5 to 10 μm (Johnson and Shoesmith 1988), and when used as an electrode, appears to have a roughness factor of ~3 (Shoesmith et al. 1984). Cracking of the fuel pellets in reactor leads to an increase in the fuel surface area (Johnson and Shoesmith 1988). Also, the water in the cracks in the fuel can receive alpha particles from several directions, resulting in increased water radiolysis. Therefore, we believe that the alpha radiolysis experienced by a water layer in contact with the fuel surface could be significantly greater than that calculated using the apparent geometric area, as in Equation (G.1).

Thus, while Equation (G.1) overestimates the extent of alpha radiolysis because of the factors discussed in section (a) above, it underestimates it because of the factors discussed in (b). Therefore, we accept Equation (G.1) as a reasonable approximation for establishing a relationship between the time profile of the alpha plus beta activity of the irradiated fuel and the alpha source strength used in experiments.

REFERENCES

Garisto, F. 1989. The energy spectrum of α-particles emitted from used CANDU™ fuel. Annals of Nuclear Energy 16, 33-38. Also Atomic Energy of Canada Limited Reprint, AECL-9822.

Hosoe, M., Y. Takami, F. Shiraishi and K. Tomura. 1984. Stopping power measurement using thick alpha sources. Nuclear Instruments and Methods of Physics Research 223, 377-381

Johnson, L.H. 1982. The dissolution of irradiated UO_2 fuel in groundwater. Atomic Energy of Canada Limited Report, AECL-6837.

Johnson, L.H. and D.W. Shoesmith. 1988. Spent fuel. In Radioactive Waste Forms for the Future (W. Lutze and R.C. Ewing, editors), Elsevier Publishers, 635-698. Also Atomic Energy of Canada Limited Reprint, AECL-9583.

Nitzki, V. and Hj. Matzke. 1973. Stopping power of 1-9 MeV He^{++} Ions in UO_2, $(U, Pu)O_2$, and ThO_2. Physical Review B. 8, 1894-1900.

Smith, H.J., J.C. Tait and R.E. Von Massow. 1987. Radioactive decay properties of Bruce "A" CANDU™ UO_2 fuel and fuel recycle waste. Atomic Energy of Canada Limited Report, AECL-9072.

Shoesmith, D.W., S. Sunder, M.G. Bailey, G.J. Wallace and F.W. Stanchell. 1984. Anodic oxidation of UO_2. Part IV. X-ray photoelectron spectroscopic and electrochemical studies of film growth in carbonate-containing solutions. Applications of Surface Science 20, 39-57. Also Atomic Energy of Canada Limited Reprint, AECL-8174.

Sunder, S., G.D. Boyer and N.H. Miller. 1990. XPS studies of UO_2 oxidation by alpha radiolysis of water at 100°C. Journal of Nuclear Materials 175, 163-169.

Tait, J.C., I.C. Gauld and G.B. Wilkin. 1989. Derivation of initial radionuclide inventories for the safety assessment of the disposal of used CANDU fuel. Atomic Energy of Canada Limited Report, AECL-9881.

List of SKB reports

Annual Reports

1977-78
TR 121
KBS Technical Reports 1 – 120
Summaries
Stockholm, May 1979

1979
TR 79-28
The KBS Annual Report 1979
KBS Technical Reports 79-01 – 79-27
Summaries
Stockholm, March 1980

1980
TR 80-26
The KBS Annual Report 1980
KBS Technical Reports 80-01 – 80-25
Summaries
Stockholm, March 1981

1981
TR 81-17
The KBS Annual Report 1981
KBS Technical Reports 81-01 – 81-16
Summaries
Stockholm, April 1982

1982
TR 82-28
The KBS Annual Report 1982
KBS Technical Reports 82-01 – 82-27
Summaries
Stockholm, July 1983

1983
TR 83-77
The KBS Annual Report 1983
KBS Technical Reports 83-01 – 83-76
Summaries
Stockholm, June 1984

1984
TR 85-01
Annual Research and Development Report 1984
Including Summaries of Technical Reports Issued during 1984. (Technical Reports 84-01 – 84-19)
Stockholm, June 1985

1985
TR 85-20
Annual Research and Development Report 1985
Including Summaries of Technical Reports Issued during 1985. (Technical Reports 85-01 – 85-19)
Stockholm, May 1986

1986
TR 86-31
SKB Annual Report 1986
Including Summaries of Technical Reports Issued during 1986
Stockholm, May 1987

1987
TR 87-33
SKB Annual Report 1987
Including Summaries of Technical Reports Issued during 1987
Stockholm, May 1988

1988
TR 88-32
SKB Annual Report 1988
Including Summaries of Technical Reports Issued during 1988
Stockholm, May 1989

1989
TR 89-40
SKB Annual Report 1989
Including Summaries of Technical Reports Issued during 1989
Stockholm, May 1990

1990
TR 90-46
SKB Annual Report 1990
Including Summaries of Technical Reports Issued during 1990
Stockholm, May 1991

Technical Reports

List of SKB Technical Reports 1991

TR 91-01
Description of geological data in SKB's database GEOTAB
Version 2
Stefan Sehlstedt, Tomas Stark
SGAB, Luleå
January 1991

TR 91-02
Description of geophysical data in SKB database GEOTAB
Version 2
Stefan Sehlstedt
SGAB, Luleå
January 1991

TR 91-03
1. The application of PIE techniques to the study of the corrosion of spent oxide fuel in deep-rock ground waters
2. Spent fuel degradation
R S Forsyth
Studsvik Nuclear
January 1991

TR 91-04
Plutonium solubilities
I Puigdomènech[1], J Bruno[2]
[1]Enviromental Services, Studsvik Nuclear, Nyköping, Sweden
[2]MBT Tecnologia Ambiental, CENT, Cerdanyola, Spain
February 1991

TR 91-05
Description of tracer data in the SKB database GEOTAB
SGAB, Luleå
April, 1991

TR 91-06
Description of background data in the SKB database GEOTAB
Version 2
Ebbe Eriksson, Stefan Sehlstedt
SGAB, Luleå
March 1991

TR 91-07
Description of hydrogeological data in the SKB's database GEOTAB
Version 2
Margareta Gerlach (ed.)
Mark Radon Miljö MRM Konsult AB, Luleå
December 1991

TR 91-08
Overview of geologic and geohydrologic conditions at the Finnsjön site and its surroundings
Kaj Ahlbom[1], Sven Tirén[2]
[1]Conterra AB
[2]Sveriges Geologiska AB
January 1991

TR 91-09
Long term sampling and measuring program. Joint report for 1987, 1988 and 1989. Within the project: Fallout studies in the Gideå and Finnsjö areas after the Chernobyl accident in 1986
Thomas Ittner
SGAB, Uppsala
December 1990

TR 91-10
Sealing of rock joints by induced calcite precipitation. A case study from Bergeforsen hydro power plant
Eva Hakami[1], Anders Ekstav[2], Ulf Qvarfort[2]
[1]Vattenfall HydroPower AB
[2]Golder Geosystem AB
January 1991

TR 91-11
Impact from the disturbed zone on nuclide migration – a radioactive waste repository study
Akke Bengtsson[1], Bertil Grundfelt[1], Anders Markström[1], Anders Rasmuson[2]
[1]KEMAKTA Konsult AB
[2]Chalmers Institute of Technology
January 1991

TR 91-12
Numerical groundwater flow calculations at the Finnsjön site
Björn Lindbom, Anders Boghammar, Hans Lindberg, Jan Bjelkås
KEMAKTA Consultants Co, Stockholm
February 1991

TR 91-13
Discrete fracture modelling of the Finnsjön rock mass
Phase 1 feasibility study
J E Geier, C-L Axelsson
Golder Geosystem AB, Uppsala
March 1991

TR 91-14
Channel widths
Kai Palmqvist, Marianne Lindström
BERGAB-Berggeologiska Undersökningar AB
February 1991

TR 91-15
Uraninite alteration in an oxidizing environment and its relevance to the disposal of spent nuclear fuel
Robert Finch, Rodney Ewing
Department of Geology, University of New Mexico
December 1990

TR 91-16
Porosity, sorption and diffusivity data compiled for the SKB 91 study
Fredrik Brandberg, Kristina Skagius
Kemakta Consultants Co, Stockholm
April 1991

TR 91-17
Seismically deformed sediments in the Lansjärv area, Northern Sweden
Robert Lagerbäck
May 1991

TR 91-18
Numerical inversion of Laplace transforms using integration and convergence acceleration
Sven-Åke Gustafson
Rogaland University, Stavanger, Norway
May 1991

TR 91-19
NEAR21 - A near field radionuclide migration code for use with the PROPER package
Sven Norman[1], Nils Kjellbert[2]
[1]Starprog AB
[2]SKB AB
April 1991

TR 91-20
Äspö Hard Rock Laboratory. Overview of the investigations 1986-1990
R Stanfors, M Erlström, I Markström
June 1991

TR 91-21
Äspö Hard Rock Laboratory. Field investigation methodology and instruments used in the pre-investigation phase, 1986-1990
K-E Almén, O Zellman
June 1991

TR 91-22
Äspö Hard Rock Laboratory. Evaluation and conceptual modelling based on the pre-investigations 1986-1990
P Wikberg, G Gustafson, I Rhén, R Stanfors
June 1991

TR 91-23
Äspö Hard Rock Laboratory. Predictions prior to excavation and the process of their validation
Gunnar Gustafson, Magnus Liedholm, Ingvar Rhén, Roy Stanfors, Peter Wikberg
June 1991

TR 91-24
Hydrogeological conditions in the Finnsjön area. Compilation of data and conceptual model
Jan-Erik Andersson, Rune Nordqvist, Göran Nyberg, John Smellie, Sven Tirén
February 1991

TR 91-25
The role of the disturbed rock zone in radioactive waste repository safety and performance assessment. A topical discussion and international overview.
Anders Winberg
June 1991

TR 91-26
Testing of parameter averaging techniques for far-field migration calculations using FARF31 with varying velocity.
Akke Bengtsson[1], Anders Boghammar[1], Bertil Grundfelt[1], Anders Rasmuson[2]
[1]KEMAKTA Consultants Co
[2]Chalmers Institute of Technology

TR 91-27
Verification of HYDRASTAR. A code for stochastic continuum simulation of groundwater flow
Sven Norman
Starprog AB
July 1991

TR 91-28
Radionuclide content in surface and groundwater transformed into breakthrough curves. A Chernobyl fallout study in an forested area in Northern Sweden
Thomas Ittner, Erik Gustafsson, Rune Nordqvist
SGAB, Uppsala
June 1991

TR 91-29
Soil map, area and volume calculations in Orrmyrberget catchment basin at Gideå, Northern Sweden
Thomas Ittner, P-T Tammela, Erik Gustafsson
SGAB, Uppsala
June 1991

TR 91-30
A resistance network model for radionuclide transport into the near field surrounding a repository for nuclear waste (SKB, Near Field Model 91)
Lennart Nilsson, Luis Moreno, Ivars Neretnieks, Leonardo Romero
Department of Chemical Engineering,
Royal Institute of Technology, Stockholm
June 1991

TR 91-31
Near field studies within the SKB 91 project
Hans Widén, Akke Bengtsson, Bertil Grundfelt
Kemakta Consultants AB, Stockholm
June 1991

TR 91-32
SKB/TVO Ice age scenario
Kaj Ahlbom[1], Timo Äikäs[2], Lars O. Ericsson[3]
[1]Conterra AB
[2]Teollisuuden Voima Oy (TVO)
[3]Svensk Kärnbränslehantering AB (SKB)
June 1991

TR 91-33
Transient nuclide release through the bentonite barrier - SKB 91
Akke Bengtsson, Hans Widén
Kemakta Konsult AB
May 1991

TR 91-34
SIMFUEL dissolution studies in granitic groundwater
I Casas[1], A Sandino[2], M S Caceci[1], J Bruno[1], K Ollila[3]
[1]MBT Tecnologia Ambiental, CENT, Cerdanyola, Spain
[2]KTH, Dpt. of Inorganic Chemistry, Stockholm, Sweden
[3]VTT, Tech. Res. Center of Finland, Espoo, Finland
September 1991

TR 91-35
Storage of nuclear waste in long boreholes
Håkan Sandstedt[1], Curt Wichmann[1], Roland Pusch[2], Lennart Börgesson[2], Bengt Lönnerberg[3]
[1]Tyréns
[2]Clay Technology AB
[3]ABB Atom
August 1991

TR 91-36
Tentative outline and siting of a repository for spent nuclear fuel at the Finnsjön site. SKB 91 reference concept
Lars Ageskog, Kjell Sjödin
VBB VIAK
September 1991

TR 91-37
Creep of OFHC and silver copper at simulated final repository canister-service conditions
Pertti Auerkari, Heikki Leinonen, Stefan Sandlin
VTT, Metals Laboratory, Finland
September 1991

TR 91-38
Production methods and costs of oxygen free copper canisters for nuclear waste disposal
Hannu Rajainmäki, Mikko Nieminen, Lenni Laakso
Outokumpu Poricopper Oy, Finland
June 1991

TR 91-39
The reducibility of sulphuric acid and sulphate in aqueous solution (translated from German)
Rolf Grauer
Paul Scherrer Institute, Switzerland
July 1990

TR 91-40
Interaction between geosphere and biosphere in lake sediments
Björn Sundblad, Ignasi Puigdomenech, Lena Mathiasson
December 1990

TR 91-41
Individual doses from radionuclides released to the Baltic coast
Ulla Bergström, Sture Nordlinder
Studsvik AB
May 1991

TR 91-42
Sensitivity analysis of the groundwater flow at the Finnsjön study site
Yung-Bing Bao, Roger Thunvik
Dept. Land and Water Resources,
Royal Institute of Technology, Stockholm, Sweden
September 1991

TR 91-43
SKB - PNC
Development of tunnel radar antennas
Lars Falk
ABEM, Uppsala, Sweden
July 1991

TR 91-44
Fluid and solute transport in a network of channels
Luis Moreno, Ivars Neretnieks
Department of Chemical Engineering,
Royal Institute of Technology, Stockholm, Sweden
September 1991

TR 91-45
The implications of soil acidification on a future HLNW repository.
Part I: The effects of increased weathering, erosion and deforestation
Josefa Nebot, Jordi Bruno
MBT Tecnologìa Ambiental, Cerdanyola, Spain
July 1991

TR 91-46
Some mechanisms which may reduce radiolysis
Ivars Neretnieks, Mostapha Faghihi
Department of Chemical Engineering, Royal Institute of Technology, Stockholm, Sweden
August 1991

TR 91-47
On the interaction of granite with Tc(IV) and Tc(VII) in aqueous solution
Trygve E Eriksen, Daquing Cui
Royal Institute of Technology, Department of Nuclear Chemistry, Stockholm, Sweden
October 1991

TR 91-48
A compartment model for solute transport in the near field of a respository for radioactive waste (Calculations for Pu-239)
Leonardo Romero, Luis Moreno , Ivars Neretnieks
Department of Chemical Engineering, Royal Institute of Technology, Stockholm, Sweden
October 1991

TR 91-49
Description of transport pathways in a KBS-3 type repository
Roland Pusch[1], Ivars Neretnieks[2], Patrik Sellin[3]
[1] Clay Technology AB. Lund
[2] The Royal institue of Techonology Department of Chemical Engineering, Stockholm
[3] Swedisch Nueclear Fuel and Waste Management Co (SKB), Stockholm
December 1991

TR 91-50
Concentrations of particulate matter and humic substances in deep groundwaters and estimated effects on the adsorption and transport of radionuclides
Bert Allard[1], Fred Karlsson[2], Ivars Neretnieks[3]
[1]Department of Water and Environmental Studies, University of Linköping, Sweden
[2]Swedish Nuclear Fuel and Waste Management Company, SKB, Stockholm, Sweden
[3]Department of Chemical Engineering, Royal Institute of Technology, Stockholm, Sweden
November 1991

TR 91-51
Gideå study site. Scope of activities and main results
Kaj Ahlbom[1], Jan-Erik Andersson[2],
Rune Nordqvist[2], Christer Ljunggren[2], Sven Tirén[2],
Clifford Voss[3]
[1]Conterra AB
[2]Geosigma AB
[3]U.S. Geological Survey
October 1991

TR 91-52
Fjällveden study site. Scope of activities and main results
Kaj Ahlbom[1], Jan-Erik Andersson[2],
Rune Nordqvist[2], Christer Ljunggren[2], Sven Tirén[2],
Clifford Voss[3]
[1]Conterra AB
[2]Geosigma AB
[3]U.S. Geological Survey
October 1991

TR 91-53
Impact of a repository on permafrost development during glaciation advance
Per Vallander, Jan Eurenius
VBB VIAK AB
December 1991

TR 91-54

Hydraulic evaluation of the groundwater conditions at Finnsjön. The effects on dilution in a domestic well

C-L Axelsson[1], J Byström[1], Å Eriksson[1], J Holmén[1], H M Haitjema[2]
[1]Golder Geosystem AB, Uppsala, Sweden
[2]School of Public and Environmental Affairs, Indiana University, Bloomington, Indiana, USA
September 1991

TR 91-55

Redox capacity of crystalline rocks. Laboratory studies under 100 bar oxygen gas pressure

Veijo Pirhonen, Petteri Pitkänen
Technical Research Center of Finland
December 1991

TR 91-56

Microbes in crystalline bedrock. Assimilation of CO_2 and introduced organic compounds by bacterial populations in groundwater from deep crystalline bedrock at Laxemar and Stripa

Karsten Pedersen, Susanne Ekendahl, Johanna Arlinger
Department of General and Marine Microbiology, University of Göteborg, Göteborg, Sweden
December 1991

TR 91-57

The groundwater circulation in the Finnsjö area - the impact of density gradients

Part A: Saline groundwater at the Finnsjö site and its surroundings

Kaj Ahlbom
CONTERRA AB

Part B: A numerical study of the combined effects of salinity gradients, temperature gradients and fracture zones

Urban Svensson
CFE AB

Part C: A three-dimensional numerical model of groundwater flow and salinity distribution in the Finnsjö area

Urban Svensson
CFE AB
November 1991

TR 91-58

Exploratory calculations concerning the influence of glaciation and permafrost on the groundwater flow system, and an initial study of permafrost influence at the Finnsjön site - an SKB 91 study

Björn Lindbom, Anders Boghammar
Kemakta Konsult AB, Stockholm
December 1991

TR 91-59

Proceedings from the technical workshop on near-field performance assessment for high-level waste held in Madrid October 15-17, 1990

Patrik Sellin[1], Mick Apted[2], José Gago[3] (editors)
[1]SKB, Stockholm, Sweden
[2]Intera, Denver, USA
[3]ENRESA, Madrid, Spain
December 1991

TR 91-60

Spent fuel corrosion and dissolution

R S Forsyth[1], L O Werme[2]
[1]Studsvik AB, Nyköping, Sweden
[2]Swedish Nuclear Fuel and Waste Management Co, Stockholm, Sweden
December 1991

TR 91-61

Heat propagation from a radioactive waste repository. SKB 91 reference canister

Roger Thunvik, Carol Braester
Royal Institute of Technology, Stockholm, Sweden
March 1991

TR 91-62

The kinetics of pitting corrosion of carbon steel applied to evaluating containers for nuclear waste disposal. Final report 1991

G P Marsh[1], K J Taylor[2], A H Harker[3]
[1]Strategic Studies Department, AEA Environment and Energy, AEA Technology, Harwell Laboratory
[2]Applied Electrochemistry Department, AEA Industrial Technology, AEA Technology, Harwell Laboratory
[3]Theoretical Studies Department, AEA Industrial Technology, AEA Technology, Harwell Laboratory
July 1991